

Electronic Thesis and Dissertation Repository

6-7-2023 10:00 AM

Catalytic Consequences of Catalyst Pellet Architecture on the Methanol to Oxymethylene Process

Sebastian M K Cook, *Western University*

Supervisor: Herrera, Jose E., *The University of Western Ontario*

A thesis submitted in partial fulfillment of the requirements for the Master of Engineering Science degree in Chemical and Biochemical Engineering

© Sebastian M K Cook 2023

Follow this and additional works at: <https://ir.lib.uwo.ca/etd>

 Part of the [Catalysis and Reaction Engineering Commons](#)

Recommended Citation

Cook, Sebastian M K, "Catalytic Consequences of Catalyst Pellet Architecture on the Methanol to Oxymethylene Process" (2023). *Electronic Thesis and Dissertation Repository*. 9316.
<https://ir.lib.uwo.ca/etd/9316>

This Dissertation/Thesis is brought to you for free and open access by Scholarship@Western. It has been accepted for inclusion in Electronic Thesis and Dissertation Repository by an authorized administrator of Scholarship@Western. For more information, please contact wlsadmin@uwo.ca.

Abstract

A critical step for the synthesis of renewable oxy methyl ethers (OME) targeted towards diesel substitution, is the catalytic production of a dimethoxymethane/formaldehyde mixture from methanol and air. The bifunctional catalyst requirements needed for methanol to undergo both the acidic and oxidative steps required for dimethoxymethane formation have been recently established for TiO₂-supported vanadia catalysts. However, translating these requirements to a catalyst capable of industrial operation remains a challenge. This thesis examines the considerations and adjustments needed to translate the molecular active phase to a large-scale catalytic pellet, including active phase distribution and possibility of hot-spot creation during catalysis. Multiple formulations are explored to evaluate the consequences on catalytic performance of systematic changes on vanadia dispersion as well as its distribution throughout the solid catalyst pellet. By controlling the distribution of vanadia, we constrained undesirable pathways in the reaction maximizing dimethoxymethane production; however, formaldehyde production was still slightly limited.

Keywords

Catalysis, reaction engineering, dimethoxymethane synthesis, vanadium oxide and titanium oxide, atomic layer deposition, catalyst scale-up

Summary for Lay Audience

Bio-derived oxy methyl ethers (OMEs) have the capacity to partially substitute diesel fuels providing an additional sustainable additive to transportation fuels, similar to the role ethanol plays in gasoline. A key starting stage in the manufacturing process of OMEs molecules is reacting a pure methanol gas stream with air to create an intermediate stream of dimethoxymethane (DMM) and formaldehyde, which can then be used for OME production. Methanol transformation to DMM and formaldehyde can be accomplished in a single step by exposing methanol to material that can speed up a process that involves both proton (acid reaction) and electron exchanges (redox reaction) between the molecules of methanol and air. This type of material is known as a bifunctional catalyst. Current work done on catalysts able to carry these transformations is conducted at the microscale, using milligram amounts of catalyst in laboratories, focusing on designing the molecular structure of the catalyst. For industrial operation to be realized, the size of the catalyst material must be scaled up. Scaling up requires in turn that the material preserves its original catalytic properties, but also that the material can offer performance levels required to handle industrial amounts of feedstock.

This thesis attempts to bridge the gap between the knowledge of the molecular structure required to produce DMM and the general industrial requirements for a scaled-up version of the catalyst and combine them to establish a protocol for the preparation of a catalyst capable of industrial production of an OME feed stream comprised of DMM and formaldehyde. To accomplish this several formulations of catalyst pellets were prepared, evaluated, and tested with altered molecular structures and/or altered distribution of catalytic material throughout the pellet. Altering the distribution of the catalytic phase through the pellet had a significant effect on the reaction as pellets with less vanadium available in the material core resulted in an increase on the production of unwanted side products. By improving the distribution of the catalytic phase material, the sites identified to be responsible for methyl formate production were covered. However, undesired by-products began to be produced via alternative routes.

Co-Authorship Statement

This thesis was written in accordance with the guidelines for an Integrated Article specified by the School of Graduate and Postgraduate Studies at the University of Western Ontario.

The candidate is responsible for the collection and analysis of numerical and laboratory data and drafting all chapters of this thesis. Dr. José Herrera provided initial motivation for this research, assisted with designing laboratory experiments, provided analysis for the resulting data, and provided revisions of this thesis. The co-authorship breakdown of this Thesis is as follows:

Authors: Sebastian Cook, José Herrera

Contributions:

Sebastian Cook conducted laboratory experiments, data analysis, and was the lead author for this thesis providing the initial document upon which he and Dr. José Herrera jointly revised.

Dr. José Herrera supervised the laboratory experiments, provided insight for the results, and reviewed and revised the draft document of this thesis with Sebastian Cook.

Acknowledgments

First, I would like to thank my supervisor, Dr. José Herrera, without whose guidance and mentorship I would not have been able to write this document. I am incredibly appreciative of all the support he has provided me since my 2nd year of undergraduate studies, allowing me to reach my academic potential. Words cannot begin to describe how grateful I am for everything Dr. Herrera has done for me so I hope this tiny blurb can suffice and do some justice.

Next, I would like to extend my thanks to my research group: Wei Tian for showing me the “ropes” of graduate studies; Andrés Rodrigues for helping me navigate post-grad academia; Adam Schubert for always being willing to lend a hand; our summer students Greg Dietrich, Ryan Alfonso, and PC Ascherl whose assistance was invaluable; and finally, Adrian Hucal who I am happy to call a colleague and a friend.

My deepest gratitude is also extended to William Broomhead, Dr. Cathy Chin, and the rest of her research group at the University of Toronto. They were gracious enough to host and allow me to use their equipment to run several crucial experiments for this thesis as well as taking the time to run additional tests required.

I would also like to thank Josh Laughton for his assistance and guidance in obtaining the WDS scans used throughout this paper and to the group at Surface Science Western for their guidance in obtaining distribution maps for my samples.

I would like to express my undying appreciation to my girlfriend, Andie Micheli, whose love and support helped keep me sane throughout the writing process and who always brings out the best in me.

Finally, I would like to thank my family and friends for their unwavering support and for always being there for me, allowing me to accomplish anything I set my mind to. I truly could not have done any of this without you.

Table of Contents

Abstract.....	ii
Summary for Lay Audience.....	iii
Co-Authorship Statement.....	iv
Acknowledgments.....	v
Table of Contents.....	vi
List of Tables.....	ix
List of Figures.....	x
Chapter 1.....	1
1 Background Information.....	1
1.1 Oxymethylene Ethers as a Carbon-Neutral Fuel Source.....	1
1.2 Thesis Outline.....	2
Chapter 2.....	4
2 Literature Review.....	4
2.1 Dimethoxymethane and Oxymethyl Ethers as a Renewable Fuel Source.....	4
2.2 Longer Chain OMEs Production.....	5
2.3 Current Industrial Dimethoxymethane Production.....	10
2.4 Reaction Network for Dimethoxymethane (DMM) Production.....	12
2.4.1 Indirect DMM Synthesis Reaction Network.....	14
2.4.2 Direct DMM Reaction Network.....	16
2.5 One-Step Direct Dimethoxymethane Production.....	18
2.6 Catalysts for Direct DMM Production.....	20
2.6.1 Unsupported Catalysts.....	21
2.6.2 Supported Catalysts.....	23
2.6.3 Titanium Supported Vanadium Catalysts.....	27
2.7 Industrial Catalyst Production Methods.....	31

2.7.1	Different Preparation Methods for Industrial Catalysis.....	33
2.7.2	Integrating Industrial Catalysis with DMM Production	40
Chapter 3.....		42
3	Design and Structure/Activity Relationships in Catalytic Pellets hosting the VO _x /TiO ₂ System for Oxymethylene Production.	42
3.1	Materials and Methods.....	42
3.1.1	Materials and Catalyst Preparation using Wetness Impregnation	42
3.1.2	Materials and Catalyst Preparation for ALD Catalysts.....	44
3.1.3	Evaluation of Titania and/or Vanadia Incorporation	47
3.1.4	Catalytic Activity Testing.....	48
3.2	Results Obtained on Initial Catalyst Formulations	52
3.2.1	Introduction.....	52
3.2.2	1 st Generation Catalyst: “Proof-of-Concept” and Testing	56
3.2.3	Catalyst Characterization Results	56
3.2.4	Catalyst Activity Evaluation.....	62
3.2.5	Interaction of the Vanadium Impregnating Complex with the Titania Pellet	65
3.3	Effect of Impregnation Time on the Impregnation Depth of the Vanadia Phase .	71
3.3.1	Introduction.....	71
3.3.2	Characterization Results of the Catalyst.....	72
3.4	Control of Vanadium Penetration by Weakening the Support Interaction	74
3.4.1	Introduction.....	74
3.4.2	Characterization Results	75
3.4.3	Catalytic Activity	77
3.4.4	Discussion.....	82
3.5	Utilizing ALD to Address the Shortcomings of Previous Catalyst Iterations	87
3.5.1	Introduction.....	87

3.5.2	Depositing Titania onto SiO ₂	87
3.5.3	Wetness Impregnation of Vanadium onto Ti/Si	92
3.5.4	Discussion	95
3.5.5	ALD Impregnation of Vanadium onto TiO ₂ /SiO ₂	98
Chapter 4	109
4	Conclusions and Recommendations	109
4.1	Conclusions and Summary	109
4.2	Direction for Future Work	110
References	112
Appendices	122
Appendix A:	Large-Scale Catalytic Testing Experimental Setup.....	122
Appendix B:	Determining Mass and Heat Transfer Limitations using Calculations.	122
Curriculum Vitae	126

List of Tables

Table 2-1 Conversions and Selectivity towards DMM for Select Metal Oxide Catalysts	21
Table 2-2 Overview of Different Catalyst Preparation Technique	33
Table 3-1 List of Wetness Impregnation Catalysts Prepared and Formulation Conditions ...	44
Table 3-2 List of ALD Catalysts Prepared and Formulation Conditions	46
Table 3-3 Thermodynamic Limitations for Methanol/Formaldehyde Acetalization if System Approaches Equilibrium	49
Table 3-4 Catalytic Activity for Vanadium Free Ti/Si Pellet and Ti Pellet in Large-Scale Reactor	90
Table 3-5 Catalytic Activity for Vanadium Free Ti/Si Pellet and Si Pellet on a Differential Reactor	91
Table 3-6 UV Bandgap at Different Sections of V-ALD/Ti/Si Pellets	99

List of Figures

Figure 2-1 Molecular Structures of DME, DMM, and OME _n	4
Figure 2-2 Proposed Eley-Rideal Mechanism for Chain Growth of OMEs.....	6
Figure 2-3 PFD of a Long Chain OME Production Scheme using Current Industrial Technology	8
Figure 2-4 PFD of the Proposed Long Chain OME Production Scheme using One-Step DMM Synthesis	9
Figure 2-5 OME _n Production Pathways from Methanol via Direct and Indirect Synthesis ...	13
Figure 2-6 Formaldehyde Production via the Mars-van Krevelen Cycle using a Hexavalent Metal Oxide as Example.....	15
Figure 2-7 Reaction Network showing Methyl Formate Production from Formaldehyde during DMM Production.....	18
Figure 2-8 Reaction Network for One-Stage DMM Synthesis Illustrating Oxidative and Acidic Pathways.....	19
Figure 2-9 Raman Spectra of Various Loadings of Fe:Mo on SiO ₂	24
Figure 2-10 Effect of Support Material on the Rate of Oxidative Dehydrogenation and Reducibility of RuO ₂	26
Figure 2-11 Amount of V-O Bonds Present in Different Vanadium Structures	28
Figure 2-12 Effect the Number of V-O-V bonds has on the Bandgap Energy of the Surface for Supported V/Ti Structures and Crystalline Vanadium Structures.	29
Figure 2-13 Effect of the O ^I and O ^{II} Coordination on the C-H Bond Scission Rate and the Methanol Adsorption Constant	30
Figure 2-14 Interconnectivity of the Considerations for Catalyst Design and Scaling Up	32

Figure 2-15 Different Active-Phase Distributions for Large-Scale Catalysis	36
Figure 2-16 ALD mechanism and Process for Titanium Tetraisopropoxide Deposition	39
Figure 3-1 Experimental System used for Atomic Layer Deposition of Metal Oxide Phases on Solid Pellets	45
Figure 3-2 Different Vanadium Dispersions on Titania Surface	53
Figure 3-3 Supported Vanadia UV Bandgap vs Cluster Size with Vanadium Dispersions ...	54
Figure 3-4 UV Bandgaps and Transformed UV Spectra for Powdered Catalyst Samples.....	55
Figure 3-5 UV Spectra of 5% V-WI _(EtOH) /Ti and 2% V-WI _(EtOH) /Ti	57
Figure 3-6 Optical Pictures of Typical 5% V-WI _(EtOH) /Ti Pellet and UV Bandgap at Cross- Section.....	58
Figure 3-7 WDS Mapping of Vanadium on the Cross-Section of the 5% V-WI _(EtOH) /Ti Catalyst Pellet	59
Figure 3-8 XRD Data for a 5% V-WI _(EtOH) /Ti Pellet after Calcination	60
Figure 3-9 FT-IR Spectra of Pure V ₂ O ₅ , blank TiO ₂ Pellet, and 5% V-WI _(EtOH) /Ti Sample..	61
Figure 3-10 Catalytic Activity for V-WI _(EtOH) /Ti Catalysts at Two Space Velocity Conditions	63
Figure 3-11 UV Data Obtained on the Vanadium Precursor Solution at each Impregnation Stage.....	68
Figure 3-12 Effect of Impregnation Time on UV Bandgap and Vanadium Dispersion	72
Figure 3-13 Vanadium WDS Scans of 5% V-WI _(EtOH) /Ti and 5% V-WI _(EtOH) /Ti-46 Days....	73
Figure 3-14 Optical Pictures of the 5% V-WI _(Aq) /Ti Pellet's Cross-Section	76
Figure 3-15 WDS scans of 5% V-WI _(EtOH) /Ti and 5% V-WI _(Aq) /Ti	76

Figure 3-16 Bandgap Energy Gradient throughout the 5% V-WI _(Aq) /Ti Pellet	77
Figure 3-17 Catalyst Activity Data for the 5% V-WI _(Aq) /Ti Sample at Two Space Velocity Conditions	78
Figure 3-18 Effect of Crushing Pellet on Catalytic Activity	81
Figure 3-19 Titanium Distribution through Silica Pellet after ALD.....	88
Figure 3-20 Comparison of Silicon and Titanium Distributions showing Signal Artefacts of a Pellet after ALD	89
Figure 3-21 Vanadium Distribution for 0.5% V-WI _(EtOH) /Ti/Si Sample.....	93
Figure 3-22 Catalyst Activity Data for the 0.5% V-WI _(EtOH) /Ti/Si Sample ¹	94
Figure 3-23 Vanadium WDS Scans of 8% V-ALD/Ti/Si and 11% V-ALD/Ti/Si.....	99
Figure 3-24 Catalytic Activity for V-ALD/Ti/Si Catalysts at Two Space Velocity Conditions	101
Figure 3-25: Rates of Formation for Different Products in a Pure Formaldehyde and Formaldehyde/Methanol Feed	104
Figure 3-26 Relationship between Methyl Formate Rate and Exposed Titania	107
Figure A-1: P&ID Diagram of Large-Scale Experimental System	122
Figure A-2 Weisz-Prater Criterion for 5% V-WI _(Aq) /Ti Sample at 50 SCCM.....	124

Chapter 1

1 Background Information

1.1 Oxymethylene Ethers as a Carbon-Neutral Fuel Source

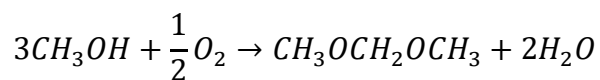
With the goal of curtailing the impact of greenhouse gas emissions on the climate, the 2015 Paris agreement imposed a limit to the global temperature rise of 1.5°C from pre-industrial levels (Rhodes, 2016). After almost 8 years since the Paris Agreement, despite progress, countries are still heavily reliant on fossil fuels for energy, and emissions consistently keep increasing (International Energy Agency, 2022). The transportation sector accounts for a quarter of the total energy demand which is largely met by consuming non-renewables such as oil (International Energy Agency, 2022). As such, renewable fuel insertion in the transportation sector has been targeted as a strategy to significantly reduce global emissions. While electric vehicles are currently a popular solution to lower these emissions, there are multiple logistical issues such as supply of rare-earth metals for battery production that make this technology difficult to implement globally (Pavid, 2016). Therefore, other options for fueling transportation which are not only able to meet the large energy demand required by society but also able to significantly reduce the current level of carbonemissions, must be formulated.

Biofuels have long been thought of as an alternative to fossil fuels as any carbon dioxide emissions derived from their combustion would be recaptured when the biomass regrows (Demirbas, 2007). One such biofuel, which has high promise as diesel fuel alternative, is oxymethylene ethers (OMEs) derived from bio-methanol (Sun et al., 2019).



This is due to OMEs only containing C-O bonds, resulting in low soot formation, and the easy blending capability that higher chain OMEs have with diesel (Burger et al., 2010). To industrially produce OMEs with a molecular weight in the range of diesel fuel, a crucial starting point is the synthesis of the simplest molecule in the OME family: dimethoxymethane (DMM also known as OME₁) (Sun et al., 2019). However, current

industrial practices for producing this molecule are hazardous and costly due to the liquid acid catalyst that is required (Thavornprasert et al., 2016), as well as the use and handling of formaldehyde derivatives. These issues can be solved using a direct synthesis route where methanol forms DMM in the gas phase in a single process, while also significantly reducing the amount of stage operations required (Sun et al., 2019):



This process requires a catalyst that possesses both a redox capability and acidic sites. While many studies have looked for the optimum catalyst formulation for direct synthesis of DMM from methanol, few have examined incorporating this synthesis into an industrial process, especially one optimized for longer chain OME production downstream (Broomhead et al., 2022). In an effort to bridge this gap, we have studied the catalytic scale-up (from powder to 1/8" pellets) of vanadium (V) oxide deposited on a titanium dioxide support as a catalyst for the direct production of DMM from methanol. By manufacturing multiple catalyst formulations with altered preparation procedures, an extensive roster of catalysts, capable of producing DMM, were obtained. Along with catalytic activity tests, these catalysts were characterized using UV-Vis, XRD, FT-IR and WDS to link the structure of the active-phase and support with the catalyst's oxidative and acidic capabilities, rationalizing the catalyst structure impact on catalyst performance. Using these techniques, we found that the two-dimensional distribution of the active phase on the catalyst pellets is critical to address mass-transfer limitations and non-isothermal temperature profiles taking place on the catalytic pellet. These characteristics are normally not addressed on kinetic studies in lab-scale experiments but are critical considerations for catalyst scale up to industrial applications. Without these considerations, mechanisms which form unwanted side-products take precedence in the reaction scheme and limit the useful product yield.

1.2 Thesis Outline

Chapter 1 provides the reader with context for the work as well as an outline for the structure of the thesis. Chapter 2 is an encompassing literature review looking at the dimethoxymethane reaction kinetics and synthesis scheme, dimethoxymethane

production methods, longer oxy-methyl ether chain production, and methods and considerations for industrial production of heterogenous catalysts. Chapter 3 describes the experimental methodology and presents the results and discussion of these results. Finally, the work is summarized in key conclusions that can be drawn from this research in Chapter 4. This Chapter also provides recommendations for future work to further the understanding of the subject matter.

Chapter 2

2 Literature Review

2.1 Dimethoxymethane and Oxymethyl Ethers as a Renewable Fuel Source

Dimethoxymethane (DMM) did not see significant industrial interest until the 19th century when it was used primarily as a solvent (Weaver et al., 1951). Today it has a wide array of industrial applications, from polymer manufacturing to pharmaceuticals production (Peláez et al., 2021). DMM was initially considered as a potential diesel fuel additive to combat particulate release, which are hazardous to human health, commonly found in diesel emissions (Maricq et al., 1998). This strategy was supported by several studies showing a significant reduction of particulates using a similar molecule, dimethyl ether (DME), as a diesel additive (Sorenson et al., 1998). While successful at reducing particulates, dimethyl ether is a gas at room temperature and as such significant changes to infrastructure and engine modifications are required to incorporate its use in diesel engines (Maricq et al., 1998). On the other hand, dimethoxymethane is a liquid with similar cetane ratings to diesel and has the carbon-oxygen bond structure found in DME, potentially providing similar particulate reductions with little impact to engine operation and the fuel distribution chain. The structures of DME and DMM as well as longer chain oxy methyl ethers (OMEs) are given below in Figure 2-1.

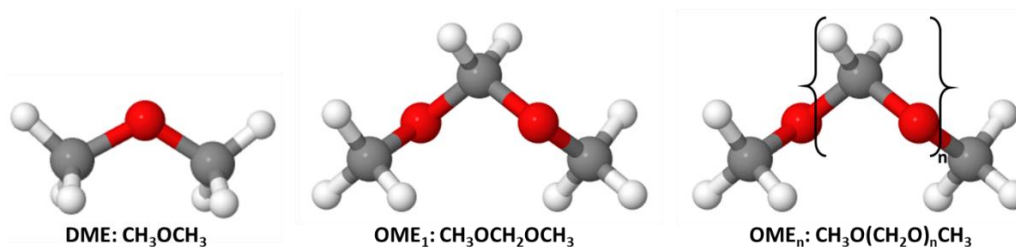


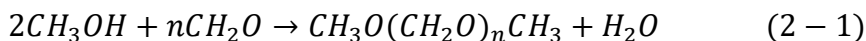
Figure 2-1 Molecular Structures of DME, DMM, and OME_n (from left to right) Grey: Carbon, White: Hydrogen, Red: Oxygen

In a study by Vertin et al. DMM was found to significantly reduce the particulate emissions when blended with diesel; however, they found DMM was more volatile than

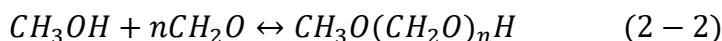
diesel leading to safety concerns (1999). Longer chain OMEs have significantly higher flash points and maintain a similar safety standard to diesel (Omari et al., 2019). Ultimately a mixture of OMEs primarily consisting of chain lengths from 3-5 were found to have properties most consistent with diesel fuel: this mixture could be easily blended with diesel and have a sufficiently low freezing point compared with longer chain lengths (Omari et al., 2019). The reinvigorated interest into these molecules as a fuel has largely come from the idea that the starting point for DMM (which itself is the starting point for larger OMEs) is methanol, which has experienced a significant market shift since methanol can now be obtained from renewable pathways (Schmitz et al., 2016). The current scheme for OMEs production will be examined in the next section.

2.2 Longer Chain OMEs Production

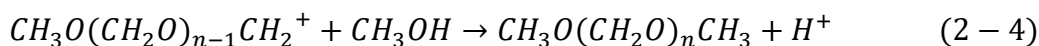
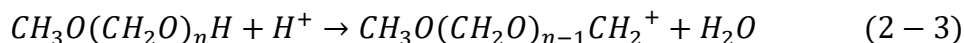
The reaction that leads to formation of OME_n ($2 < n < 6$) can be depicted as formaldehyde oligomerization, capped at both ends by methoxy units and is depicted in Equation 2-1.



This oligomerization step (i.e., formation of the C-O-C chains) occurs in two stages. The first is the formation of a hemiformal molecule given below in Equation 2-2.



This first step happens spontaneously in solution and does not require a catalyst, however; the process is reversible since the hemiformal is highly unstable and readily reforms to methanol and formaldehyde (Baranowski et al., 2017). The second stage requires a catalyst with an acidic function, to enable the final acetalization step between a molecule of methanol and the hemiformal which is illustrated below in Equations 2-3 and 2-4. It should be noted that in the case of a solid acid catalyst, the proton is provided by a hydroxyl group on the surface with the formed carbocation adsorbing to the catalyst thus stabilizing the molecule.



Due to the higher boiling points of the OME_n products obtained, the reaction is carried in the liquid phase and is equilibrium limited (Burger et al., 2010). Experimentally, the process has been assessed using different starting sources for formaldehyde such as trioxane, paraformaldehyde, and formalin, as well as different initiators such as DMM and methanol (Baranowski et al., 2017). A few studies have reported the use of dimethyl ether (DME) as the monomer source, but in those cases the largest molecule obtained was OME_2 (Zhang et al., 2014, Zhang et al., 2016).

The mechanism for OME_n chain growth from formaldehyde is still under debate. There is some disagreement in terms of the specific pathway for C-O-C-O bond formation. Two different pathways have been proposed (Baranowski et al., 2017). Some studies have proposed an Eley-Rideal mechanism where formaldehyde adsorbs and reacts with OME_n chains further increasing the chain length (Wu et al., 2015; Zheng et al., 2013; Zheng et al., 2015). This mechanism is given below in Figure 2-2.

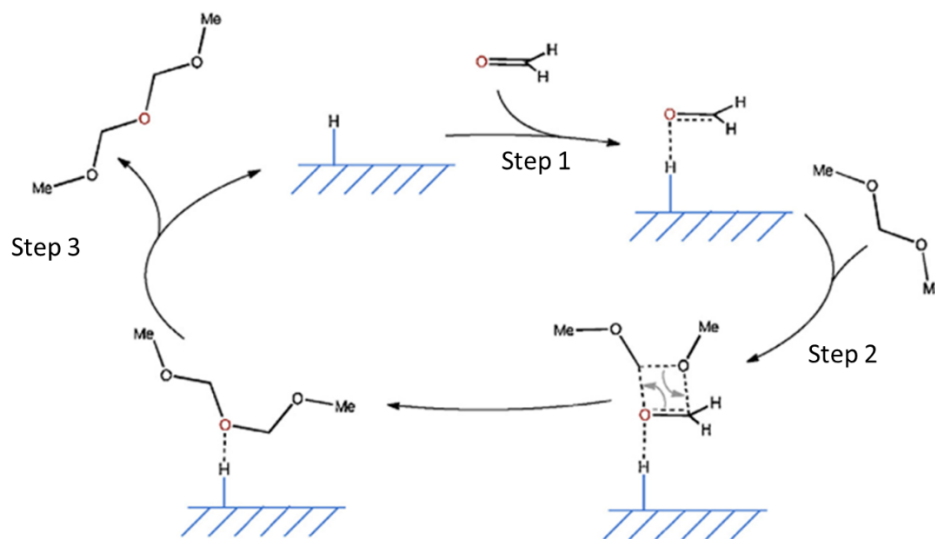
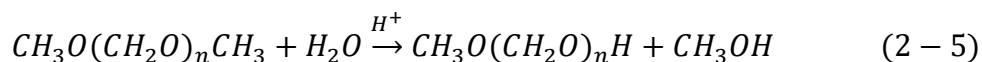


Figure 2-2 Proposed Eley-Rideal Mechanism for Chain Growth of OMEs adapted from Baranowski et al., 2017

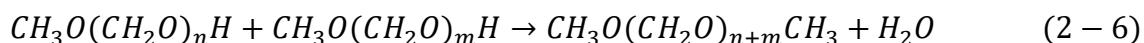
This chain-growth mechanism can be broken down into three distinct steps. The first step (step 1) involves the formaldehyde adsorbing to a Brønsted acid on the catalyst surface (Wu et al., 2015). The next step (step 2) involves an OME_n chain (pictured as DMM in

Figure 4) interacting with this adsorbed formaldehyde and forming a new intermediate (Wu et al., 2015). This intermediate decomposes to OME_{n+1} (step 3) releasing the Bronsted site (Wu et al., 2015). It is important to mention that this mechanism neglects the role of hemiformals in the chain growth process. Indeed, it has been reported that hemiformals could form during the chain growth process, forming via the hydrolysis of formed OME_n molecules in the presence of an acid, shown in Equation 2-5 (Klokic et al., 2020).



Once these hemiformals form they begin to spontaneously decompose to lower hemiformals due to equilibrium limitations, following the reverse process depicted in Equation 2-2; this ultimately leads to higher selectivity of smaller OME chains (Klokic et al., 2020). Smaller OME chains are favoured due to instability of the intermediate necessary to increase the chain length grows (Wang et al., 2015). Alternatively, these hemiformals can be capped with methanol and reformed into OME_n through an alternative mechanism described in detail below.

In addition to the chain growth mechanism proposed for solid-acid catalytic systems, homogenous systems have several termination mechanisms. Hemiformals or carbocations are formed in solution and are grown with additional formaldehyde molecules before being capped to form an OME chain. The capping method either occurs when methanol reacts with a long chain hemiformal to produce a larger OME molecule (Equations 2-3 and 2-4 happening simultaneously) or two hemiformals undergo a condensation reaction to produce a longer OME chain (Equation 2-6) (Zhang et al., 2014). Some reports indicate, that in the presence of a homogenous acid catalyst, it is possible for carbocations that are formed in Equation 2-3 to be stabilized in solution, allowing them to later directly react with methanol to cap the OME molecule (Equation 2-4) (Baranowski et al., 2017).



The processes described above implicitly delineate the need to have both formaldehyde and methanol fed into a reactor if OME_n is to be produced. Moreover, there is a clear need to have an excess of formaldehyde as the length of the desired OME chain grows. An

excess of water is also required along with this formaldehyde to prevent formaldehyde polymerization (Millar and Collins, 2017). Typical formaldehyde synthesis processes (FORMOX®) include water as steam before synthesis and as an additive after reaction to produce the formalin solution (Bahmanpour et al., 2014; Thrane et al., 2021). As OME_n synthesis is severely equilibrium limited, the presence of excess water negatively impacts the yield of OME_n (Schmitz et al., 2015). Figure 2-3 provides a process flow diagram (PFD) of the current industrially proposed methods to form OME_{3-5} .

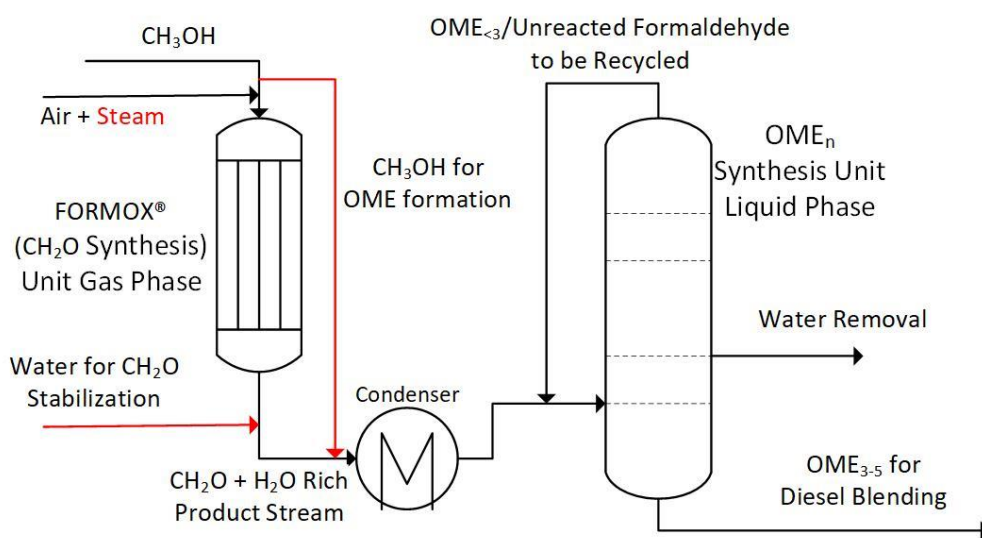


Figure 2-3 PFD of a Long Chain OME Production Scheme using Current Industrial Technology. FORMOX® Process based upon work from Bahmanpour et al., (2014) and OME_n unit proposed by Lautenschütz et al., (2017). Streams that could be removed by using one-stage DMM synthesis are highlighted in red

Alternative pathways limiting the amount of water in the reactant stream could be beneficial. For instance, an OME_n synthesis using OME_1 (DMM) as a starting material rather than methanol, would allow for interstage water removal. The ideal case could be to combine the feedstock resulting from a DMM (OME_1) synthesis unit (obtained in turn from methanol and air reacting together to produce DMM and formaldehyde) into a

single reactor. If the yields of DMM and formaldehyde on the first stage are carefully tuned, there may no longer be a need for cofeeding additional formaldehyde, as shown in the process flow diagram below (Figure 2-4).

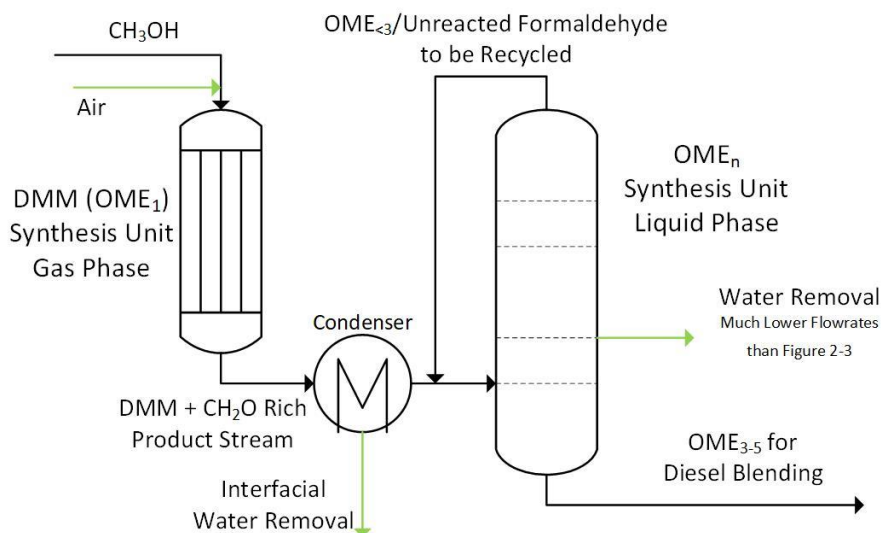


Figure 2-4 PFD of the Proposed Long Chain OME Production Scheme using One-Step DMM Synthesis. Benefits highlighted in green

When examining the ideal feedstock composition required to maximize the desirable cut of OME chains for diesel blending, two parameters are of critical importance: the DMM to formaldehyde ratio obtained in the first stage and the amount of water generated during this stage. Water, which is the coproduct in the DMM synthesis reaction, significantly limits the yield of longer OME chains (Schmitz et al., 2015; Klokic et al., 2020). This is due to the OME_n chain growth reaction being equilibrium limited, i.e., the presence of water favours the reactant side of the equation. As such water removal may need to occur after DMM synthesis to increase the yield of OME₃₋₅. This demonstrates the potential benefit of using DMM over methanol as a starting point for longer OME chain synthesis. By using DMM over methanol the amount of water in the oligomerization reactor may be limited by easily separating the formed water from the DMM and formaldehyde mixture after the first stage as shown in Figure 2-4. Ultimately a complete technological

assessment would need to be performed to evaluate the process economics and determine the extent or presence of any improvements using the scheme in Figure 2-4 vs that in 2-3; however, this is outside the scope of this thesis.

Burger et al. (2010). found that when the DMM to trioxane (used as formaldehyde precursor) ratio decreased, the fraction of OME₂ obtained in the reactant mixture decreased, favoring those of larger ($n > 2$) OME_n products. However, the smallest DMM to trioxane mass ratio that was assessed was 2:1 (equivalent to a 2:3 mass ratio DMM to formaldehyde). A more recent study, carried in a batch reactor, achieved mass yields of ~30% OME₃₋₅ when the molar ratio of DMM to formaldehyde was near 1:1 (Lautenschütz et al., 2017). These values were near the theoretical equilibrium and as such represent the maximum yield attainable in a single pass (Lautenschütz et al., 2017). This data illustrates the ideal feed composition for a potential OME₃₋₅ oligomerization reactor. As such a 1:1 DMM to formaldehyde ratio in the stream obtained from a methanol to DMM reactor (stage 1) provides the best starting point for a downstream oligomerization unit. In other words, a reactor unit that maximizes the selectivity to DMM at the expense of formaldehyde is not desirable if the overarching process targets the production of OME_n mixtures. Since DMM synthesis is crucial to the synthesis of longer chain OMEs this will be examined further in the next section.

2.3 Current Industrial Dimethoxymethane Production

As outlined above, the synthesis of diesel alternative OME mixtures can be largely simplified if DMM is used as starting material. Currently DMM is produced industrially using a two-stage process which separates the oxidative and acid reactions into two separate units (Thavornprasert et al., 2016). The first unit carries the oxidation of methanol to formaldehyde. This is an industrially mature process due to formaldehyde being an essential building block chemical (Zhang et al., 2018). While both silver and iron-molybdate based catalysts are used industrially to produce formaldehyde from methanol, iron molybdate was quickly adopted by commercial facilities in the 1950s and has become the preferred catalyst due to lower reaction temperatures and longer catalyst stability (Andersson et al., 2016; Soares et al., 2005).

Industrial formaldehyde production using iron-molybdates occurs in a multi-tubular reactor in order to minimize any temperature increase profile that is created due to the exothermic nature of the reaction (Thrane et al., 2021). The heat removed from the reactor is then used to evaporate and preheat the incoming feed (Thrane et al., 2021). Reactor temperatures are kept below 673K with an excess of oxygen used to dilute the methanol feed between 6-10% (by volume) to keep the reaction mixture below the explosive limit for methanol while also ensuring maximum methanol conversions (Thavornprasert et al., 2016; Andersson et al., 2016).

The second stage of the industrial DMM process starts after the formaldehyde is produced. The products obtained from the methanol partial oxidation (formaldehyde and water) are cooled down to form an aqueous solution to which more methanol is added (Sun et al., 2019). This liquid mixture undergoes a reaction using a liquid acid catalyst, such as sulfuric acid, to form DMM (Sun et al., 2015). There are many issues with using sulfuric acid, including recovery, corrosion, and environmental impact (Thavornprasert et al., 2016; Sun et al., 2015). As such there has been an effort to substitute the homogenous liquid catalyst with solid acid catalysts or ionic liquids to minimize the drawbacks of the process. Ionic liquids have been tested as an alternative and are able to achieve high conversions and selectivity (at bench scale) while also improving on recyclability, but are hampered by significantly higher cost (Sun et al., 2015).

Schemes using solid acid catalysts have also been developed. Typically, these solid catalysts are combined with the distillation unit, thus performing reactive distillation: separating and forming DMM at the same time, which helps overcome the thermodynamic equilibrium limitations (Sato and Tanigawa; 1999; Masamoto et al., 1989; Sun et al., 2019). However, if a DMM purity above 93% is required further process units are required due to an azeotropic mixture of DMM and methanol being formed (Sun et al., 2019). Unfortunately, compared to homogenous processes, issues persist due to lower catalytic activity and lower catalyst lifespans, making sulfuric acid the only viable industrial alternative at this point (Masamoto et al., 1989; Sato and Tanigawa; 1999; Sun et al., 2015).

Besides formaldehyde, other feedstocks can be used in presence of an acid catalyst, which eliminates the need for the first stage (methanol oxidation). These include using trioxane as a formaldehyde source in conjunction with DME (Schmitz et al., 2015; Breitkreuz et al., 2022). As these feedstocks are significantly more expensive than methanol, they have not been significantly explored as they pose little economic viability for an industrial process. All potential pathways for DMM synthesis from methanol will be further explored in the next section.

2.4 Reaction Network for Dimethoxymethane (DMM) Production

As discussed in Section 2.2, there are two distinct production routes to form longer chain OMEs from methanol and formaldehyde, and all of them involve DMM as an intermediate. These production routes are classified in terms of either having methanol initially converted exclusively to formaldehyde or if the methanol is first directly converted into a mixture of DMM (OME_1) and formaldehyde. The first route, as reported in the previous section, involves an indirect synthesis pathway where methanol is first reacted to form formaldehyde in the gas phase. This formaldehyde is then condensed and mixed with more methanol to form DMM and longer chain OMEs in a liquid system in the presence of a homogenous acid catalyst. The direct route involves methanol being reacted to form DMM in the gas phase. The DMM then is condensed and combined with formaldehyde (from the previous reaction or a formaldehyde precursor) to form longer OME chains in an acidic environment. These synthesis routes are illustrated in Figure 2-5 below. Note that for the indirect pathways OME_n is listed as the final product; this can be substituted for $n = 1$ for DMM synthesis.

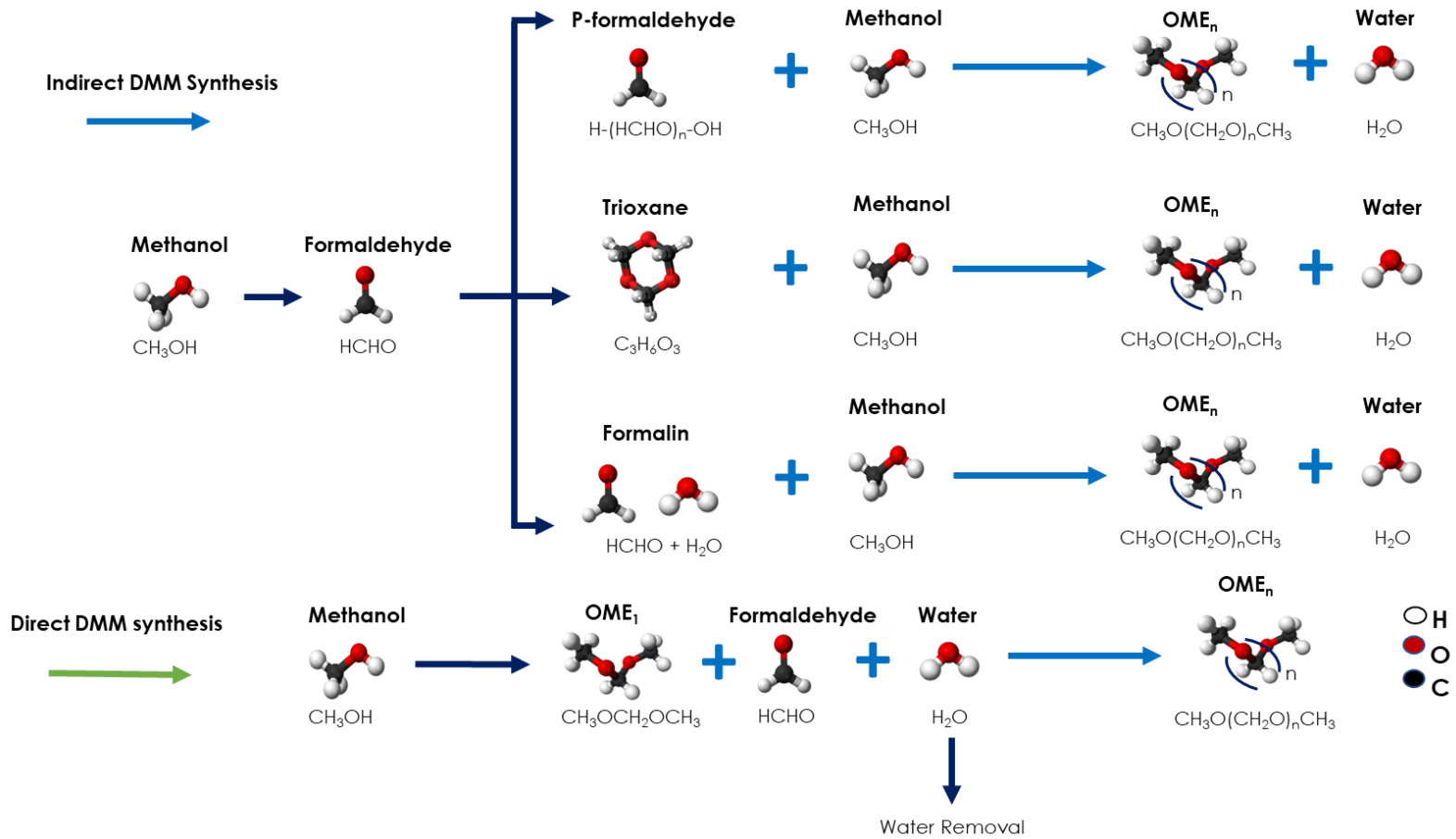
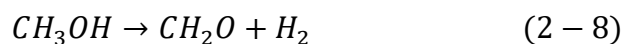
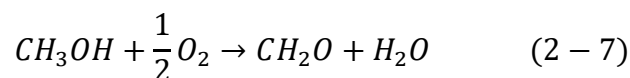


Figure 2-5 OME_n Production Pathways from Methanol via Direct and Indirect Synthesis

2.4.1 Indirect DMM Synthesis Reaction Network

The first step in the indirect synthesis of DMM is an oxidation step wherein methanol is oxidized to formaldehyde. Currently two different reaction pathways are used to produce formaldehyde, the direct dehydrogenation of methanol and the partial oxidation of methanol (Bahmanpour et al., 2014). The stoichiometries of these respective reactions are given below in Equations 2-7 and 2-8. The direct dehydrogenation of methanol is an endothermic pathway only seen at high temperatures in tandem with the oxidative pathway (Bahmanpour et al., 2014). As mentioned previously industrial formaldehyde production is trending towards exclusively utilizing the partial oxidation route (Bahmanpour et al., 2014). As such this thesis will not explore this direct dehydrogenative route (Equation 2-8) as the partial oxidative pathway is much more relevant within the scope of the work presented here.



The reaction given by Equation 2-7 utilizes the partial oxidation pathway in a catalytic route typical of Mars-van Krevelen cycles (Soares et al., 2005). The Mars-Van Krevelen cycle involves the oxidation of a chemical species through abstraction of an oxygen atom from a metal oxide species (Doornkamp and Ponc, 2000). The reduced metal oxide is then re-oxidized by a gas phase oxidant. As such the kinetics of the reaction can be described as a two-step process. In the first step, the adsorbed methanol experiences C-H scission, which is the rate-limiting step, creating formaldehyde (Soares et al., 2005). This formaldehyde desorbs along with water, leaving behind a reduced catalytic center that is re-oxidized by oxygen in the second step (Soares et al., 2005). This mechanism is illustrated for the methanol to formaldehyde reaction below in Figure 2-6.

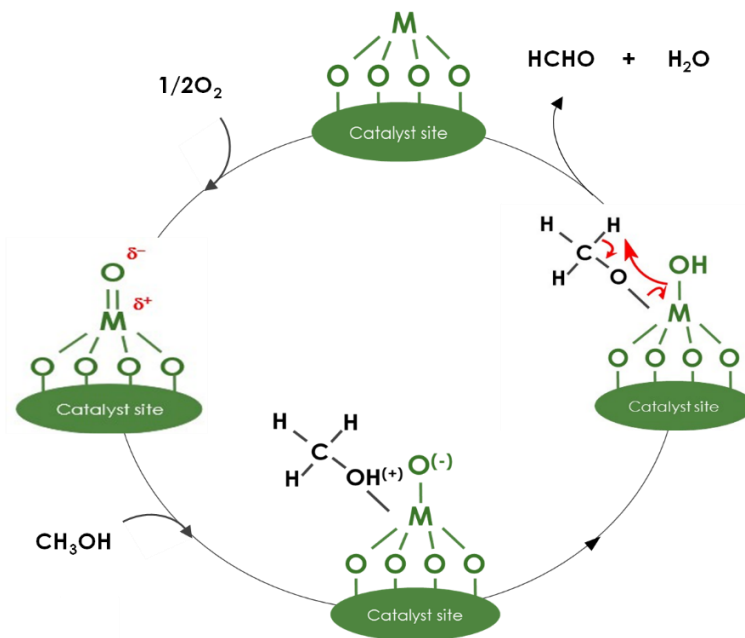
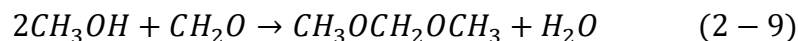
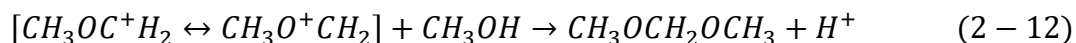
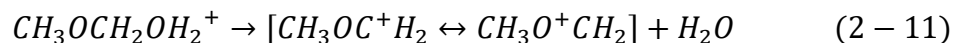
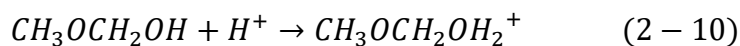


Figure 2-6 Formaldehyde Production via the Mars-van Krevelen Cycle using a Hexavalent Metal Oxide as Example

After completion of the oxidation step, the newly formed formaldehyde is combined with a methanol stream to react in a homogenous liquid reactor to form a DMM molecule. As with longer OME chain synthesis, the acetalization to form DMM is an equilibrium limited reaction (Sun et al., 2019). The stoichiometry for this acetalization step for DMM, is given below in Equation 2-9.



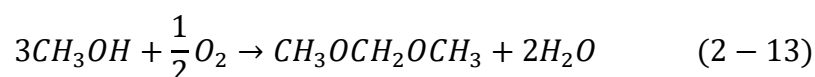
This follows a similar mechanism to longer chain OME production given in Section 2.2. Industrially the indirect synthesis is conducted as a liquid phase reaction, its mechanism will now be discussed. The first step is the spontaneous forming of a hemiformal molecule from one molecule of methanol and formaldehyde similar to that presented in Equation 2-2 but where $n=1$ (Sun et al., 2019). The next step is the rate-limiting step and involves methanol combining with a hemiformal to form DMM (Sun et al., 2019) This occurs over several steps given below in Equations 2-10 through 2-12 (Kolah et al., 1996).



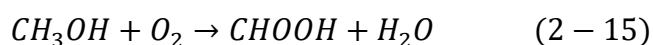
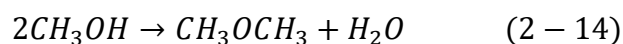
The first step requires the hemiformal to react with a proton in solution which initiates a carbocation to be formed (Equation 2-10) (Kolah et al., 1996). Afterwards, the carbocation is stabilized from removal of a water molecule (Equation 2-11) (Kolah et al., 1996). The final step has methanol acting as the nucleophile to react with the carbocation, forming a protonated DMM molecule which loses this proton to complete the cycle (Equation 2-12) (Kolah et al., 1996).

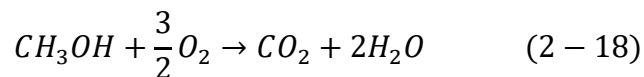
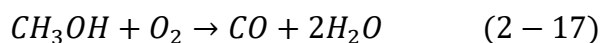
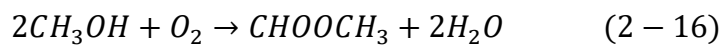
2.4.2 Direct DMM Reaction Network

The direct pathway for methanol to DMM is achieved in the gas phase by combining the oxidative and acid reactions, seen in the indirect pathway, over a single catalyst. As such we get an overall reaction occurring according to the below stoichiometry, illustrated in Equation 2-13.



While the above equation describes the desired reaction pathway for the synthesis of DMM, there are several undesired side reactions that can take place through both the acidic and oxidative pathways due to the dual nature of the catalyst. These typically are not seen in the indirect pathway due to the separation of the acid and oxidative pathways (Thavornprasert et al., 2016). These side-products are typically DME, formic acid, methyl formate (MF), carbon monoxide and carbon dioxide. The chemical reactions for methanol to form these compounds are given below in Equations 2-14 through 2-18.





DME (Equation 2-14) is formed by two molecules of methanol reacting in an acid catalyzed dehydration process, this is regulated by the acid strength of the catalyst (Liu and Iglesia, 2003). Instead of producing a hemiformal with formaldehyde, two methanol molecules react with each other and go down the acetalization pathway, forming DME (Blaszkowski and van Santen, 1996). Other potential side products are the result of over-oxidation reactions where methanol continues down the oxidation pathway of the Mars-van Krevelen cycle instead of stopping at formaldehyde. As such these products are impacted by the redox properties of the catalyst. It should be noted that carbon monoxide production is formed through the decomposition of gaseous formic acid which forms carbon monoxide (CO) and water (Akiya and Savage, 1998; Tatibouët, 1996). Typically, formic acid acts as an intermediate towards methyl formate or CO production and is not seen in methanol oxidative reactions (Tatibouët, 1996).

Methyl formate is unique as a side product in the sense that there are several pathways towards it, with one of them not requiring oxidation past formaldehyde (Sun et al., 2019; Broomhead et al. 2022). Figure 2-7 below illustrates the three different methyl formate pathways. Herein the oxidative pathway from formic acid reacting with methanol to form methyl formate (Pathway 1a and 1b in Figure 2-7) is illustrated as outlined by Tatibouët (1996). Additionally, the hemiformal intermediate that leads to DMM, formed initially when one methanol reacts with formaldehyde in an acid-catalyzed reaction, can form methyl formate through oxidation (Pathway 1d in Figure 2-7) or react with a methanol to continue towards DMM formation (Liu and Iglesia, 2003). The final pathway involves two formaldehyde molecules reacting to form methyl formate via the Tishchenko reaction (Pathway 1c in Figure 2-7), and primarily occurs on Lewis type acid sites (Broomhead et al., 2022).

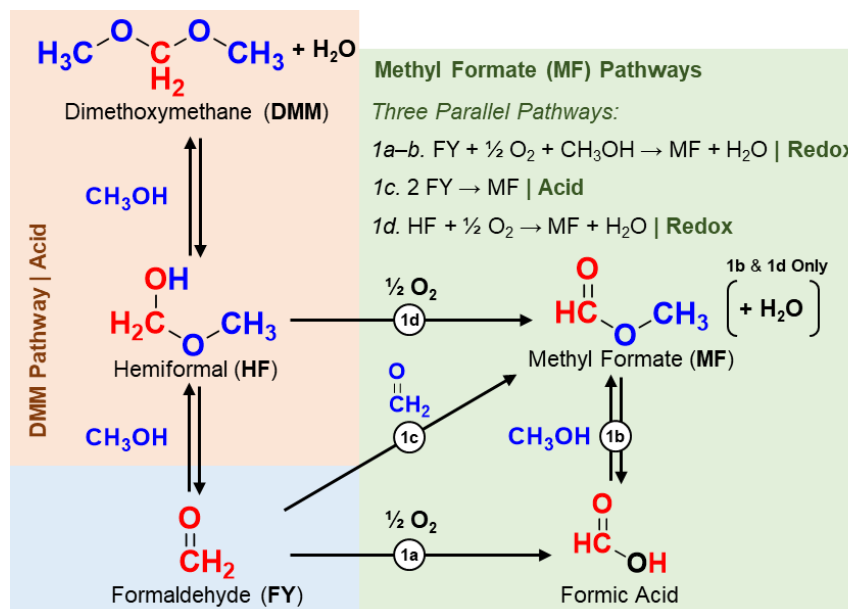


Figure 2-7 Reaction Network showing Methyl Formate Production from Formaldehyde during DMM Production adapted from Broomhead et al., 2022

Based on this scheme it becomes apparent that a chemical process to produce high yields of DMM will need to selectively oxidate methanol to formaldehyde without further overoxidation. The catalyst used will need to also contain an acidic component strong enough to form DMM but tailored to avoid DME production. Additionally, this acid catalyst needs to minimize the amount of Lewis acid sites to limit formaldehyde reacting with itself to form methyl formate.

2.5 One-Step Direct Dimethoxymethane Production

As opposed to the current two-stage reaction process outlined in Section 2.3 for DMM synthesis, a one-step process for DMM formation provides clear benefits to the existing industrial technology. By using a pathway where both the oxidative and acid-catalyzed reactions occur simultaneously in the gas phase, a single stage process for DMM can be tailored to accomplish longer OME synthesis downstream. This one-step method is desirable since DMM could be efficiently manufactured from a simple starting point (methanol and air) without the need of additional stage operations. To create this

simplified and industrially viable process, a bifunctional catalyst is required. This catalyst must contain redox sites along acid functions in order to bring methanol along the pathway required for successful DMM synthesis (Broomhead et al., 2022; Thavornprasert et al., 2016; Sun et al., 2019). However, the ability to perform oxidation and acid-catalyzed condensation is not sufficient to ensure a catalyst achieves high DMM yields. The oxidative and acid strengths of the catalyst must be carefully tuned to avoid side reactions resulting from overoxidation or acid catalyzed dehydration processes (Figure 2-8). (Thavornprasert et al., 2016).

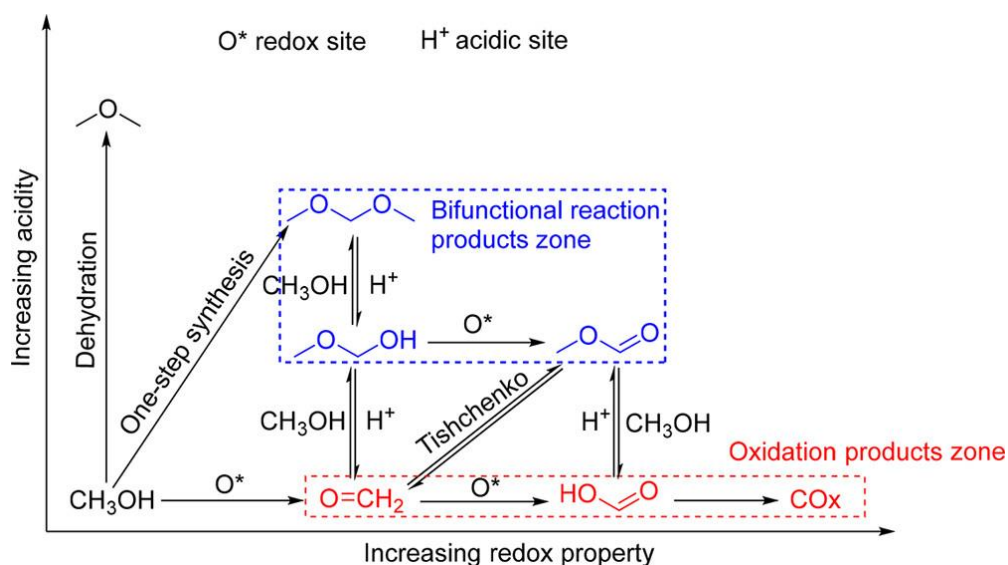


Figure 2-8 Reaction Network for One-Stage DMM Synthesis Illustrating Oxidative and Acidic Pathways from Sun et al., 2019

The tuning of the catalytic sites is important in harmonizing both the oxidative and acetalization catalytic cycles to ensure one does not outperform the other, leading to the formation of the unwanted side products discussed in Section 2.4.1 and highlighted in Figure 2-8. To ensure sufficient yields of DMM, potential catalysts must have the proper oxidative strength to readily convert methanol to formaldehyde while ensuring this formaldehyde does not subsequently participate in the Mars-van Krevelen cycle itself, further oxidizing to formic acid or carbon oxides. The acid strength subsequently must be strong enough to dehydrate the hemiformal molecule to DMM before it oxidizes and

forms methyl formate, while not too strong as to allow methanol to react with itself to form DME.

In determining which of the cycles is dominant, the rate-limiting steps of the oxidative and acetalization pathway can be compared to determine which is determinant of the overall rate of DMM formation. Studies consistently indicate that the C-H bond scission step, where methanol is converted into formaldehyde, in the Mars van-Krevelen cycle, has a larger activation energy than the hemiformal formation in the methanol acetalization cycle, and therefore is rate-determining for DMM production (Broomhead et al., 2022; Liu and Iglesia, 2005). This means the oxidation function of a catalyst is much more consequential to the process kinetics than its acid function, as any formaldehyde produced should undergo acetalization at a much faster rate than methanol turning into formaldehyde. Due to this behaviour, catalysts with a sound redox activity should be used as a starting point, with the acid function modified as required. The DMM production capability of several catalyst candidates will be examined in the next section.

2.6 Catalysts for Direct DMM Production

Catalyst formulations that exhibit the properties required for DMM production (bifunctional) typically involve unsupported/supported transition metal oxides as these compounds have shown a good ability for oxidation of organic compounds, while providing an acid function. (Lee et al., 2020; Bernholc et al., 1987). Catalysts that have strong DMM production capability can be grouped into two categories: unsupported and supported. Unsupported catalysts describe pure metals and metal oxides, while supported describes metals/metal oxides attached to a support structure to enhance certain characteristics of the catalyst. In general, pure metal oxides have a lower surface area and therefore less activity than their supported counterparts but can provide important information on the mechanistic requirements for DMM synthesis. The methanol conversions as well as the selectivity towards DMM for select catalysts are presented below in Table 2-1 while more detailed examinations of these catalysts can be found in the following subsections.

Table 2-1 Conversions and Selectivity towards DMM for Select Metal Oxide Catalysts adapted from Rodrigues and Herrera, (2023) and Sun et al., (2019)

Catalyst	Methanol Concentration	Temperature	Methanol Conversion	DMM Selectivity	Reference
RuO ₂	4	393	20*	2.2	Liu and Iglesia, 2005
4.3% RuO ₂ /SiO ₂	4	393	20**	56.1	Liu and Iglesia, 2005
4.4% RuO ₂ /Al ₂ O ₃	4	393	20***	57.4	Liu and Iglesia, 2005
Fe ₂ (MoO ₄) ₃	40	553	55.7	89.7	Gornay et al., 2010
Fe ₂ (MoO ₄) ₃ /HZSM-5	40	653	89.1	88.7	Yuan et al., 2022
SbRe ₂ O ₆	4	573	6.5	92.5	Yuan et al., 2000a
ReO ₃	4	513	12.4	99.0	Yuan et al., 2000b
ReO ₂	4	513	65.3	64.6	Yuan et al., 2000b
10% Re- γ Fe ₂ O ₃	4	513	48.4	91.0	Yuan et al., 2000b
10% Re-TiO ₂ (anatase)	4	513	59.5	78.5	Yuan et al., 2000b
12.5% V-TiO ₂ (anatase)	4	393	59.7	57.0	Kaichev et al., 2014

*20% conversion obtained using a 2.3 h⁻¹ space velocity for more information see reference

**20% conversion obtained using an 8.3 h⁻¹ space velocity for more information see reference

***20% conversion obtained using a 14.9 h⁻¹ space velocity for more information see reference

2.6.1 Unsupported Catalysts

When examining unsupported metal/metal oxide catalysts there are three different catalysts that have received most of the research attention: ruthenium oxide, rhenium oxide, and iron-molybdenum oxide catalysts. One of the first catalysts reported to have activity for DMM production was iron-molybdate. Since its main use is historically for formaldehyde production, any DMM observed was an unwanted side product and thus very few studies sought to maximize these yields, as the amount of DMM formed was minimal (Thavornprasert et al., 2014). Researchers found that by subjecting iron-molybdate catalysts to low methanol conversions and low temperatures which are atypical to formaldehyde production, DMM selectivity is greatly improved (Machiels and

Sleight, 1982). By utilizing these process conditions researchers were able to achieve significantly higher DMM production rates than those that had been achieved using other catalysts with a rate of 4.6 kg/h DMM per kg of catalyst at 553 K (Gornay et al., 2010). These researchers found that iron-molybdate exhibited near zero selectivity to DMM, when using low methanol concentrations in the feed (oxygen rich conditions), which is typically associated with formaldehyde production (Gornay et al., 2010). Once methanol was fed at higher concentrations than oxygen (methanol rich conditions) high yields of DMM were obtained (Gornay et al., 2010). While the researchers didn't offer a mechanistic framework onto why this behaviour was occurring, it is possible to speculate that the oxygen potential in the catalyst surface increased under oxygen rich conditions, hence directing the catalyst to mainly carry partial oxidations on the organic substrate. The link between iron/molybdenum ratios in the catalyst and DMM yield has also been examined. Thavornprasert et al., performed a study which showed the optimum DMM yields between 0.2-0.3 Fe/Total metal with an apparent maximum at 0.24 (2014). This was attributed to the addition of iron oxide boosting the redox capability of the catalyst but impacting the acid strength of the molybdenum trioxide (Thavornprasert et al., 2014).

Ruthenium oxide is a versatile redox catalyst, historically used for the oxidation of carbon monoxide to carbon dioxide and the oxidation of high carbon alcohols at near ambient conditions (333-393K) (Liu and Iglesia, 2005). When evaluated for DMM production, extremely low selectivity towards DMM was attained and methyl formate was observed instead, suggesting that with an enhancement of acid function DMM could achieve better yields (Liu and Iglesia, 2005). The proposed mechanism for this reaction was ruthenium oxide undergoing a Mars-van Krevelen cycle where an oxygen atom is abstracted from the catalyst surface to perform the oxidation of methanol and subsequently replenished (Liu and Iglesia, 2005). This transformation of methanol to formaldehyde was found to be the rate-determining step highlighting the importance of utilizing catalysts with good redox potential (Liu and Iglesia, 2005). Unfortunately, the acid pathway leading to DMM and MF was not explored; however, it has been proposed by other authors that reduced ruthenium species (Ru^{+3}), acting as Lewis acid sites, are responsible for the production of DMM and MF from methanol (Li et al., 2015).

The use of rhenium oxide as a catalyst for DMM synthesis has also been explored, as it can exist in many oxidation states and has been used in hydro-desulfurization and metathesis reactions (Yuan et al., 2000a). However, at standard operating conditions for methanol oxidation rhenium is highly volatile and is lost via sublimation (Yuan et al., 2000a). As such researchers have explored ways to stabilize the rhenium oxide species using antimony, which forms mixed SbReO structures exhibiting better thermal stability (Yuan et al., 2000a). Researchers have identified SbRe_2O_6 , as the most active structure for DMM production, and attributed this to the reducibility of this phase (which makes its oxygen easier to transfer during methanol oxidation), compared to others with a higher antimony to rhenium ratio ($\text{Sb}_4\text{Re}_2\text{O}_{13}$) (Yuan et al., 2000a). Isolated rhenium oxide in oxidation states +6 and +4 were tested as well at lower temperatures (513K), displaying better performances than the antimony-rhenium oxide (Yuan et al., 2000b). The rhenium in a +6 state exhibited significantly better selectivity towards DMM albeit a lower conversion than the rhenium in the +4 state (Yuan et al., 2000b). However, issues associated with thermal stability and low surface areas impact the viability of these materials as industrial catalysts.

2.6.2 Supported Catalysts

Supported catalysts have been studied extensively, since their use increases the available surface area of the active phase and also dramatically enhances its thermal stability (Munnik et al., 2015; Bagheri et al., 2014). When discussing supported catalysts, it is important to distinguish between the catalytic metal-bearing functionality, which is considered the active phase, and the support, which may or may not be inert. Materials used as support include activated carbon, aluminum oxide, titanium dioxide, cerium dioxide, silicon dioxide, zeolites, lanthanum oxide, and zirconium oxide (Bagheri et al., 2014). A critical factor in choosing an adequate support is the interaction between the active phase and the support, as this can play a critical role in activity and in most cases changes the electronic properties of the active phase (Bagheri et al., 2014).

As discussed above, iron-molybdenum catalysts have been assessed in the past for DMM synthesis; however, due to low mechanical and thermal resistance iron-molybdates have not been extensively used in bulk form (Thavornprasert et al., 2016). SiO_2 and Al_2O_3

have been tested as potential supports for this system. It has been demonstrated that anchoring these species in the support results in a strong interaction between the metal species and the support, particularly at low metal oxide loadings (Hill and Wilson, 1991). When examining Raman spectra of silica-supported catalysts, at different metal oxide loadings, characteristic peaks for bulk iron-molybdate and molybdenum trioxide were not observed in the spectra until a metal loading of 10% (for iron) and 33% (for molybdenum) were reached. (Figure 2-9) (Hill and Wilson, 1991).

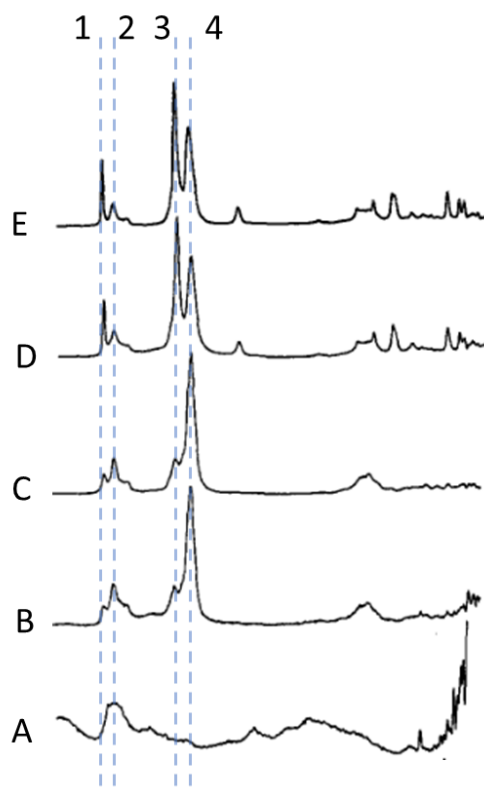


Figure 2-9 Raman Spectra of Various Loadings of Fe:Mo on SiO₂; A: 5wt% B:10 wt%, C:18 wt%, D: 33 wt%, E: Bulk Catalyst (100 wt%) Peaks at 1 and 3 represent signals associated with the presence of MoO₃ and peaks 2 and 4 represent peaks associated with Fe₂(MoO₄)₃. Figure adapted from Hill and Wilson, 1991

This signal masking was also found when using Al₂O₃ as support (Hill and Wilson, 1991). In this case the signals for iron molybdate and molybdenum oxide were not observable even at metal oxide loadings above 30%, which were clearly visible on the

supported SiO₂ catalyst with similar loadings, indicating a stronger interaction of the metal oxide phases with the alumina support (Hill and Wilson, 1991).

Even though the Mo-Fe oxide system has been well studied, there is a limited number of reports on one-stage production of DMM with supported iron-molybdates. A study reported iron-molybdate impregnated on a zeolite (HZSM-5) being able to achieve significant yields towards DMM in a fluidized bed system with a catalyst regeneration loop (Yuan et al., 2022). In their study, the authors attributed the redox activity to iron-molybdenum oxide phase and the acid-catalyzed acetalization path to Lewis and Brønsted acid sites present on the zeolite support (Yuan et al., 2022). It should be noted that several discrepancies exist between this study and previous ones on supported iron-molybdenum systems. For instance, the reported amount of oxygen that was co-fed in with methanol does not seem to be sufficient to achieve the reported yield of oxidation products. Additionally, total metal loadings of 13% were evaluated, which would have significant support interactions and reduced activity on a pure Al₂O₃ or SiO₂ support, but no support effects were mentioned for the catalyst. While these results are intriguing, more mechanistic studies need to be conducted on DMM production over supported iron-molybdenum to gain a better understanding of the effect the support has on DMM yields.

Supported ruthenium-based catalysts have also been evaluated for DMM production, showing much better performance compared to their unsupported counterparts. This was attributed to the ability for the ruthenium to highly disperse on the support, limiting the formation of unreactive ruthenium metal oxide clusters present on the bulk unsupported catalyst (Liu and Iglesia, 2005). Figure 10 shows the methanol oxidation turnover rates for a series of ruthenium oxide catalysts prepared using different supports. The results clearly indicate the chosen support has a significant effect on the catalyst activity, with tin oxide showing the best performance. The authors attributed the trend observed in Fig. 2-10 to the redox properties of the support, proposing that supports able switch between redox states under reaction conditions (i.e., support reducibility) significantly promote the ability of ruthenium oxide to carry methanol oxidation. (Liu and Iglesia, 2005)

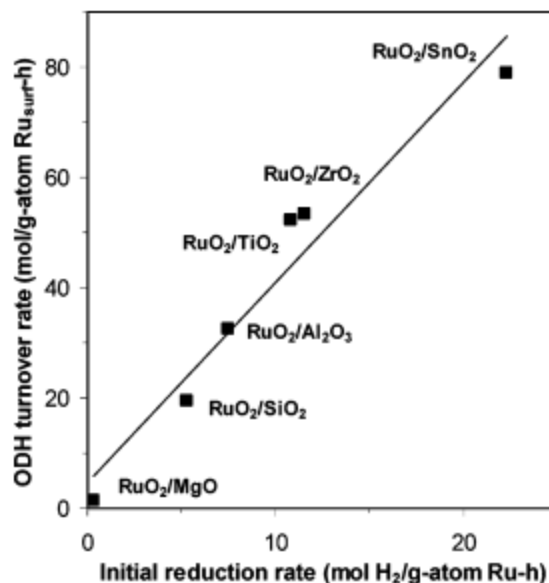


Figure 2-10 Effect of Support Material on the Rate of Oxidative Dehydrogenation and Reducibility of RuO₂ from Liu and Iglesia, 2005.

The authors also evaluated the formation of acid products and found it to be highly dependent on the support; with the best DMM yields achieved over SiO₂ and Al₂O₃ supported catalysts, while titanium, and magnesium oxide increased methyl formate formation. The authors attributed the formation of methyl formate to acid or dehydrogenation sites in the support, dehydrogenating the hemi-acetal DMM precursor to MF rather than enabling the dimerization of formaldehyde (Liu and Iglesia, 2005). Other researchers were able to improve the amount of methanol converted by dispersing the RuO₂ on carbon nanotubes, but this did not increase DMM yields as this support provided too much acidity (Yu et al., 2008). Ultimately these catalysts are hampered by high methyl formate yields, regardless of support, which leads to concerns about purification for industrial adoption (Sun et al., 2019).

Supported rhenium catalysts have also been assessed for these processes (Yuan et al., 2000a; Yuan et al., 2000b). When examining these supported catalysts, the amount of rhenium deposited becomes important for determining DMM yields. When the loading of rhenium dispersed on the support is below two monolayers thick, rhenium remains in the Re⁺⁶ state, but started to reduce to Re⁺⁴ above two monolayer thickness (Yuan et al.,

2000b). As mentioned in Section 2.6.2, unsupported Re 6+ has a better selectivity towards DMM, but lower total conversions of methanol, indicating that loading has a severe effect on product yield (Yuan et al., 2000b). However, the researchers did not normalize loadings based on the surface area of the support (Yuan et al., 2000b), and as such it is difficult to determine that the change in catalyst performance was due to changes in the support-rhenium oxide interaction or the changing dispersion observed using supports with different chemical identities, as well as different surface areas. While rhenium has promise as a catalyst for DMM production, its cost can be considered a drawback (Gothe et al., 2021). In addition, further studies need to be conducted to gain a better understanding of the identity of the active sites carrying the acid-catalyzed pathway, understanding how the support affects the supported rhenium in enhancing or limiting DMM formation.

2.6.3 Titanium Supported Vanadium Catalysts

Vanadium (+5) oxide has been extensively studied, being identified as a good redox catalyst when supported on titania and other similar supports (Guerrero-Pérez, 2017). The most active vanadium-oxide based catalyst for redox processes to be recognized to date is obtained when vanadia is anchored in titanium oxide (Wachs, 2013). For the specific case of DMM production, Broomhead et al. observed that while the rate of methanol conversion was an order of magnitude lower than that of TiO₂-supported vanadia (423K), the purely crystalline phase had a 100% selectivity to DMM (2020).

The activity for partial oxidation for the VO_x-TiO₂ system has been linked to the role of the V-O bonds present in these structures, differentiating between vanadyl groups (V=O), vanadia bridges (V-O-V) and vanadia/titania bridges (V-O-Ti). Each of these species possess different redox activities, and there is debate in the literature on which of these three participate in the Mars-van-Krevelen cycle for alcohol partial oxidation (Yun et al., 2018; Zabilska et al., 2022). Figure 2-11 illustrate this differentiation, O^I describes one of the oxygens anchoring the vanadium to its support (absent in the crystalline phase), O^{II} describes the oxygen bridging two atoms of vanadium found at a ratio of 5 oxygens per vanadium (5+) in the crystalline phase, and O^{III} describes the oxygen in the vanadyl group and is found at a 0.5 oxygen to vanadium ratio (Broomhead et al., 2022).

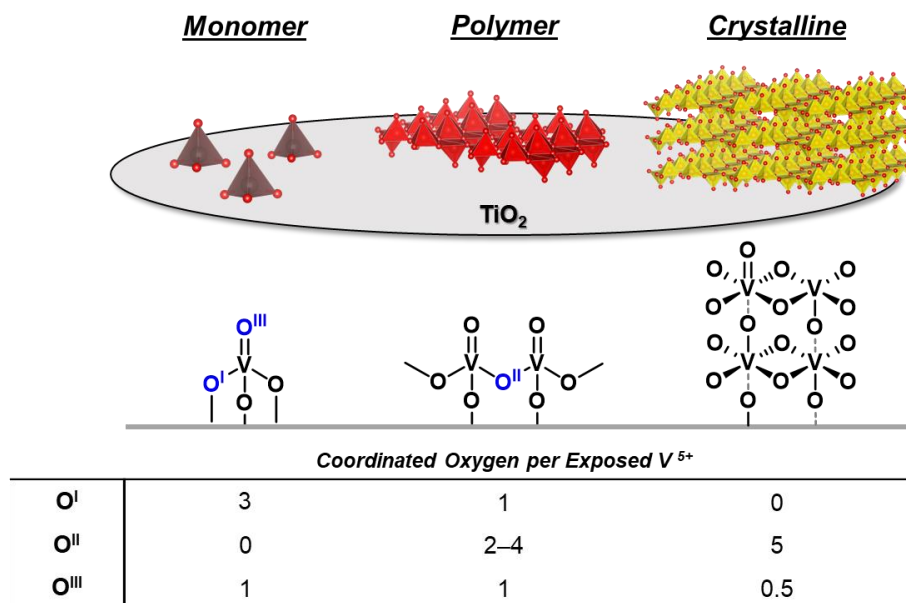


Figure 2-11 Amount of V-O Bonds Present in Different Vanadium Structures from Broomhead et al., 2022

When examining their catalytic activity, multiple studies have confirmed that O^{III} has no effect on the reactivity and O^{II} is active in oxidation but is not as crucial as the O^I bond (Wachs and Weckhuysen, 1997; Broomhead et al., 2022). This would explain the significantly lower activity of the crystalline vanadium as opposed to the supported versions as the C-H bond scission, leading to formaldehyde formation, cannot be performed as effectively due to the lack of O^I in the catalyst (Broomhead et al., 2022). If this O^I bond is indeed highly critical to the oxidative activity of the catalyst, the vanadium-support interaction then becomes crucial to maximize DMM production.

When examining the support effect for vanadium oxide, Wachs and Deo found that the best supports for oxidation reactions were surface-reducible such as ZrO₂, TiO₂, Nb₂O₅, etc. as compared to non-reducible supports such as SiO₂ and Al₂O₃ (1993). This hierarchy is similar to the one observed on rhenium catalysts, which showed a similar trend (Yuan et al., 2000b). The authors further theorized that below monolayer coverage the vanadium loading had no effect on the activity (Wachs and Deo, 1993). However, it

should be noted that the authors were examining the process at higher temperatures (503K) as opposed to those favored for DMM production on supported vanadium. When examining the effect of vanadium loadings on the oxidation step for DMM production at 423K Broomhead et al., observed that the vanadium loading was highly critical for the methanol oxidation step (2022).

Indeed, it is widely acknowledged that vanadium exhibits different electronic behaviour as it becomes more agglomerated, and the number of V-O-V bonds increases for both the supported and crystalline phases. This has been consistently reported in the literature through the observed changes in the electronic bandgap, which occur as the vanadium oxide agglomerates. (Broomhead et al., 2022; Gao and Wachs, 2000). Unlike supported rhenium the oxidation state does not change as the vanadium becomes more isolated, but instead a monomeric vanadate molecule attached to the surface is formed as illustrated in Figure 2-12 (Broomhead et al., 2022) This relationship is illustrated below in Figure 2-12 where the electronic bandgap observed for TiO₂-supported catalysts with different loadings of vanadium are reported.

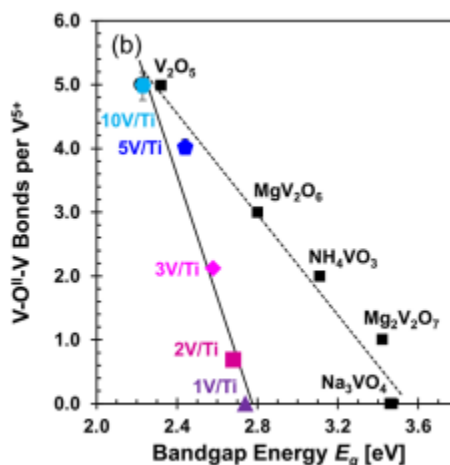


Figure 2-12 Effect the Number of V-O-V bonds has on the Bandgap Energy of the Surface for Supported V/Ti Structures and Crystalline Vanadium Structures from Broomhead et al., 2022; crystalline data from Gao and Wachs, 2000. The number before the V/Ti complex denotes the vanadium loading as a mass percentage.

Using the electronic bandgap information, it is easy to correlate the degree of agglomeration of the vanadium oxide species with its observed catalytic activity. Broomhead and coworkers demonstrated that the best redox catalytic performance (methanol oxidation step) is observed at 2 atoms of vanadium per square nanometer (Figure 2-13) (et al., 2022). This result indicates that dispersion below monolayer coverages is necessary to achieve optimum partial oxidation performance at low temperatures.

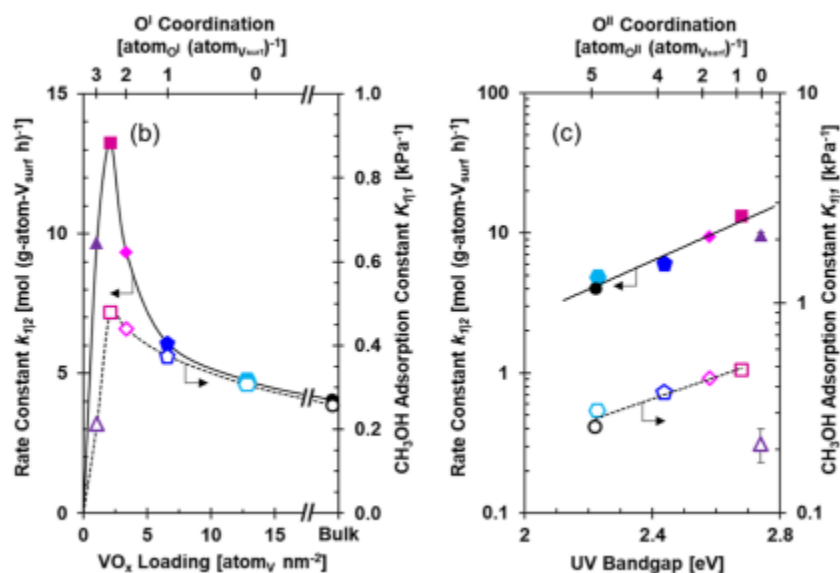


Figure 2-13 Effect of the O^I and O^{II} Coordination on the C-H Bond Scission Rate and the Methanol Adsorption Constant from Broomhead et al., 2022. Note the symbols correspond to the loadings presented above in Figure 12 with the hollowed-out symbols corresponding to the adsorption constant

When looking at the acid function of bulk V₂O₅, acidity was primarily attributed to Brønsted sites. DMM formation rates did not change after the crystalline catalyst was reduced, indicating that Lewis sites on crystalline vanadium oxide were likely not responsible for DMM production (Broomhead et al., 2022). However, a correlation between DMM formation and the amount of O^I available in the supported phase was observed, leading to attribute the acid function responsible for DMM formation in the TiO₂-supported catalyst to V-O-Ti moieties in the surface (Broomhead et al., 2022).

An additional catalytic cycle was observed in the VO_x-TiO₂ system: the methyl formate production cycle. Rather than a product of over-oxidation or over-acidification, Broomhead et al., proposed methyl formate was produced through dimerization of formaldehyde over Lewis acid sites via the Tishchenko reaction (2022). Anaerobic conditions of pure methanol and formaldehyde revealed that these Lewis sites are created when vanadium oxide reduces (oxidation state less than 5) or over vanadium free exposed titanium oxide surfaces (Broomhead et al., 2022). This is in opposition to what was proposed by Liu and Iglesia on supported ruthenium catalysts; however, given that Iglesia and coworkers used a different metal oxide species, a different mechanistic pathway is plausible to reconcile this discrepancy.

When accounting for all three mechanisms, a specific range of vanadium loading is necessary to achieve good DMM selectivity, while maintaining high methanol conversions (normalized by Vanadium atom), specifically 3-10 wt% vanadium oxide on titanium dioxide (Broomhead et al., 2022). Vanadium deposited on titanium catalysts addresses several of the drawbacks seen on other DMM producing catalytic systems, such as cost, low DMM yields, poor stability, and most importantly, a lack of atomic-level mechanistic understanding of catalyst behaviour. Using these advantages and mechanistic information, we embark on the considerations required to scale up this catalytic system.

2.7 Industrial Catalyst Production Methods

When scaling up a catalyst formulation, initially formulated for optimization of active site distribution and strength in a microreactor system operating in a kinetically controlled regime, to a system producing thousands of tonnes of feed in an industrial grade reactor, several design factors have to be taken into consideration. At lab-bench scale, the constraints associated with the elucidation of mechanistic steps and reaction kinetics demand the use of catalyst morphologies of relatively small particle size, to ensure the reactant can readily access any active sites and the reaction is not limited by mass-transfer (Munnik et al., 2015). This regime is satisfactory for catalyst beds with minimal height as found in typical bench scale-research reactors, but when industrial reactors where bed heights are multitude of magnitudes larger, the pressure drop through

the bed becomes unfeasible for operation. As a result, while catalyst particles of 50-200 microns are used at bench scale, catalysts sizes in the order of 1-10 mm are typically used in industrial applications (Munnik et al., 2015). This increase in particle size means transport effects must be incorporated into catalyst pellet design. Additionally, the energy lost/gain in the reactor system due to the reaction increases exponentially, affecting product distribution and catalyst stability. In addition to these concerns numerous other issues exist from mechanical strength to bed voidage, which also need to be taken into consideration to maximize the effectiveness of the reactor system. These issues are often the reason for which scaling up a catalyst for industrial use takes years of development and extensive capital (Armor, 2011). The relationship between the small-scale and large-scale aspects of catalyst preparation are illustrated in Figure 2-14. Both the large-scale mechanical properties and physio-chemical characteristics are shaped by the preparation methods used to formulate the catalyst, with both aspects impacting catalyst performance dramatically.

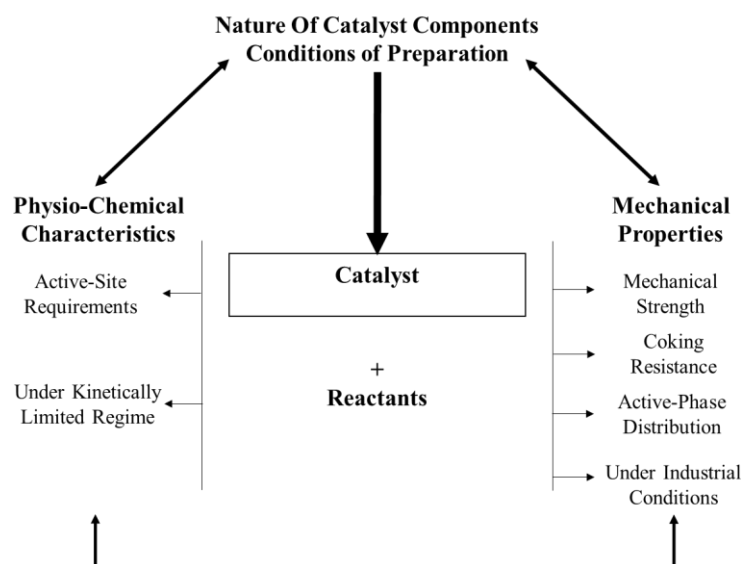


Figure 2-14 Interconnectivity of the Considerations for Catalyst Design and Scaling Up

Section 2.6.2 covered the physio-chemical requirements for the vanadium/titania catalyst used for DMM synthesis, the section below will focus on catalyst manufacturing techniques and the factors that must be controlled when a catalyst is scaled up for use under industrial conditions.

2.7.1 Different Preparation Methods for Industrial Catalysis

As mentioned above, there are multiple factors that must be considered in industrial catalyst pellet production. The methodology selected for loading of the active phase in a suitable support is paramount to minimize the volume of catalyst and reactor space required, while at the same time the surface area of exposed catalytic material must be maximized (Afandizadeh and Foumeny, 2001). Finally, the mass and heat transfer properties of the catalyst need to be optimized to limit gradients in concentration or heat throughout the pellet and bed (Hlavacek, 1970). Both factors are heavily influenced by the preparation method of the catalyst, meaning the right method should be chosen according to the needs of the process. Below, Table 2-2 describes several different catalytic preparation methods with the ones relevant to this thesis italicized.

Table 2-2 Overview of Different Catalyst Preparation Techniques, adapted from Zhang, 2020

Catalyst Preparation Method	Brief Description of Synthesis Technique
<i>Precipitation</i>	<i>With all component precursors fully dissolved, a change in the liquid phase results in precipitation of the support and/or active phase precursor.</i>
<i>Deposition Precipitation</i>	<i>The solid support is mixed with a solution of the active phase ionic precursors, the active-phase component ions diffuse on the solid and solution conditions are changed to induce their precipitation onto the support.</i>
<i>Impregnation</i>	<i>The support is immersed in a solution containing active components. After reaching equilibrium, the remaining liquid is removed.</i>
Sol-Gel	Using high pH or organic molecules support precursors are hydrolyzed to form a colloidal solution (sol) directly or lysed to form a solution, and then a solution of the active phase precursors is added to form an aggregated gel, which then is dried.
<i>Atomic Layer Deposition (ALD)</i>	<i>Active phase precursors are used to produce monolayer films by chemical reactions between the surface chemical functionalities of the supports and the active phase precursors in a highly controlled and ordered fashion</i>

Active phase deposition in an industrial catalyst pellet can be conducted using two distinct general methods: impregnation or precipitation (Munnik et al., 2015). Both these methods encompass multi-step approaches that can affect the structure and activity of the active phase created on the pellet substrate, making it critical that the right methodology is selected. Precipitation relies on the change in conditions in a precursor solution (usually aqueous) that triggers the precipitation of the active phase. This methodology can be used as well to prepare the catalyst support (Munnik et al., 2015). Precipitation methodology used to simultaneously create both the support and active phase is called co-precipitation and involves the precipitation of two or more phases at the same time to form the catalyst, followed by aging to grow larger particle sizes, the material obtained is washed to remove ions in solution, and calcined to convert the precursor to the metal oxide active phase (Munnik et al., 2015). Precipitation can be induced by changing the pH, the temperature, polarity of the solvent mixture and/or evaporation, with each of these stages potentially affecting the final physical and chemical characteristics of the catalyst material obtained (Baltes et al., 2008). Typically, coprecipitation produces materials with relatively low surface areas. The iron-molybdate unsupported catalysts, described in Section 2.6.1, are traditionally prepared via co-precipitation, with obtained surface areas around $10 \text{ m}^2/\text{g}$ (Pudge et al., 2022). It should be noted that the washing steps required to remove dissolved precursor ions create numerous waste streams (Munnik et al., 2015).

Deposition-precipitation involves one or more phases precipitated onto a solid support. This is achieved by having the solid support suspended in the precursor solution (Munnik et al., 2015). To successfully perform deposition precipitation, conditions must be selected to have the support acting as a seed for nucleation (Burattin et al., 1998). By acting as a seed, active-phase precipitation would rather occur on the support's surface than in the bulk solution (undesirable as a segregated usually crystalline phase is obtained), thus maintaining the crucial interaction between the active-phase and support (Burattin et al., 1998). As such, homogenous control of the solution's pH must be obtained to avoid local areas with differing pH values that may lead to bulk precipitation of the metal oxide precursor (Burattin et al., 1998). The use of deposition-precipitation methodology enables the preparation of catalysts with extremely high loadings of active

phase being well distributed onto the surface of a support, as opposed to other preparation methods which are usually limited by the solubility of the metal salt precursors (Bitter et al., 2003).

Impregnation involves the use of capillary action to deposit a solution containing the active phase precursor onto a catalyst support (Munnik et al., 2015). This method has been shown to provide optimum dispersion in comparison to co-precipitation as it helps prevent sintering of the active phase during heat treatment (Li et al., 2006). Impregnation produces less waste than the co-precipitation method; since, unlike co-precipitation, it foregoes the washing step and a drying step is instead used to remove any lingering solvent (Munnik et al., 2015). There are two main types of impregnation-based methodologies: wetness impregnation and incipient wetness impregnation. These methods differ on the amount of liquid used; incipient wetness impregnation utilizes a volume of solution equal to the total pore volume available on the support. In wetness impregnation, the solution volume is substantially more than the total pore volume (Munnik et al., 2015). Incipient wetness impregnation is limited by the solubility of the active phase precursor salts (Schwarz et al., 1995). Precursor metal salts with low solubility may need several rounds of impregnation and drying to deposit the required loading, which may alter the distribution of the active phase throughout the pellet. Wetness impregnation avoids this issue as extra solvent is used, however; as undeposited precursor metals ions may remain in the solution, metal loadings obtained may be lower than expected, after filtration. Both impregnation methods require that the active phase precursor is first dissolved in the solution before the support is added. Reversing these steps limits the distribution of the active phase to diffusion rather than capillary action, which takes significantly longer to occur (Neimark et al., 1981; Schwarz et al., 1995; Munnik et al., 2015).

Wetness impregnation allows for the creation of macro distributions of the active phase throughout the catalytic support. These forms of macro phase segregation take place through both the impregnation and drying stages. As supported industrial catalysts are several magnitudes larger than those typically used in bench scale kinetic experiments, there are several distributions possible for the catalytic pellets obtained, which greatly

impact their behaviour inside a reactor (Munnik et al., 2015). The four possible active phase distributions are depicted in Figure 2-15. While some of these distributions may be achieved using other catalyst preparation techniques, wetness impregnation is the only way to achieve any of the four types of phase distribution in a catalytic pellet consistently. Extra emphasis should be placed that the phase segregation described herein is at the macro scale. A uniform active phase distribution indicates that there is no segregation, and the solid phases are physically well mixed at the macroscopic scale but does not imply that a solid solution between the two phases has been formed, nor that a new chemical phase incorporating the support and active phase atoms has been created.

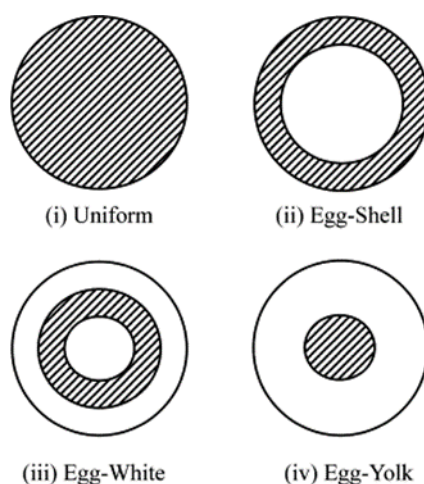


Figure 2-15 Different Active-Phase Distributions for Large-Scale Catalysis from Lekhal et al., 2001. Shaded areas represents the active phase and blank areas represents the bare support

The first type of phase distribution described is obtained when the active catalyst phase is homogeneously deposited throughout the entirety of the support “Uniform” on Figure 2-15. This macro distribution is commonly found using impregnation, deposition, or atomic layer deposition techniques (Munnik et al., 2015). Typically, uniform distributions are rarely used in industry, as it is used in scenarios where the intrinsic rate of the catalytic reaction is very slow compared to reactant diffusion rate, requiring the reactant mixture to have a long residence time and exposure to active sites (Munnik et al., 2015). Eggshell distributions are the result of the active phase of the catalyst distributed only upon the outer layer of a support. Due to the active phase being concentrated at the surface of the

catalyst, these distributions are beneficial towards processes which are diffusion-limited (Neimark et al., 1981). In diffusion-limited reactions the reaction occurs very fast and as such any active material located closer to the center of the catalyst is unlikely to interact with unreacted product once the reactant has diffused past the active phase in the outer layer. (Neimark et al., 1981). As a result, this distribution is also beneficial if the desired product is an intermediate product in a sequential reaction network (Russo et al., 2020). By limiting the reactant's exposure to the active phase, there is less opportunity for a reactant to continue down a reaction pathway thus increasing selectivity towards the intermediate (Russo et al., 2020; Neimark et al., 1981). An egg-yolk distribution has an active phase concentrated in the center of the support and is the type of distribution preferred if substances that can poison the catalyst are present in the reactor feedstock (Munnik et al., 2015). By distributing the active phase in the center of the catalyst pellet, poisons can adsorb onto support sites before reaching the active phase, as opposed to egg-shell or homogenous distributions where the poison can easily interact with the active phase on the surface. Essentially the active phase is "protected" by an outer layer of support which provides no catalytic value to the process and as such can be poisoned/subject to attrition. Finally, egg-white catalysts can be described as an intermediate between an eggshell and egg-yolk distribution and combine aspects of both these morphologies (Munnik et al., 2015). This distribution is used when risk of attrition or poisoning are present and the active phase should not be located at the pellet surface, but the process is diffusion limited making an egg-yolk distribution unnecessary as reactants need short exposure to active sites to react (Neimark et al., 1981).

Obtaining these different distributions occurs through the alteration of various aspects of the catalyst pellets' manufacturing process. For example, researchers have found a correlation between a higher drying temperature and depth of active phase penetration as higher temperatures lead to a more defined egg-shell distribution for weakly adsorbed materials (Lekhal et al., 2001). This was attributed to the convective forces from evaporation bringing the dissolved metals towards the surface as opposed to lower drying temperatures, which are subject to back diffusion of the active phase towards the catalyst center, due to longer drying times (Lekhal et al., 2001). An additional way to create an eggshell distribution is to create a diffusion-limited impregnation. While capillary effects

fill the catalyst with solution in a few minutes, dispersing the dissolved active phase very quickly; diffusion can take several days (Neimark et al., 1981). This diffusion limitation occurs when the active-phase is added to the solution after the support material so that the dissolved active-phase is not present during capillary action (Munnik et al., 1981).

Altering the chemistry of the precursor solution (such as a pH change) can also affect the active phase distribution morphology. Competitive adsorption can allow for migration of the active phase towards the center of the catalyst forming an egg-yolk catalyst, such as the case of the impregnation of cobalt on Al_2O_3 with citric acid at low pHs (Bergwerff et al., 2008). At low pH Co^{2+} ions compete for adsorption sites in the support with citrate ions (Bergwerff et al., 2008), while at higher pH the citrate chelates the cobalt ions acting as a complexation agent. This limits the complex's diffusivity by increasing its interaction with the support, forming a catalyst with an eggshell distribution containing a very sharp, distinct active phase gradient that does not penetrate significantly towards the catalyst center (Bergwerff et al., 2008). Egg-white distributions can be similarly engineered using a competitive adsorbent, but also altering the impregnation time or the pH so that the active-phase does not fully migrate towards the center (Zandbergen et al., 2012, Bergwerff et al., 2008).

Another alternative, albeit more sophisticated, for catalyst pellet preparation is "atomic layer deposition" (ALD) synthesis, where molecules are able to form a highly structured 2-D, atomic monolayer on the surface (Munnik et al., 2015). While gas phase ALD has been extensively used for the preparation of nanomaterials, liquid phase ALD was developed for the preparation of heterogenous catalysts (Herrera et al., 2005). In this specific case organic metal precursors dissolved in a non-aqueous solvent are used (Herrera et al., 2006; Munnik et al., 2015). Liquid ALD is a much more industrially friendly process compared to gas ALD process as it eliminates the need for vacuum while maintaining highly ordered depositions (Graniel et al., 2021). The ALD technique takes advantage of a self-terminating reaction between the metal precursor and the support surface hydroxyl groups (Hu et al., 2017). As the solution is anhydrous, metal ions are unable to agglomerate and thus are forced to bond to surface hydroxyls (Hu et al., 2005). For instance, if titanium dioxide is to be incorporated on a silicon dioxide phase, titanium

tetraisopropoxide (TTIP) could be used. TTIP contains a Ti^{+4} ion bonded to four oxygens connected to isopropyl groups via alkoxy ligand bonds. Since the alkoxide group is labile, one of these alkoxy ligands can be substituted with a former surface silanol (Si-OH) group and the metal precursor ion becomes bonded to the support. This process can occur as long as there are neighboring silanol groups available or stop if there are no longer more silanol groups available (Herrera et al., 2006). The exclusive interaction between support and active phase allows for the entire support to be coated with a monolayer thickness of active phase if enough precursor is available. After monolayer formation, unreacted precursor still in solution is removed and another reactant (typically water or oxygen) is added to remove any remaining organo-metallic bonds and replenish the hydroxyls on the newly formed monolayer so that further monolayers may be obtained if desired (Graniel et al., 2021; O'Neil et al., 2015). This process is illustrated in the diagram given in Figure 2-16 below.

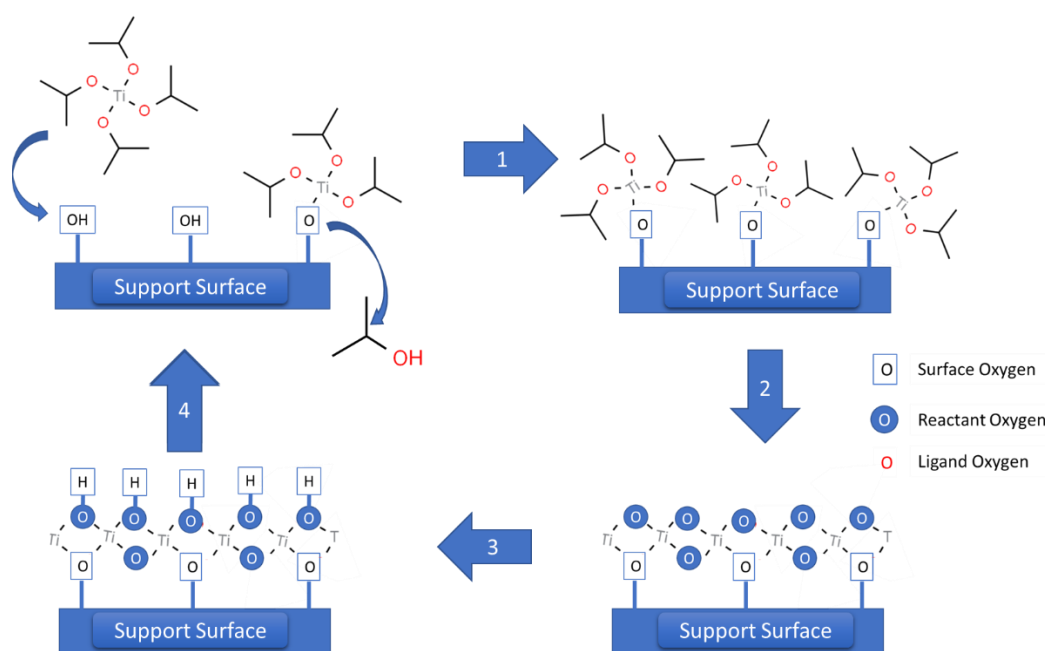


Figure 2-16 ALD mechanism and Process for Titanium Tetraisopropoxide Deposition using TiO_2/SiO_2 Scheme proposed by Capel Sanchez et al., 2009. Note that Steps 2 and 3 often occur simultaneously

As evidenced by Figure 2-16 Liquid ALD allows for the creation of a catalyst pellet with a layer of governable thickness. By enabling atomic level manipulation to the active phase-support interactions and the dispersion of the active-phase during synthesis, ALD provides a degree of control which is not seen in more conventional synthesis methods.

2.7.2 Integrating Industrial Catalysis with DMM Production

Under the right conditions and taking advantage of the interaction of the support with the active phase, wetness impregnation allows for a relative control of the two-dimensional dispersion (surface metal oxide cluster size) of the active phase throughout the support in a powder version of a catalyst. As discussed in Section 2.6.3, for the specific case of DMM synthesis from methanol, a two-dimensional monolayer of vanadium oxide anchored on a titania surface results in the most efficient catalytic formulation. The ability to translate these active site requirements and consistently manufacture it at the macro-scale can only be achieved by incorporating the macro-scale considerations discussed in Section 2.7.1.

As catalyst moiety regulating the activity of the VO_x/TiO_2 catalyst for both the acid and oxidative cycles, required for formation of DMM from methanol is the V-O-Ti site; these interactions must be preserved while scaling up to create an active catalyst for DMM formation. The preservation of these sites ensures there are enough oxygen atoms to participate in the Mars-van Krevelen mechanism as well as Brønsted acid sites to acetalize formed hemiformals. To maximize the amount of these bonds located between the active-phase and the support, the vanadium should be well-dispersed along the titanium dioxide surface to maintain high active-phase support interactions and minimize excess V-O-V and V=O bonds. The two best synthesis methods to ensure a high dispersion are wetness impregnation and ALD. While ALD is very effective at forming a 2D monolayer, which is the ideal molecular dispersion for DMM selectivity, it is less effective at being able to control the macro distribution throughout the pellet. As such ALD catalysts will technically result in homogenous distributions of the vanadium phase over a titania pellet support. Meanwhile wetness impregnation may result in more vanadium agglomeration, but it is significantly cheaper and provides the opportunity to control the solid phase macro-distribution. If the DMM synthesis process is assumed to

be conducted under similar conditions as the ones used in the FORMOX® process, the catalyst will not be subject to abrasion or catalyst poisons meaning an egg-yolk or egg-white distribution are not necessary. However, the preferred product of the sequential oxidation reaction from the reaction network is formaldehyde, an intermediate of a combustion reaction. As such an eggshell distribution may be preferential to ensure high formaldehyde selectivity. The issue with an eggshell distribution for DMM synthesis is that this distribution could leave substantial amounts of bare support towards the center of the pellet and the main active site for formaldehyde to methyl formate production are Lewis sites on bare titania sections. As such the benefits/drawbacks of eggshell and homogenous distributions will have to both be examined to determine the right approach for catalyst pellet design for the DMM process.

Chapter 3

3 Design and Structure/Activity Relationships in Catalytic Pellets hosting the VO_x/TiO_2 System for Oxymethylene Production.

3.1 Materials and Methods

3.1.1 Materials and Catalyst Preparation using Wetness Impregnation

Catalytic materials with two different macroscale morphologies were prepared: powder form (average particle diameter: 125-180 μm or 425-600 μm , and pellet form: (average particle diameter 3.18 mm). The supports utilized consisted of sulfated TiO_2 pellet (3.18 mm diameter, 261 m^2/g , 1.09 cc/g pore volume, Median Pore diameter 140 \AA , 1% Sulfur Content, Alfa Aesar) and a SiO_2 pellet (3.18 mm diameter, 261 m^2/g , 1.09 cc/g pore volume, median pore diameter 115 \AA , Alfa Aesar). It should be noted that based on the SDS for the silica pellets it specifies that the pellets also contain up to 10 wt% alumina; however, WDS analysis could not detect any aluminum oxide suggesting if present content is much lower than 10 wt%.

Incorporation of the active phase on the pellets took place using two main methodologies: wetness impregnation and atomic layer deposition. Wetness impregnation was carried out over TiO_2 pellets and Ti/Si pellets prepared via atomic layer deposition (ALD, methodology described below). A solution containing oxalic acid (anhydrous, $\geq 99\%$, Sigma-Aldrich) was prepared using ethanol (anhydrous) as solvent, to obtain a 1.5 M solution. Ammonium metavanadate (ACS Reagent grade, $\geq 99\%$, Sigma-Aldrich) was then added to this solution, The amount of vanadate salt was adjusted based on the desired final vanadium oxide loading in the catalyst (0.5%-5%). After the vanadium salt was completely dissolved in solution, either 1/8" diameter Titanium Pellets (261 m^2/g , 1.09 cc/g pore volume, Median Pore diameter 140 \AA , 1% Sulfur Content, Alfa Aesar) or ALD coated titania- SiO_2 pellets (see below) were added at a ratio of 10 mL of solution to 1 gram of solid support. After addition of the solid, the solution was stirred using a MAXQ 2000 shaker table (Thermo Scientific) at a rate of 90 RPM to ensure fracturing of

the pellets did not occur. This step was run for 24hrs. Once impregnation was completed, the contents were transferred to a round bottom flask and placed in a rotary evaporator (Heidolph) and heated gradually from 333K to 353K under vacuum. After the solvent was recovered, the remaining solid was dried in an oven at 373-393 K to remove any residual solvent between 24-48 hours. After drying the solids were calcined in air (Extra-Dry grade, Linde) at a flowrate of 80 SCCM at 723K for 4 hours. Table 3-1 lists all the catalyst prepared utilizing wetness impregnation. In the case of using water as a solvent the same methodology was followed substituting de-ionized water for ethanol and without the addition of oxalic acid.

Table 3-1 List of Wetness Impregnation Catalysts Prepared and Formulation Conditions

Catalysts Sample	Preparation Method	Solvent	Support Pellet	Vanadium Loading (wt%)	Impregnation Time (Days)
5% V-WI _(EtOH) /Ti	Wetness Impregnation	EtOH/ Oxalic Acid	TiO ₂	5	1
2% V-WI _(EtOH) /Ti	Wetness Impregnation	EtOH/ Oxalic Acid	TiO ₂	2	1
5% V-WI _(EtOH) /Ti-3 days	Wetness Impregnation	EtOH/ Oxalic Acid	TiO ₂	5	3
5% V-WI _(EtOH) /Ti-6 days	Wetness Impregnation	EtOH/ Oxalic Acid	TiO ₂	5	6
5% V-WI _(EtOH) /Ti-12 days	Wetness Impregnation	EtOH/ Oxalic Acid	TiO ₂	5	12
5% V-WI _(EtOH) /Ti-24 days	Wetness Impregnation	EtOH/ Oxalic Acid	TiO ₂	5	24
5% V-WI _(EtOH) /Ti-33 days	Wetness Impregnation	EtOH/ Oxalic Acid	TiO ₂	5	33
5% V-WI _(EtOH) /Ti-46 days	Wetness Impregnation	EtOH/ Oxalic Acid	TiO ₂	5	46
5% V-WI _(Aq) /Ti	Wetness Impregnation	Water	TiO ₂	5	1
0.5% V-WI _(EtOH) /Ti/Si	Wetness Impregnation	EtOH/ Oxalic Acid	Ti/Si pellet via ALD	0.5	1

3.1.2 Materials and Catalyst Preparation for ALD Catalysts

ALD deposition of either titania or vanadia phases was conducted in an anhydrous environment. An anaerobic atmosphere for metal oxide incorporation was created by using a three neck round bottom flask attached to a continuous flow of nitrogen. Silica Pellets (3.18 mm diameter, 261 m²/g, 1.09 cc/g pore volume, median pore diameter 115Å, Alfa Aesar) and 120 ml toluene (anhydrous, 99.8%, Sigma-Aldrich) were added to the flask and N₂ (Ultra-High grade, Linde) flow to the system immediately started. The experimental setup is depicted in Fig. 3-1. The toluene mixture was stirred and heated to reflux (393K, toluene boiling point) keeping a constant bubbling of nitrogen through the

system. The flask was attached to a reflux condenser and a Dean-Stark apparatus, to ensure toluene was refluxed back into the system and water removed. Desiccant was added to the top of the reflux column to ensure atmospheric moisture did not enter the system. The system was left at reflux for 24hrs.

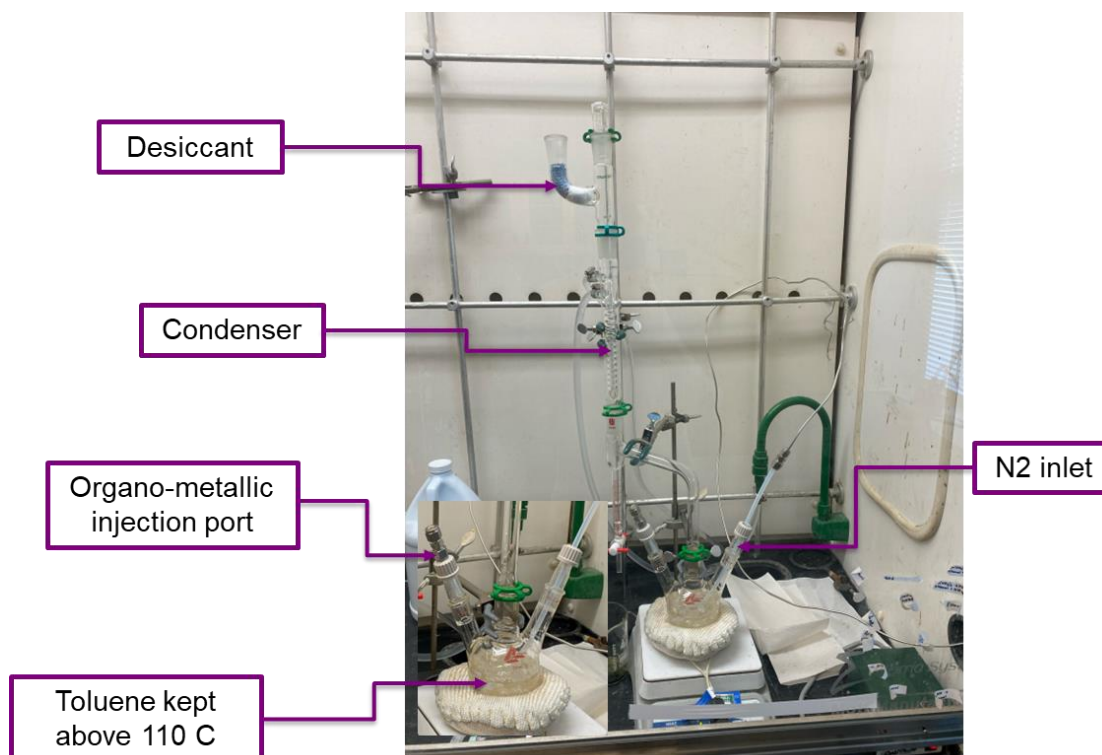


Figure 3-1 Experimental System used for Atomic Layer Deposition of Metal Oxide Phases on Solid Pellets

After this time elapsed, an alkoxide precursor for TiO_2 or VO_x was added using a syringe. The amount of alkoxide added was adjusted based on the desired loading of metal oxide in the solid, for the case of titania incorporation the amount of precursor used corresponded to the amount needed to achieve complete monolayer coverage of SiO_2 , calculated based on the silica pellet surface area, which equates to ~ 10 wt%. For the case of TiO_2 , titanium (IV) isopropoxide, (99.999%, Sigma-Aldrich) was used, for impregnation of VO_x the precursor used was vanadium tri-isopropoxide oxide (96%, Sigma-Aldrich).

After addition of the alkoxide precursor the system was left at reflux and under N₂ flow for another 24 hours to ensure any water formed during the deposition process was removed. After 24 hours the system was cooled down in N₂ atmosphere. The suspension was then transferred to a round bottom flask where it was then subject to vacuum distillation using a rotary evaporator (Heidolph) to remove the solvent. The pellets were dried in an oven at 413K for 24 hours to remove any remaining toluene. Afterwards the pellets were calcined at 823K for 8 hours in air (80 SCCM, Extra-Dry Grade, Linde) to generate the desired metal oxide phase. Materials prepared following this methodology included titanium oxide ALD impregnated over SiO₂ pellets and vanadium oxide ALD impregnated over the formed Si/Ti pellets and. After these materials were prepared, the pellets were analyzed using UV/Vis spectroscopy to confirm the presence of the deposited metal oxide phase on the pellets.

For the case of the TiO₂ impregnated/SiO₂ a second deposition step followed to incorporate the vanadium oxide phase. Either through wetness impregnation methodology, following the procedure described in Section 3.1.1, or through a second ALD step using the amount of vanadium tri-isopropoxide oxide required to achieve the desired vanadium loading (8-11 wt%). This was conducted following a similar process to the ALD methodology described above, calcination of the vanadium loaded pellets occurred at 723K for 4 hours in air (80 SCCM, Linde, Extra-Dry Grade). Table 3-2 lists all the materials prepared using ALD.

Table 3-2 List of ALD Catalysts Prepared and Formulation Conditions

Catalysts Sample	Preparation Method	Support Pellet	Titanium Loading (wt%)	Vanadium Loading (wt%)
Ti/Si	ALD	SiO ₂	10	0
8% V-ALD/Ti/Si	ALD	Ti/Si	10	8
11% V-ALD/Ti/Si	ALD	Ti/Si	10	11

3.1.3 Evaluation of Titania and/or Vanadia Incorporation

We used UV/Visible spectroscopy in diffuse reflectance mode to confirm the incorporation of the vanadia and titania phases on the materials and to evaluate the degree of dispersion of the incorporated phases at the nanoscale. Whole and cross section areas of the pellets were evaluated, both vanadium oxide and titania have distinct UV/Vis signals that correspond to their band gap transition energies. These analyses were carried using both a Cary 4000 (Agilent) and UV-VIS-NIR model 3600 spectrometer (Shimadzu) equipped with a Harrick Praying Mantis for DRS analysis. Spectra was collected in the 200-800 nm region using a step-size of 1 nm. Barium sulfate (99%, Sigma-Aldrich) was used as a reflectance standard.

The area of analysis of the pellet was controlled by visually positioning the light beam (set at 530 nm, green color) on the pellet surface at the spot selected for spectral collection. After data acquisition, the contributions from the TiO₂ pellet, SiO₂ pellet, or Ti/Si pellet were subtracted, and the spectra transformed to a Kubelka-Munk function. The UV bandgap energy E_g was then obtained using the David and Mott's correlation for a direct allowed formalism for the electronic transition and extrapolate the linearized part of the band edge profile to obtain the axis intercept (eV) (Nobbs, 1985).

UV/Vis of the vanadium precursor solution was also measured using a Shimadzu 2100 instrument in transmission mode using quartz cuvettes. Absorbance spectra was obtained between 350-800nm at a step-size of 0.5nm. Three samples of 50 mL solution were prepared following procedures for catalyst preparation of 5 wt% loaded vanadium on 5g of support. Aliquots were taken at selected times during catalyst preparation (see Section 3.1.1) Before UV the spectra were taken a 1.5 M oxalic acid in ethanol solution was used to dilute the samples at a 4:1 dilutant to sample ratio, this solution was also used as reference for the measurements.

Wavelength Dispersive Spectroscopy (WDS) was done on sample cross-sections to determine the distribution of vanadium, titanium, and silicon throughout the cross-section. Elemental maps were obtained for several samples using a JEOL JXA-8530F electron microscope. Catalyst samples were mounted in epoxy and cut revealing the

cross-section distribution of the different phases present. These epoxy mounts were carbon-coated before WDS maps were performed at a 5-micron resolution, identifying several of the present phases such as vanadium, titanium, and silicon.

FT-IR analysis was carried on the crushed titania pellet ($261 \text{ m}^2/\text{g}$, 1.09 cc/g pore volume, Median Pore diameter 140 \AA , 1% Sulfur Content, Alfa Aesar), crystalline vanadium ($\geq 99.6\%$, Sigma-Aldrich), and 5% V-WI_(EtOH)/Ti using a Bruker Alpha II spectrometer. The pelletized sample was carefully scraped to remove the vanadium rich outer-layer and avoid contamination of the IR signal from the titanium rich pellet core. IR analysis was done within the 400-2000nm region using a step-size of 2 nm. X-Ray Diffraction (XRD) analysis was taken to determine how dominant crystalline vanadium was in the sample as well as to confirm the presence of anatase phase for TiO₂ after calcination. Whole pellets of the 5% V-WI_(EtOH)/Ti sample were crushed into a wafer and analyzed using a Inel CPS Powder Diffractometer (Cu $\kappa\alpha$ source). Testing was done in the 2-theta range of 20-80° with a step size of 0.032°

3.1.4 Catalytic Activity Testing

Catalyst reactivity including conversions and selectivity were tested using an integral reactor, via direct-injection of 2 ml of gaseous sample via syringe using a SRI 8610C gas chromatograph with N₂ as the carrier gas, equipped with a packed column (SRI Hayesep D, 2 m), an on-stream methanizer with Ni catalyst (648 K and 20 SCCM of H₂), and a flame-ionization detector (FID). Between 1.38-3.27 grams of catalyst sample was loaded into a 3/8" Swagelok tube with quartz wool (Sigma-Aldrich) and acid-washed silicon dioxide (Sigma-Aldrich) on the bottom of the bed to ensure zero blow through of active phase. After catalyst loading, the reactor is integrated into an offline sampling system as given in Figure A-1 in Appendix A. The catalyst pellets are then pretreated in a 20% O₂/Argon (both Messer Grade 5.0) under a temperature ramp to 573K for 1 hour and then at 573K for another hour before being cooled to reaction temperature. Methanol (99.8% anhydrous, Sigma-Aldrich) is then injected into the system using a micro-syringe pump at a partial pressure of 20 kPa, the methanol flowrate is adjusted depending on total flow rate used in the test. Oxygen flow rate is adjusted to reach 10 kPa partial pressure. After allowing sufficient time to allow the system to reach steady state samples of the reactor

outlet are manually taken at 15 min intervals and injected into the GC system. Several injections are taken at each condition to ensure reproducibility and consistency of results. After adequate results are obtained the next set of reaction conditions (flow rate, temperature, etc.) is selected. After a steady state for the new condition is reached for 25 minutes, sample collection under the new condition is conducted.

A temperature range of 393-573K was selected to ensure thermodynamic conditions favourable for DMM production. As the acetalization step is thermodynamically limited the maximum attainable methanol conversion as well as the selectivity towards DMM over the temperature range can be calculated if the system reached equilibrium. This data is given below in Table 3-3, calculated using relevant thermodynamic values from the NIST database and assuming methanol is first converted initially to form a 2:1 methanol to formaldehyde ratio before undergoing the acetalization step.

Table 3-3 Thermodynamic Limitations for Methanol/Formaldehyde Acetalization if System Approaches Equilibrium

Temperature (K)	Methanol Conversion (%)	DMM Selectivity (%)	Formaldehyde Selectivity (%)
393	70.6	79.2	20.8
403	66.0	74.2	25.8
413	61.3	68.5	31.5
423	56.8	62.0	38.0
433	52.6	54.9	45.1
443	48.7	47.4	52.6
453	45.3	39.6	60.4
463	42.5	32.2	67.8
473	40.1	25.4	74.6

As the system is open and not closed (such as if it were a batch reactor), these equilibrium limitations should not play a heavy factor in determining the selectivity and conversions of the presented system as the products are constantly being removed.

For the temperature range, initially a 15K change between conditions was first selected with a final 20K change between 453K-473K. This was later lowered to four conditions (393K, 423K, 453K, 473K) as the four temperatures were able to provide an equally

informative activity profile as compared to the original six points. Additionally, two flow rate conditions were selected. A high flow rate of 250 SCCM and a low flowrate condition of 50 SCCM total. There was a fluctuation for the residence times of different samples due to varying support densities and bed packing, the calculated values of the space velocities thus are adjusted accordingly all falling in the range of 2200 to 10200 ml $g_{cat}^{-1}h^{-1}$.

Selected small-scale tests were done on differential reactor systems. For these cases between 60-100mg of crushed pellet sample (sieved to 40 or 120 mesh) was loaded to a ¼ inch quartz microreactor systems with online GC analysis (in some cases, the catalyst bed was diluted using acid-washed silica (Sigma-Aldrich)). These small-scale experimental systems are similar to the experimental setup given by Yun on page 205 of his doctoral thesis and as such can be referenced for a more detailed description (2016). For the case of the 11% V-ALD/Ti/Si sample online analysis was carried using an SRI 8610C gas chromatograph with N₂ as the carrier gas, equipped with a packed column (SRI Hayesep D, 2 m), an on-stream methanizer with Ni catalyst (648 K and 20 SCCM of H₂), and a flame-ionization detector (FID). In this case 100 mg (particle size 125-180 µm) of catalyst was diluted in a glass reactor with acid-washed silica of the same particle size to get a total bed weight of 500 mg. The sample was pretreated at 573K for 1 hour in 50 SCCM a 20 O₂/Argon mixture (both Messer Grade 5.0). For the 5% V-WI_(Aq)/Ti methanol (99.8% anhydrous, Sigma-Aldrich) was fed into the reactor at a 1 kPa partial pressure with either a 10 kPa or 0.5 kPa concentration of oxygen. A balance of argon was used to achieve 101.3 kPa. The catalyst was evaluated at 423K and 453K at 3000 ml $g_{cat}^{-1}h^{-1}$ space velocity, data collected and presented were gathered at steady-state conversions.

The crushed 11% V-ALD/Ti/Si sample was analyzed using the same system. In this case 110 mg (particle size 125-180 µm) of catalyst was diluted in a glass reactor with acid-washed quartz of the same particle size to get a total bed weight of 500 mg. The catalyst was pretreated at 573K for 1 hour in 50 SCCM a 20 O₂/Argon mixture (both Messer Grade 5.0). Formaldehyde was generated by the decomposition of paraformaldehyde (95%, Aldrich) at 348 K with an argon flow of 22 SCCM, yielding a gas mixture that was

approximately 1 kPa formaldehyde. This mixture was initially fed into the reactor along with 10 kPa oxygen and balance argon to obtain a total pressure of 101.3 kPa at 453K. A constant space velocity of $27300 \text{ ml g}_{\text{cat}}^{-1}\text{h}^{-1}$ was obtained and once enough data points were generated at steady-state, 1 kPa of methanol (99.8% anhydrous, Sigma-Aldrich) was added to the feed stream and more data points at steady state were collected.

The activity tests on the Ti/Si catalyst and bare Si samples were done on a different microreactor system equipped with a Shimadzu gas chromatograph, GC-2014 with a capillary column (DB-624, $30 \text{ m} \times 0.250 \text{ mm}$, $1.40 \mu\text{m}$ thickness) connected to a flame ionization detector (FID). 60 mg of powdered sample ($425\text{-}600 \mu\text{m}$) was loaded into a quartz micro-reactor packed with quartz wool to prevent blow through. Catalyst pre-treatment conditions were kept consistent with the large-scale tests with the substitution of air (Ultra-Dry Grade, Linde) made for the 20 kPa O₂-Argon mixture. A mixture of 5% O₂ in He (Certified Mixture, Linde) and Argon (Ultra-High grade, Linde) was added to obtain a total flowrate of 13 SCCM (space velocity of $13000 \text{ ml g}_{\text{cat}}^{-1}\text{h}^{-1}$) and a total O₂ pressure of 2.5 kPa, Methanol (99.8% anhydrous, Sigma-Aldrich) was fed into the reactor to obtain a partial pressure 5 kPa (balance Helium/Argon to achieve 101.3 kPa). This maintained the 2:1 methanol to oxygen ratio used in the large-scale reaction tests. This feed stream was allowed to stabilize with the samples for 40 minutes before 10 runs for each sample were conducted to ensure repeatability of the results and that the catalyst had reached steady state, an average of 120 minutes per tested condition.

Catalyst activity is defined using the following terms: conversion and selectivity.

Conversion is defined as the amount of feed converted by the reaction and typically given as a percentage. 0% represents all the feed passing through unreacted and 100% represents complete conversion. The calculation for the conversion of a species “i” is given below in Equation 3-1. Note “N” represents the molar flow per unit time.

$$\frac{N_{i \text{ IN}} - N_{i \text{ OUT}}}{N_{i \text{ IN}}} \times 100\% \quad (3 - 1)$$

Selectivity is defined as the fraction of the product obtained as compared to the other potential products. This is typically normalized to account for stoichiometry and does not

include the unreacted feedstock. The calculation for the selectivity of a species “i” is given below in Equation 3-2. Note “ v_i ” represents the stoichiometric molar requirement from a reaction for a species, “ X_i ” represents the molar fraction of that species in the product stream, and “ v_r ” represents the stoichiometric requirement from the reactant.

$$\frac{v_r X_i}{v_i \sum_i v_r X_i} \times 100\% \quad (3 - 2)$$

3.2 Results Obtained on Initial Catalyst Formulations

3.2.1 Introduction

By coupling the previously described (Section 2.6.3) mechanistic knowledge of DMM formation obtained in microreactors operating under differential conditions and the theoretical and practical considerations constraining large scale catalysts preparation, we can arrive an idealized morphology for the industrial-scale DMM catalyst. The results available in the literature and described in Section 2.6.3 indicated that, in a V/Ti catalyst, the V-O-Ti moieties present on the catalyst surface are crucial for both the redox and acid site properties required for the DMM reaction (Broomhead, et al. 2022). In addition, the DMM reaction network contains numerous by-products as described in Section 2.5 and Figure 2-8 requiring careful catalytic tuning. As such, the degree of vanadium dispersion is essential to maximize the efficiency of these V-O-Ti moieties to produce valuable products and minimize the formation of unreactive crystalline V_2O_5 on the catalytic surface. Broomhead et al. reported that the optimum dispersion to obtain high DMM yields is achieved when a two-dimensional vanadia monolayer is formed on the titania surface. The extreme cases for possible dispersion levels that can theoretically be achieved on VO_x/TiO_2 catalysts are shown in Figure 3-2. These include isolated VO_4 monomers (Fig. 3-2, left) a two-dimensional VO_x monolayer (Fig. 3-2 center) and nanocrystalline agglomerated V_2O_5 (Fig. 3-2, right). V-O-Ti moieties are maximized in only two of these three cases.

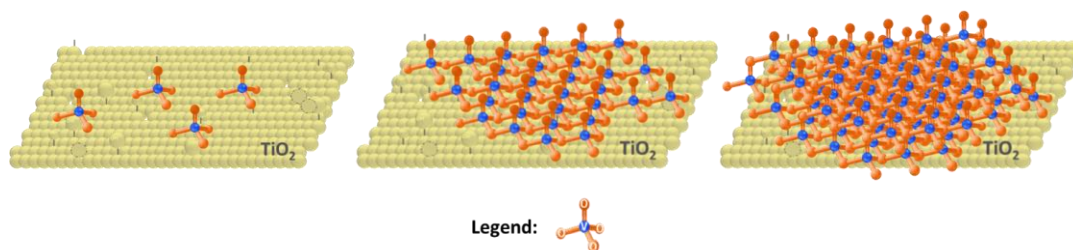


Figure 3-2 Different Vanadium Dispersions on Titania Surface. From left to right: monomeric vanadium, vanadium monolayer, crystalline vanadium. The legend refers to an isolated tetrahedral vanadium oxide monomer (VO_4^{-3})

While monomeric vanadium contains the most V-O-Ti moieties, this dispersion is very unselective towards DMM formation. This is partially due to the excess titania sites that are left exposed as evidenced in Figure 3-2. As reported in Section 2.6.3 these bare titania sites are the contributing factor to methyl formate production. The other reason is that the transition state upon methanol adsorption is less stable for monomeric vanadium than with agglomerated vanadia as the V-O-V bonds, absent in monomers, are used to delocalize the electrons from the adsorbed methanol during the C-H scission rate limiting step for formaldehyde formation (Broomhead et al., 2022). Thus, despite the higher number of V-O-Ti moieties, monomeric vanadium is not desired.

UV/Vis spectroscopy enables us to differentiate between these possible structures, as the energy bandgap is sensitive to the average domain size of the vanadia structure (Gao and Wachs, 2000). As the energy required for the electronic transition is a function of the size of the VO_x cluster this can be easily correlated to determine the vanadium dispersion on the titania surface as evidenced in Figure 3-3 below.

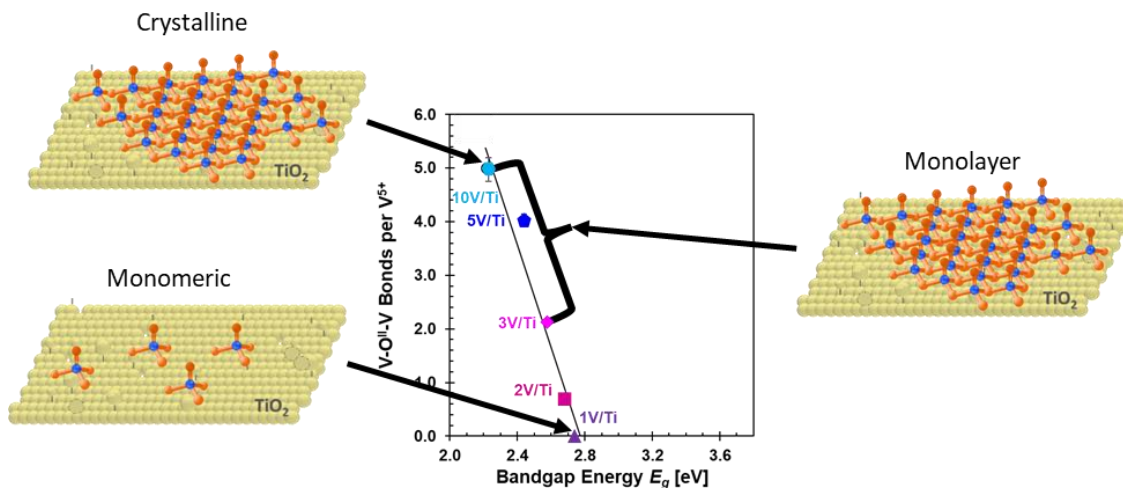


Figure 3-3 Supported Vanadia UV Bandgap vs Cluster Size with Vanadium Dispersions adapted from Broomhead et al., 2022

It is well established that two-dimensional monolayer coverage of VO_x on TiO_2 is achieved in powdered TiO_2 anatase phase ($58 \text{ m}^2\text{g}^{-1}$) at loadings above 3 wt % vanadium, as confirmed by using the UV spectra of the catalyst. As the value of the bandgap energy of vanadium oxide is a function of its dispersion, UV analysis can also be used to evaluate whether monolayer dispersion has been achieved or not (Gao and Wachs, 2000; Broomhead et al., 2022). Figure 3-4 shows the results obtained in V/Ti powder samples used for DMM production from methanol; with a more dispersed catalyst, obtained at lower vanadia loadings, having a higher bandgap energy (Broomhead et al., 2022).

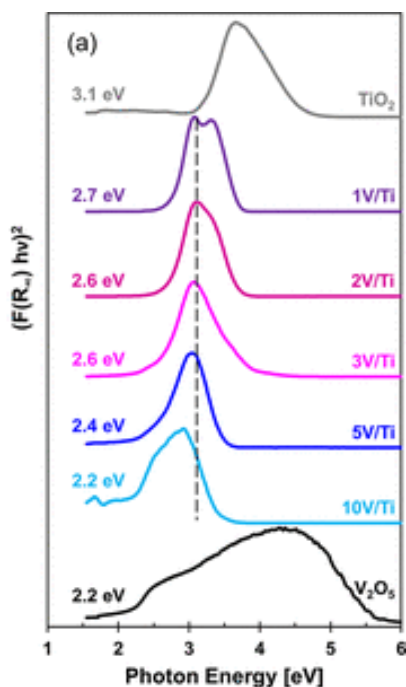


Figure 3-4 UV Bandgaps and Transformed UV Spectra for Powdered Catalyst Samples from Broomhead et al., 2022

From these recorded values for the bandgap energy and using as starting point previously obtained results (Section 2.6.3) indicating that in the powdered V/Ti the 3-10wt% catalysts performed significantly better for DMM production, we can state that vanadium oxide anchored on TiO_2 displaying a bandgap energy range between 2.2-2.5eV is forming a monolayer structure on the catalyst surface will be catalytically active for selective DMM production from methanol.

Despite this information, the ability to translate the molecular-level vanadium distribution from a powdered catalyst to a pelletized form, will require further considerations. Specifically, how the macro-distribution of a vanadium monolayer throughout a pellet can affect DMM yields. As previously discussed in Chapter 2, there are four distinct macro-level dispersions that can be attained when utilizing wetness impregnation for pelletized catalyst preparation. Three of these four (eggshell, egg-yolk, and egg-white) contain significant portions of bare support. With the V/Ti catalysts this means that bare TiO_2 will be exposed. As the Lewis acid sites associated with TiO_2 are the primary active site for methyl formate production, exposed TiO_2 should be minimized, making these

three dispersions, at least at a preliminary stage of catalyst pellet development, undesirable. Additionally, there are no known poisons in the methanol stream, and if a packed bed reactor is to be used, attrition is not a significant concern. Consequently, the benefits associated with an egg-yolk and an egg-white pellet morphology catalysts are not required for DMM synthesis. As mentioned in Section 2.7.1 Catalysts with eggshell dispersions show good selectivity toward intermediate products in sequential reactions which may help reduce over-oxidation of formaldehyde; however, any extra formaldehyde produced would be exposed to significant free titania, potentially resulting in the formation of methyl formate over exposed TiO_2 -Lewis sites, limiting the effectiveness of this dispersion. Ultimately, a homogenous dispersion would ensure that the amount of exposed TiO_2 is limited and thus methyl formate production is limited. As such the homogenous dispersion is the ideal starting point for the scaling up process for the vanadium/titania catalyst.

3.2.2 1st Generation Catalyst: “Proof-of-Concept” and Testing

Since impregnation of vanadium onto powdered TiO_2 is usually carried using wetness impregnation of a vanadate salt dissolved in a solution of oxalic acid in ethanol due to oxalic acid’s ability to create well-dispersed vanadia catalysts as opposed to other preparation methods (Satsuma et al., 2002). A modification of this methodology was first attempted for the impregnation of vanadium as a “proof-of-concept”, to first evaluate whether acceptable levels of vanadium dispersions could be achieved.

For this set of experiments, cylindrical TiO_2 pellets were chosen, since this is a preferred geometry for industrial catalysts used for formaldehyde synthesis from methanol as discussed in Chapter 2, likely due to their ability to provide adequate heat transfer to maintain bulk reaction temperatures throughout the bed (Partopour and Dixon, 2020). Two formulations were prepared using ethanolic oxalic acid solutions: one with a vanadium oxide weight loading of 2% and another one with 5% weight.

3.2.3 Catalyst Characterization Results

The UV/Vis spectra obtained for the two catalysts prepared (2 and 5 wt% vanadium on TiO_2 pellets) is shown in Fig. 3-5. As described above, a monolayer dispersion of

vanadium oxide, favourable to DMM production, will result in a bandgap energy range between 2.2-2.5eV. This “tolerance” range is also depicted in Figure 3-5. The bandgap value obtained for the 5% V-WI_(EtOH)/Ti samples was 2.26 eV and 2.46 eV for the 2% V-WI_(EtOH)/Ti formulation. As expected, a lower vanadium loading provides better dispersed vanadium, nearing the upper range of bandgaps associated with dispersions able to produce high DMM yields. Meanwhile the bandgap associated with the 5 wt% catalyst is nearing the lower bounds of the acceptable range and is close to that obtained on crystalline V₂O₅ and 10 wt% V/Ti powdered samples. As both spectra are within the tolerance range set out in Section 3.2.1 the vanadium dispersion can be described as near monolayer.

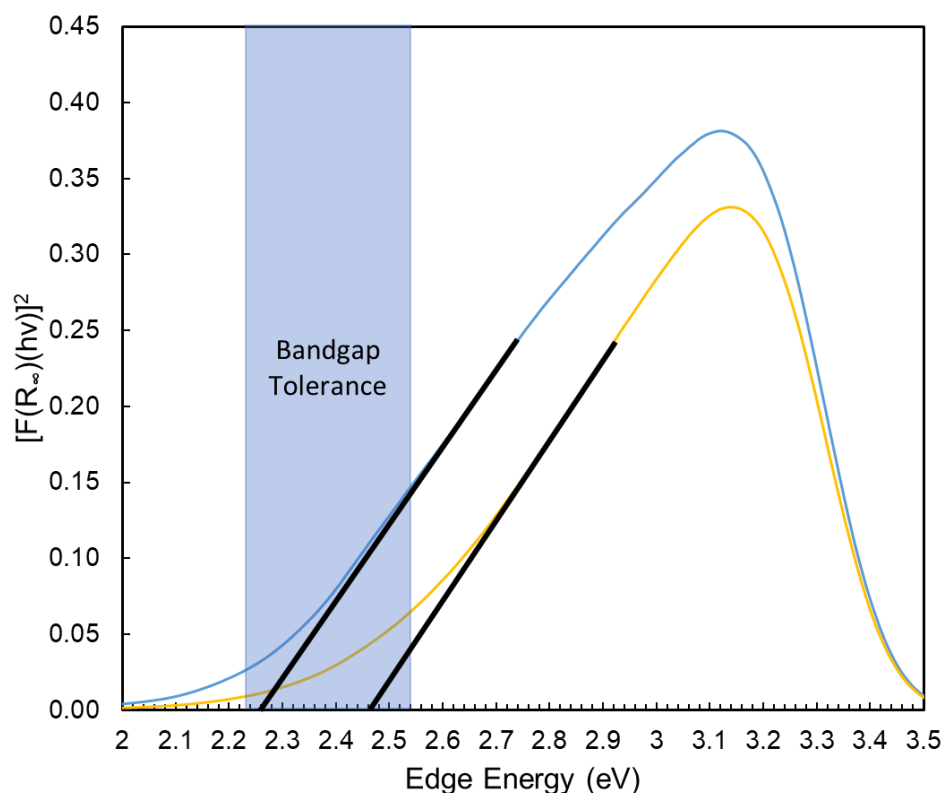


Figure 3-5 UV Spectra of 5% V-WI_(EtOH)/Ti (Blue) and 2% V-WI_(EtOH)/Ti (Yellow). The area shaded in blue represents the range of bandgap values associated with high DMM production.

Once the vanadium dispersion was evaluated, it was important to determine which macro distribution of vanadium was achieved throughout the pellet. In other words, whether a homogenous dispersion had been achieved or eggshell, egg-yolk, or egg-white morphologies had been achieved instead. Optically magnified pictures were obtained on selected catalyst pellets, typical results are depicted in Figure 3-6.

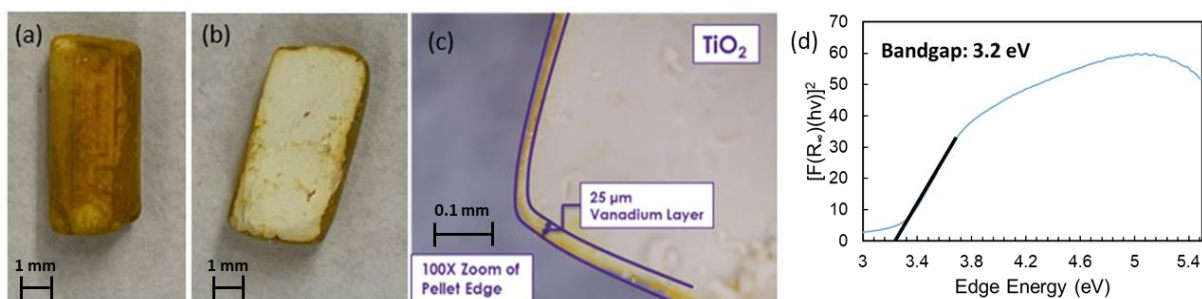


Figure 3-6 Optical Pictures of Typical 5% V-WI_(EtOH)/Ti Pellet and UV Bandgap at Cross-Section. (a) 5X zoom of whole pellet (b) 5X zoom of cross-section (c) 100X zoom of cross-section edge with depth of vanadium penetration clearly observed (d) Edge Energy of pellet cross-section taken at the center of the pellet showing a pure titania anatase phase

Figure 3-6 (a) shows the outer surface of the impregnated 5% V-WI_(EtOH)/Ti pellet where the yellow color characteristic of V₂O₅ is clearly seen covering the catalyst. Upon examination of the cross-section (Figure 3-6 (b)) a majority of the pellet is uncovered by this vanadium oxide phase past the surface. Once the cross section is zoomed-in, it is revealed that the vanadium seems to have only penetrated a few micrometers into the support (Figure 3-6 (c)). While visually the amount of bare titania seems substantial, other analyses are required to confirm this hypothesis to determine if vanadium had penetrated further than visually apparent. UV spectra was obtained for the cross-section of the pellet shown in Figure 3-6 (d). The UV obtained at the center of cross-section gave a bandgap value of 3.2 eV which is characteristic of anatase titanium (Dette et al., 2014), meaning vanadium penetration was unlikely. Wavelength Dispersive Spectroscopy (WDS) of the cross-section was also done and allows for mapping of the catalyst pellet with resolutions of less than a micron while being able to differentiate between the vanadium and titanium in the sample (Mengason and Ritchie, 2017). The vanadium

distribution throughout the pellets radial cross-section is given by the WDS scan for the 5% V-WI_(EtOH)/Ti in Figure 3-7.

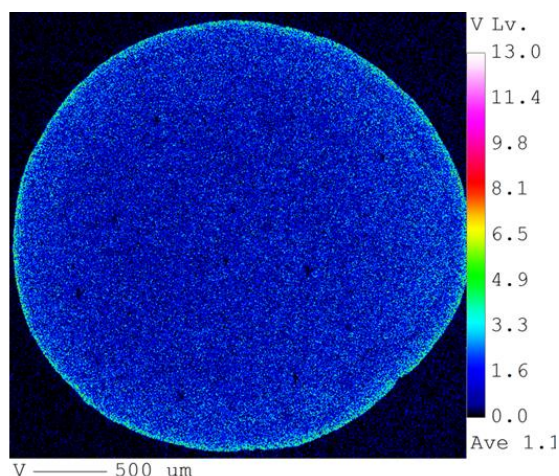


Figure 3-7 WDS Mapping of Vanadium on the Cross-Section of the 5% V-WI_(EtOH)/Ti Catalyst Pellet

Figure 3-7 confirms what was seen visually in Figure 3-6 that vanadium does not penetrate past the outer surface of the pellet and is concentrated within the first few micrometers of the support. While there was some signal from vanadium towards the center of the pellet this was most likely caused by the overlap between the vanadium κ_{α} and titanium κ_{β} electron signals in the WDS which is well known in literature (Carpenter, 1997). Based on both the optical micrographs, the UV/Vis, and WDS data it is clear that the vanadium has arranged itself in an eggshell dispersion and has not penetrated much more than a few micrometers towards the catalyst, likely in a monolayer form. To further confirm that vanadium oxide is forming mostly a two-dimensional monolayer (i.e., the absence of nanocrystalline structures) XRD analysis was conducted for the 5% V-WI_(EtOH)/Ti sample, the data obtained is presented in Figure 3-8.

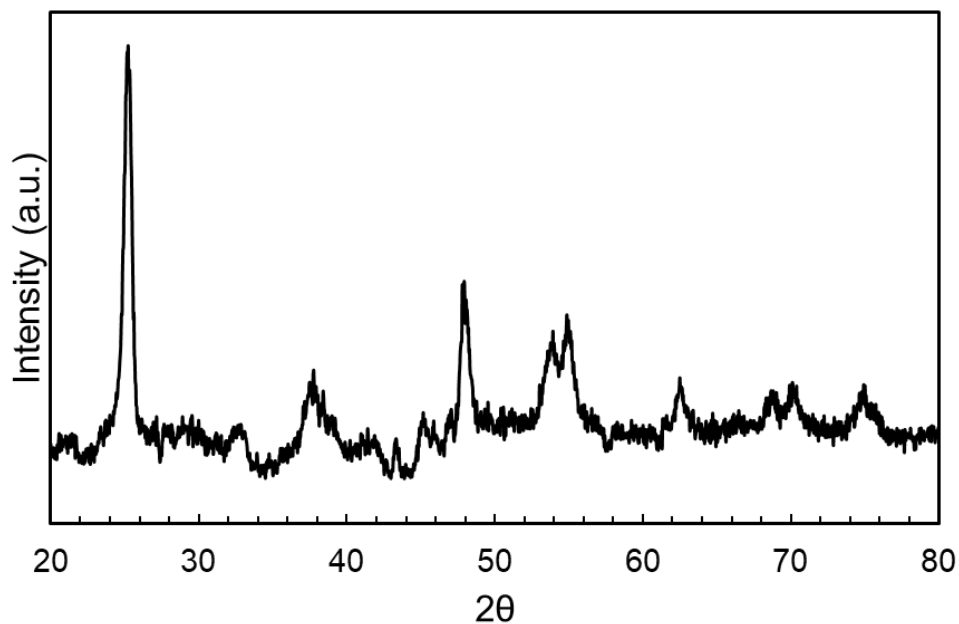


Figure 3-8 XRD Data for a 5% V-WI_(EtOH)/Ti Pellet after Calcination. The characteristic peaks for anatase (25°, 38°, 49°) are clearly observed. (JCPDS card no. 21-1272)

Based on the XRD data in Figure 3-8 all peaks present from the 5% V-WI_(EtOH)/Ti sample are associated with the presence of titania in the anatase phase. Peaks associated with crystalline vanadium +5 oxide are not observed. This could be due to several factors such as crystalline vanadium not forming large enough domains (Holder and Schaak, 2019). The vanadia present in monolayer form is also difficult to distinguish from the anatase Ti signal as the XRD signal for these vanadium-titania complexes are located closely to those of the anatase phase cannot be differentiated at the 5 wt% loading (Jin et al., 2014). It should be noted as well that reports on samples with much higher loaded V/Ti catalysts (18 wt%) provide XRD spectra that does not show the presence of vanadium oxide either (Radko et al., 2018). The lack of rutile phase titania peaks observed in Fig. 8 is also worth mentioning as vanadium ions diffuses into the rutile domains during phase transition of the titania and become unavailable for catalysis (Bañares et al., 1996) While this phase transition normally occurs on pure anatase titanium at 973K-1073K, the vanadate ions promote this transformation allowing it to occur at temperatures as low as 823 K (Radko et al., 2018). Previous literature reports a peak which is characteristic of rutile titania at a slightly higher angle than the anatase peak at 25 degrees (Radko et al.,

2018). As illustrated below, after calcination this peak does not appear in our samples confirming that the integrity of the pellet is maintained, and the dominant phase of titania remains anatase.

Another technique we used to determine the presence of crystalline vanadium was FTIR. The spectra for the un-impregnated pure titanium pellet as well as the 5% V-WI_(EtOH)/Ti sample, and bulk V₂O₅ are presented below in Figure 3-9.

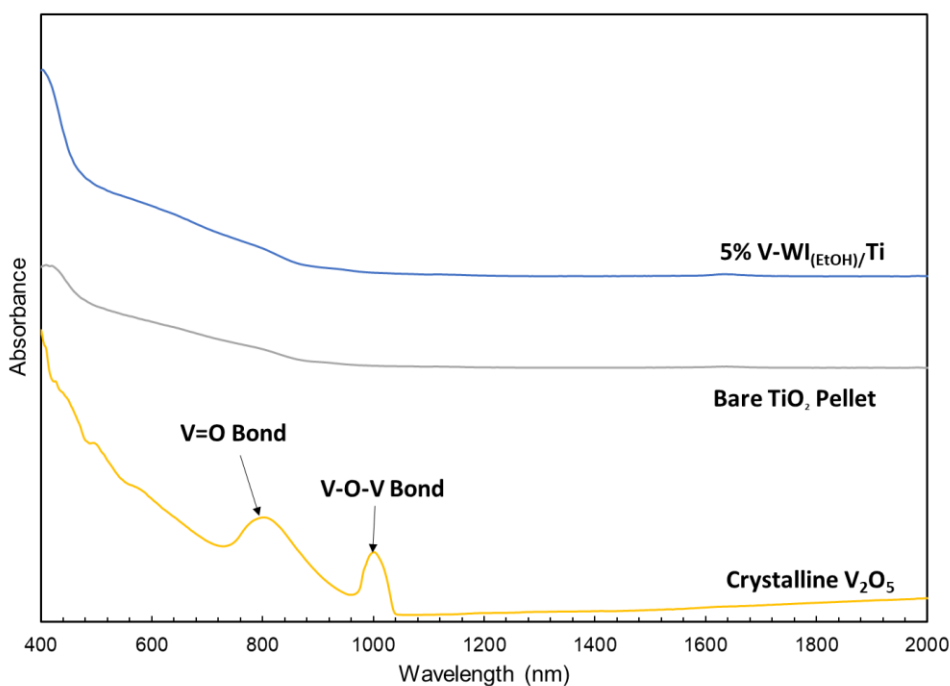


Figure 3-9 FT-IR Spectra of Pure V₂O₅, blank TiO₂ Pellet, and 5% V-WI_(EtOH)/Ti Sample. Responsible bonds labeled using data from Shafeeq et al., 2020

There are two characteristic peaks associated with the crystalline V₂O₅ representing the V=O bond and the V-O-V bridge bond located at 800 and 1000 nm, respectively (Shafeeq et al., 2020) As the TiO₂ pellet had an observable signal at 800 nm the V=O signal would be masked by titania making the V-O-V signal at 800 the determinant signal if crystalline V₂O₅ was significantly present in the 5% V-WI_(EtOH)/Ti sample. As no noticeable peak was observed at 1000 nm for the 5% V-WI_(EtOH)/Ti sample, the vanadium impregnated on this sample is not in the crystalline phase closely interacting with the titania as desired.

While the eggshell dispersion is not the desired distribution of vanadium for DMM production; hypothesized in Section 3.2.1, as needed to be homogenous, the microstructure of the catalyst is within the optimum bandgap range, indicating that the nano-dispersion of the vanadium is adequate. While the higher-loaded 5% V-WI_(EtOH)/Ti sample had a bandgap nearing the crystalline region further XRD and IR analysis showed that despite this more agglomerated dispersion, crystalline vanadium was not present in quantifiable amounts. These results confirmed that most of the vanadium active phase would be reactive towards DMM production. As a result, catalyst performance was evaluated for both loadings (5% and 2%) elucidate the effect that an improper macro-distribution might have on the catalyst when desired nano-dispersion were achieved.

3.2.4 Catalyst Activity Evaluation

The characterization results obtained of 5% V-WI_(EtOH)/Ti and 2% V-WI_(EtOH)/Ti samples indicate that we were able to successfully translate the morphology of the vanadium phase from the powder to the catalyst pellet from of the material. However, the vanadium oxide was not homogenously impregnated in the TiO₂ pellet. Therefore, we set to determine the effect this heterogenous dispersion of the vanadium phase in the pellet on catalytic activity. The results obtained are presented in Figure 3-10, which depicts conversions and product selectivity obtained at steady state at different temperatures for these two samples.

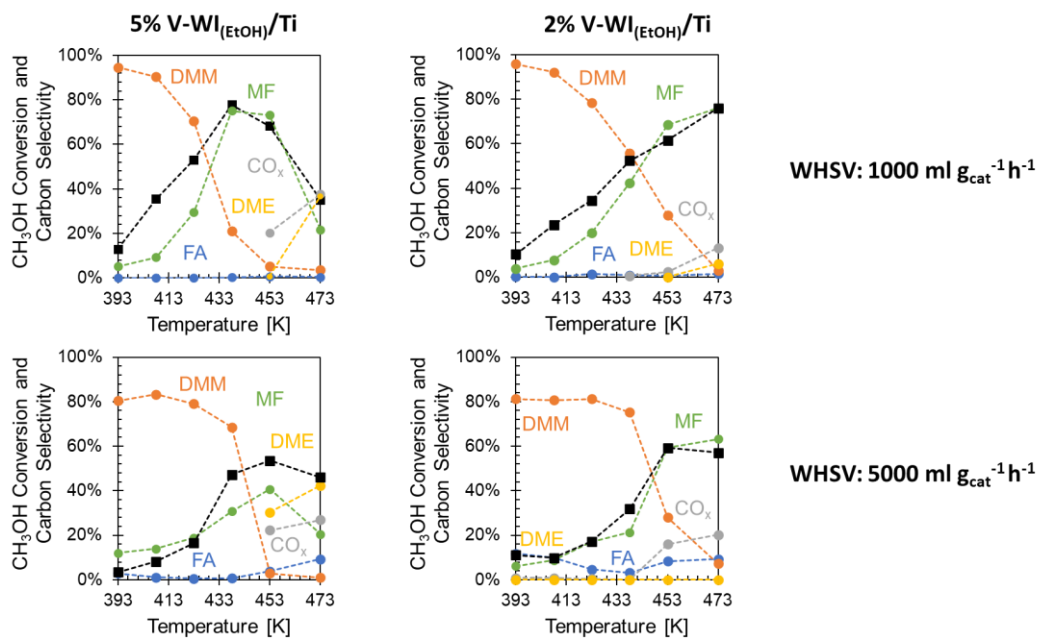


Figure 3-10 Catalytic Activity for V-WI_(EtOH)/Ti Catalysts at Two Space Velocity Conditions. Black Square: Methanol Conversion, FA: Formaldehyde, MF: Methyl Formate. 3.06g of the 5% V-WI_(EtOH)/Ti and 3.08g of the 2% V-WI_(EtOH)/Ti whole pellets tested between 393K-473K, 20 kPa methanol and 10 kPa oxygen; balance argon. 50SCCM/250SCCM

When examining the catalytic activity for the higher loaded 5% V-WI_(EtOH)/Ti at the lower space velocity (top left panel), several trends are obtained. First, total methanol conversion increases with temperature achieving a maximum of 80% at 438K. The DMM selectivity was near 100% at low temperatures and decreased at higher temperatures until it neared 0% at 473K. Formaldehyde was not produced in noticeable quantities throughout the temperature range. Methyl Formate was initially formed in low quantities and then in a trend mirroring the conversion increased to just under 80% at 438K before decreasing to 20% at 473K. DME and CO_x are not observed on the samples collected below 453K but formed substantially at higher temperatures. CO_x first appears at 453K increasing to a 40% selectivity at 473K. DME was observed only at 473K (40% Selectivity).

At the high space velocity conditions (bottom left panel), the 5% V-WI_(EtOH)/Ti catalyst exhibits much lower methanol conversions, achieving a maximum of 54%. The trend also diverges from the low space velocity conditions as the conversion does not decrease substantially with temperature instead plateauing at 50% once 438K is reached. The DMM selectivity is high, lingering between 80-70% until it sharply decreases to near zero at 453K. Formaldehyde was observed at low quantities reaching a maximum of 9% at 473K. Methyl formate was also formed at low quantities, reaching a maximum of 40% at 453K, before dropping to 20% at 473K. CO_x was also formed but at lower quantities than at low space velocities, achieving a maximum of 27% at 473K. DME also appeared at 453K and achieved a maximum of 42%. Overall, increasing the weight hourly space velocity lowered the selectivity to methyl formate, increased DMM selectivity, and slightly increased formaldehyde production. This behaviour could be explained by the location of the active sites at the pellet surface.

The lower loaded catalyst (2% V-WI_(EtOH)/Ti) evaluated displayed similar behaviour to the 5% VO_x/TiO₂ sample, with a couple differing trends at the low space velocity regime (top right panel). Understandably conversion was higher for the 5% V-WI_(EtOH)/Ti catalyst than the 2% V-WI_(EtOH)/Ti. However, when normalizing per vanadium content the 2% V-WI_(EtOH)/Ti sample has a reaction rate of 12.4 mol (mol V⁻¹) h⁻¹ vs 7.7 mol (mol V⁻¹) h⁻¹ for the 5% V-WI_(EtOH)/Ti catalyst (at 423K). This suggests the 2% V-WI_(EtOH)/Ti catalyst was more efficient in its use of the active phase. Additionally, the decrease in conversion and methyl formate selectivity at higher temperatures seen with the 5% V-WI_(EtOH)/Ti did not occur with the lower loaded 2% V-WI_(EtOH)/Ti catalyst. Instead, lowered selectivity to DME and CO_x (6% and 13%, respectively) was observed. This may suggest that the conversion and methyl formate selectivity are competing with CO_x and/or the DME production. Other trends that are observed for the 2% V-WI_(EtOH)/Ti sample were DMM selectivity having a more gradual decrease with temperature than in the 5% V-WI_(EtOH)/Ti sample at similar space velocities; formaldehyde was again not substantially produced.

At the high space velocity condition, the 2% V-WI_(EtOH)/Ti catalyst achieved slightly higher maximum conversions than the 5% V-WI_(EtOH)/Ti sample at (59% vs 54%) at

453K. This could be attributed to the increase in DMM yields for the lower loaded catalyst in comparison to the higher loaded catalyst at this condition (28% vs 3%). Formaldehyde was produced steadily throughout the temperatures at a selectivity of about 9% while DME was not seen in substantial amounts under all temperatures assessed. Finally, compared to the 5% V-WI_(EtOH)/Ti sample. CO_x selectivity decreased achieving a maximum of 20% at 473K. Methyl formate followed a similar trend as the one observed for 5% V-WI_(EtOH)/Ti until 453K where it increased substantially to 63% at 473K for the 2 wt% loaded sample.

As mentioned above, CO_x was formed at a higher selectivity at and above 453K for 5% V-WI_(EtOH)/Ti than on the 2% V-WI_(EtOH)/Ti catalyst at low space velocities. With the increased CO_x yields, a decrease was observed in the 5% V-WI_(EtOH)/Ti sample's methanol conversion at both flowrates. However, an increase in CO_x selectivity did not result in lower conversions observed for the 2% V-WI_(EtOH)/Ti at a low space velocity albeit at lower CO_x productions and only a slight decrease at high space velocities.

3.2.5 Interaction of the Vanadium Impregnating Complex with the Titania Pellet

From the characterization tests conducted on both the 2 wt% V-WI_(EtOH)/Ti and 55% V-WI_(EtOH)/Ti samples. It is clear from the UV results that the vanadium dispersions are similar with both achieving a monolayer of vanadia. Additionally, the preparation methodologies were the same, apart from the amount of vanadium loaded onto the pellet. the morphologies for both can be described as an eggshell distribution. While WDS mapping was only done on the 5% V-WI_(EtOH)/Ti sample, this is a safe assumption as the loading of the active phase has insignificant effect on the distribution of the pellet (Munnik et al., 2015). As such this eggshell morphology means the vanadia is concentrated to the outer layers which through using WDS was confirmed to be no more than a few micrometers deep.

While both samples discussed achieved a monolayer of vanadium the dispersions were not the same. 5% V-WI_(EtOH)/Ti had a bandgap of 2.26 eV bordering the crystalline region (<2.20 eV) which was much lower than bandgap for the 5% V/Ti powdered phase

presented by Broomhead et al. being 2.4 eV (2022). Meanwhile the 2% V-WI_(EtOH)/Ti had a bandgap of 2.46 eV showing it was more dispersed than the higher loaded sample. This bandgap was similar to the 5% V/Ti powdered sample from Broomhead et al., despite half the vanadium loading content on the pellet. Ultimately this difference did not seem to affect the DMM productivity as yields remained largely the same at low temperatures when DMM was the primary product (<438K). At high temperatures (>438K) the more dispersed catalyst (2% V-WI_(EtOH)/Ti) showed better selectivity towards DMM and a lower selectivity towards DME and CO_x. The formaldehyde selectivity was lower than required (1:1 DMM to Formaldehyde molar ratio for optimum OME₃₋₅ synthesis from Section 2.2) for both catalysts, despite the better dispersed catalyst having slightly better formaldehyde production at high space velocities. As such it seems that in these pellets, the vanadium dispersion seems to be inconsequential as the DMM yields are very similar. The 5% V-WI_(EtOH)/Ti is slightly more efficient (0.987 mmol_{DMM} g_{cat}⁻¹ h⁻¹ at 423K and 1000 ml g_{cat}⁻¹h⁻¹). However, both catalysts did not produce enough formaldehyde to be viable for downstream OME production.

Neither catalyst had the desired homogenous active-phase distribution, instead forming a sharp eggshell boundary with vanadium concentrated in the first few micrometers of the cylindrical pellet surface. Eggshell distributions have shown increased selectivity towards intermediate products in literature, as mentioned in Section 2.7.1. From the reaction network presented in Section 2.4, formaldehyde is an intermediate for both the DMM reaction, methyl formate production and CO_x generation. Despite the eggshell distribution's proclivity towards intermediates, very little formaldehyde was observed for either catalyst. CO_x formation was limited until higher temperatures were reached since higher temperatures favour combustion (Forzatti et al., 1997). The high DMM selectivity can be attributed to the fact that the DMM acetalization step is much faster than the formaldehyde formation step, meaning any formed formaldehyde will acetalize with two methanol molecules to form DMM quickly. Finally, it is clear from the activity data obtained that methyl formate production has increased substantially by scaling up the formulation from a powder to a catalyst pellet. As the eggshell morphology of the pellets have a distribution of the vanadium in a very narrow region of the pellet, i.e., little vanadium penetration, there are a lot of titanium Lewis sites exposed. These titanium

Lewis sites have been linked to methyl formate production and as such the eggshell distribution may be the root cause of the high methyl formate yields. To better investigate the relationship, if any, between the depth of vanadium impregnation and the methyl formate production, the reason for the lack of vanadia penetration must be determined. As discussed in Section 2.7.1, the addition of another complex to the vanadium impregnating solution can have varying effects on the active-phase distribution. As such interaction between the oxalate and vanadium ions needs to be examined during the preparation of the vanadium solution and impregnation of the pellets.

We monitored the structure of the vanadium precursor complex, using liquid phase UV/Vis analysis. When the metavanadate salt is dissolved in the oxalic acid ethanolic solution, the mixture becomes a dark green colour and upon heating this colour changes to teal. The UV spectrum of the teal-colored solution is shown in Figure 3-11 (Stage 1), clearly indicating that at this stage only vanadium +5 ions are present (Choi et al., 2013). During incorporation of the vanadium ions into the pellet, several colour changes of the vanadium solution occurred, these changes are mirrored in the changes of the UV/Vis spectra of the impregnating solution and are the result of the incorporation of oxalate ions in the first coordination sphere of the vanadium ions and changes in the redox state of the vanadium species (Tracey et al., 1987; Bruyère et al., 2001). Specifically, after 12 hours, the spectra obtained (Stage 2) shows characteristic peaks for V^{+4} coordinated by oxalic ligands. After these changes a final stage is reached (Stage 3) which occurs during the removal of the water in the rotary evaporator where the solution is heated under vacuum to 353K. The UV/Vis spectra indicate formation of vanadium +3 complexes and an increased amount of vanadium +4 species.

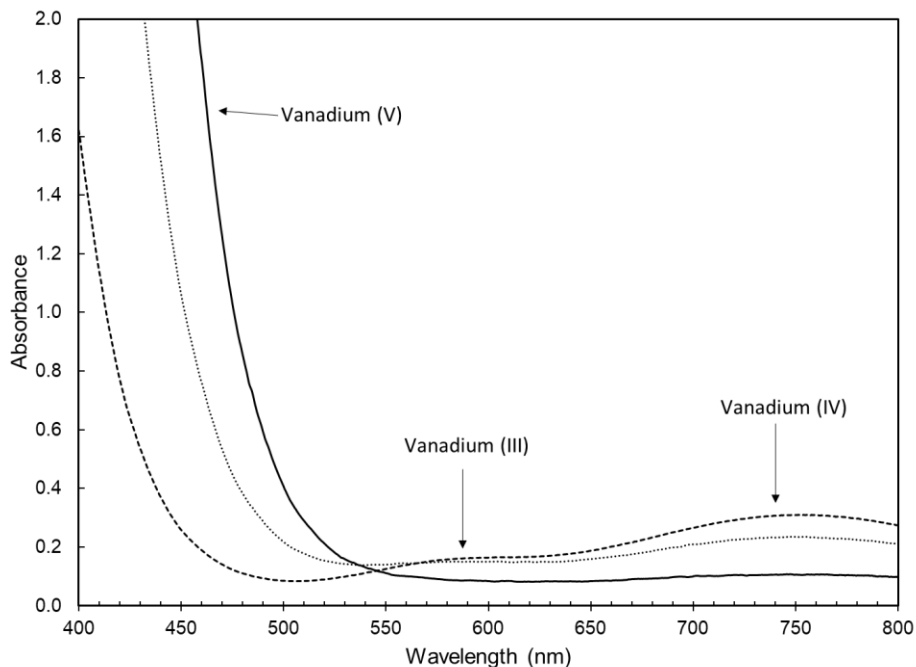


Figure 3-11 UV Data Obtained on the Vanadium Precursor Solution at each Impregnation Stage. The peaks attributed to different vanadium valence states are highlighted according to data from Choi et al., 2013

As discussed in Section 2.7.1, the use of a complexation agent during impregnation of the active phase results in sharp eggshell dispersions in the resulting catalyst pellet. For instance, when citrate is used in the precursor solution of a cobalt salt, the citrate complex strongly interacts with the pellet support, contrasting the behaviour of un-complexed cobalt (+2) ions (Bergwerff et al., 2013), which do not show this strong interaction. It is plausible then to postulate that reduced vanadium oxalate complex (formed during pellet impregnation as evidenced by Figure 3-11) has a strong interaction with the titania pellet support, causing a large distribution gradient of the vanadium phase at the macro-scale. This issue was not apparent when the powder catalyst was prepared, as the titania powder used in this case had an average particle size of 21 nm (Broomhead et al, 2022). An impregnation depth on the micrometer scale will not affect vanadia distribution on these materials, as such the powder-scale formulations were unaffected by this issue.

The effect the distinct eggshell dispersion had on the reactivity was clearly evidenced in the selectivity plots obtained for these two materials at both high and low space velocities. While DMM was obtained at high yields in both catalysts, as seen by the conversion and selectivity values in Fig. 3-10, the amount of methyl formate formed is also substantially high, increasing with temperature. These methyl formate yields are also substantially greater than those reported in the powdered version of the catalyst under the same conditions (Broomhead et al. 2022). Indeed, *in the powdered version of the catalyst, under differential reactor conditions, the main by-product observed was formaldehyde and not methyl formate.* These different behaviours can be explained in terms of the macro-distribution of the vanadium oxide in the pellet. The sharp concentration gradient observed for the vanadium oxide phase in the titania pellet clearly indicates that vanadium has not penetrated much more than a few micrometers past the titania's phase, and as such a sharp eggshell distribution is obtained. This in turn results in a large amount of exposed titania present, containing Lewis sites, which are the main active sites for methyl formate production on the vanadium/titania catalysts. Therefore, any formaldehyde that is not converted to DMM at the Brønsted sites present on the V-O-Ti interphase diffuses to the titania rich center where it is converted to methyl formate. This behaviour is similar to the high methyl formate yields reported for the powdered 1 wt% loaded V/Ti sample, which exhibits the largest number of exposed titanium sites among all powdered catalysts formulations tested (Broomhead et al., 2022), which again supports our hypothesis.

Another interesting trend that can be linked to the macro distribution of the vanadium phase on these materials is the lower normalized rates of methanol reaction observed on the 5% V-WI_(EtOH)/Ti sample. Compared to the 5% V-WI_(EtOH)/Ti sample, the sample with the lower vanadium content (2% V-WI_(EtOH)/Ti) shows lower methanol conversions, but similar selectivity profiles. However, when the rates are normalized by the amount of vanadium in the sample, the values of the normalized total rate are higher for the sample with lower vanadium oxide content (12.4 mol (mol V)⁻¹ h⁻¹ vs 7.7 mol (mol V)⁻¹ h⁻¹ at 423K). When looking at the UV results for these two catalysts, 2% V-WI_(EtOH)/Ti displays a spectrum consistent with well dispersed vanadium oxide (2.44 eV) compared to the more crystalline 5% V-WI_(EtOH)/Ti (2.26 eV). This suggests that there is more

vanadium in the unreactive crystalline phase in 5% V-WI_(EtOH)/Ti, not participating in the reaction as compared with 2% V-WI_(EtOH)/Ti, resulting in a less effective rate of conversion of methanol per mole of deposited vanadium.

While the high DMM yields obtained over by catalyst samples are desirable if the product is to be used for longer OME production, the lack of enough formaldehyde present on the product stream does not allow for the direct incorporation of a subsequent unit able to produce OMEs with a longer chain (OME_n, n=3-5). As such if either of the product streams obtained over these catalysts were to be used to feed an OME oligomerization reactor the feed streams to a OME production unit would need to be supplemented with additional formaldehyde to achieve the ideal 1:1 DMM: formaldehyde molar ratio needed for OME₃₋₅ synthesis. (Section 2.2). While the formaldehyde selectivity increases slightly when the space velocity was increased for the 2% V-WI_(EtOH)/Ti catalyst formulation, the higher selectivity is not sufficient to justify the significantly lower methanol conversion seen with high DMM yields at this space velocity.

If we take into consideration that the main by-product observed was methyl formate, and that methyl formate is the result of two formaldehyde molecules undergoing the Tishchenko reaction, there is a clear window of opportunity where *the formaldehyde selectivity can be boosted at the expense of the Tishchenko reaction*. In other words, if the mechanism for methyl formate production could be blocked, the formaldehyde selectivity should be much higher. With the exposed titania sites in the center of the pellet catalyzing the Tishchenko reaction, by blocking the accessibility of formaldehyde to these sites, the formaldehyde yields should increase. A straightforward way to block these sites is by achieving a homogenous vanadium distribution throughout the pellet. This strategy will also offer an additional advantage: a homogenous vanadium distribution will lead to less crystalline vanadium dispersions on the surface, as a homogenous distribution would spread vanadium oxide throughout the entirety of the support, and therefore to an improved atomic efficiency in the use of the vanadium centers.

With the information gained at this stage of the work, now we embark on a three prong approach to achieve the necessary homogenous dispersion of vanadia through the titania bearing pellet: 1) a longer impregnation time in an attempt to overcome any diffusion rate limitations during the impregnation of the vanadium phase on the titania pellet, 2) utilizing a different solvent to lower the interaction the vanadium ions in solution have with the pellet support, and 3) utilizing ALD to build a vanadium monolayer throughout the catalyst able to cover all titanium centers present on the solid. The outcome of these methods will be presented in subsequent sections.

3.3 Effect of Impregnation Time on the Impregnation Depth of the Vanadia Phase

3.3.1 Introduction

The first effort to increase the penetration of the vanadium oxide phase into the pellet was to ensure the depth of vanadium penetration was not limited by diffusion rates, preventing the precursor ions reaching the center of the catalyst pellet. Solutions containing active materials that have a strong interaction with the support have been found to need more time to impregnate if a deeper penetration of the active phase is desired (Munnik et al., 2015). Since the “proof-of-concept” catalysts, 5% V-WI_(EtOH)/Ti and 2% V-WI_(EtOH)/Ti, were prepared with an impregnation time of one day, we systematically evaluated different impregnation times, from 1 day up to 46 days. The methodology used to prepare these samples was the same as described at the beginning of Section 3.1.1, with the only difference being that instead of 24 hours, the samples were left impregnated for longer times. This length of time is more than sufficient to achieve a deeper impregnated catalyst as in similar systems, the impregnation equilibrium for 2 mm radius catalysts limited by diffusion is reported to be reached after ~3 days (Neimark et al., 1981).

3.3.2 Characterization Results of the Catalyst

The UV bandgap energy values obtained for these series of samples are presented in Figure 3-12 as a function of the impregnation time used. The results indicate that there is a decrease in the bandgap energy value that takes place after the first day of impregnation. After three days the bandgap value drops below the tolerance threshold (Section 3.2.1) and the spectra are dominated by the crystalline phase and below the “engineering tolerance” lower limit of 2.23 eV characteristic of a vanadium oxide monolayer dispersion.

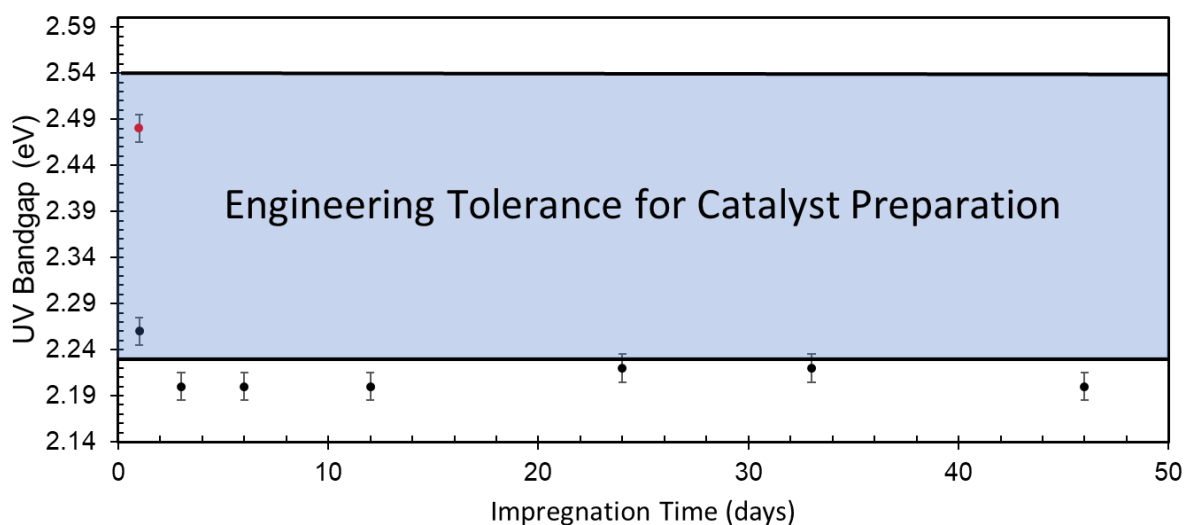


Figure 3-12 Effect of Impregnation Time on UV Bandgap and Vanadium Dispersion. (Black dots represent series of 5% V-WI_(EtOH)/Ti samples; red dot represents 5% V-WI_(Aq)/Ti sample)

Visually there was virtually no change to the depth of penetration of the vanadium oxide phase after 46 days of impregnation compared to the sample obtained after impregnation for 24 hours. This is clearly depicted by the WDS scans of the two pellets where similar vanadia distributions are observed for both samples (Figure 3-13). However, 5% V-WI_(EtOH)/Ti-46 days showed a slightly higher agglomeration of vanadium at the outer edge than the 5% V-WI_(EtOH)/Ti sample, which is consistent with the bandgap energies observed (monolayer 2.26 eV monolayer for the sample obtained after 24 hours vs.

2.2eV, nanocrystalline for the sample obtained after 46 days). As such, while the impregnation time does affect the degree of dispersion of the vanadium on the pellets surface it has virtually no impact on distribution and pellet penetration depth of the vanadium oxide phase.

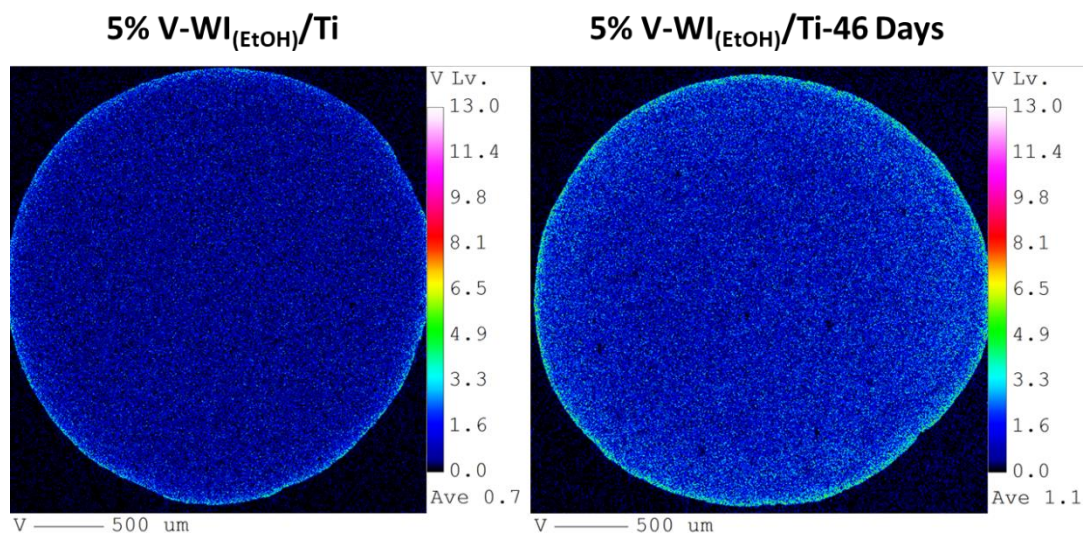


Figure 3-13 Vanadium WDS Scans of 5% V-WI_(EtOH)/Ti (left) and 5% V-WI_(EtOH)/Ti-46 Days (right)

The results indicate that our attempt to affect the penetration depth of the vanadium oxide phase by changing the impregnation time was unsuccessful, based on the characterization results it was deemed to not be warranted to test these formulations for catalytic activity as both the macro distribution and the micro dispersion of the active phase are not beneficial to DMM nor formaldehyde production. The results indeed clearly indicate vanadium oxide did not penetrate further towards the center of the catalyst with increasing impregnation times. This suggests that the strong interaction of the support with the oxalo-vanadate species likely regulates this process, and it cannot be overcome by letting the support interact with the solution for longer times. In other words, these vanadium-oxalate species in solution essentially prevent the diffusion of the vanadate ions once they are bonded to the surface. Substantial time was given for this impregnation to occur; therefore, it is unlikely that further increasing the time would have an effect. The UV bandgap clearly indicated that increasing the impregnation time did

influence the vanadium dispersion but at the molecular level. After one day of impregnation, the vanadium-oxalate species began to agglomerate. It is unclear if this agglomeration is occurring on the surface of the titania with other previously bonded vanadium-oxalates or in the bulk solution where large oxalo-vanadate oligomers form which then bond to the titania surface. Either way this agglomeration occurs rapidly as the bandgap plateaus past 1 day of impregnation, exhibiting UV bandgaps indicative of crystalline vanadium oxide already at 3 days of impregnation with slight change onwards. The vanadium dispersion being worse than those obtained on the samples prepared using 24 hours of impregnation time and the distribution also showing no improvement suggest that these catalysts would have worse conversions and lower normalized rates due to the increase of unreactive crystalline vanadium agglomerating at the outer surface of the pellet. As such the catalyst activity does not need to be evaluated due to the lack of improvement of the distribution of vanadium oxide at the macro and nanoscale observed.

3.4 Control of Vanadium Penetration by Weakening the Support Interaction

3.4.1 Introduction

On the previous section we hypothesized that the oxalate complexation of vanadium ions during impregnation resulted in a decrease of penetration of the created vanadium oxide in the titania pellet. Studies suggest that this must be due to the complex ions having a strong interaction to the hydroxyl groups present on the support (Bergwerff et al., 2013). If our hypothesis is correct, by removing the oxalate species from the solution, the vanadium ions would have a weaker interaction with the titania support resulting in further depth of impregnation of the vanadium oxide phase. For this purpose, we created a new vanadium precursor solution, where vanadium ions are surrounded exclusively by water molecules on their first coordination sphere, as such the impregnation method was systematically modified, oxalic acid was not used, and ethanol was replaced with water during the impregnation stage. A sample containing 5% VO_x loading was prepared, all other parameters and protocols used for catalyst preparation remained the same.

3.4.2 Characterization Results

The degree of vanadium oxide dispersion on the sample prepared using water as solvent was evaluated, once again, using UV/vis spectroscopy. The result obtained for this sample is shown in Figure 3-12 (red sample labeled “water impregnation”), the value obtained for the band gap energy was 2.48 eV. This result is remarkable, it indicates that a high dispersion of the vanadium oxide has been reached at the nanoscale, indeed this value is similar to the one obtained for the bandgap energy of the 2% V-WI_(EtOH)/Ti catalyst, despite the fact the 5% V-WI_(Aq)/Ti sample has a loading of vanadium that is significantly higher (5% vs 2%).

Following the methodology developed, to assess if the distribution of vanadium penetrated past the outer surface of the support, optical magnification pictures were taken of the cross section of the pellet (Figure 3-14) and WDS analysis carried (Figure 3-15). Visually at least, the vanadium had penetrated much further into the pellet structure. There was also a clear visual gradient between the vanadium and titanium, with a clear titanium core observed.

The WDS results differed slightly from the visual depictions. The WDS showed vanadium at high concentrations reaching further into the pellet, in agreement with the visual inspection results; however, the WDS showed a homogenous dispersion of vanadium throughout the entire cross-section. This was in direct opposition to there being a clear gradient observed on the magnified photos. Two potential causes for this discrepancy are that vanadium is attached but at a lesser concentration on the “bare titania” than can be visually determined by the photos. Alternatively, the cross-section may have been taken towards the ends of the catalytic pellet such that axial distribution of the active phase played a role in the overall distribution throughout the cross-section.

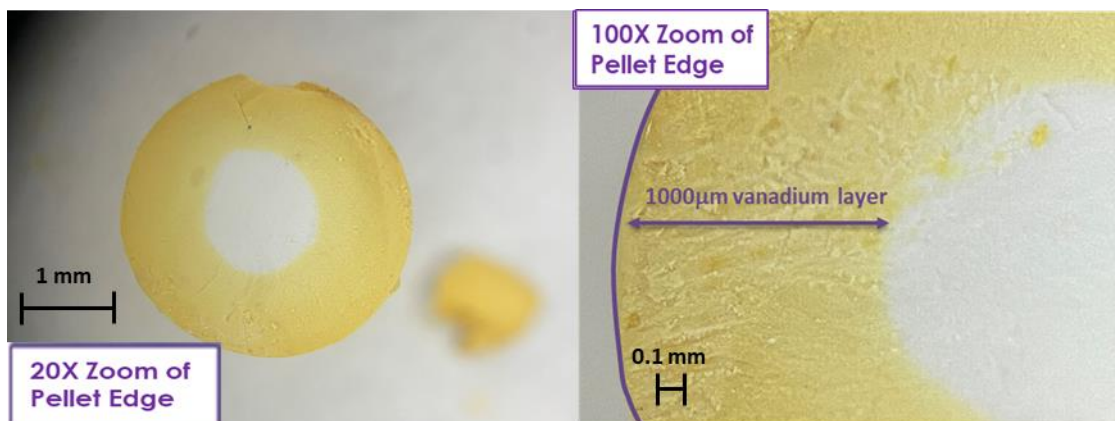


Figure 3-14 Optical Pictures of the 5% V-WI_(Aq)/Ti Pellet's Cross-Section

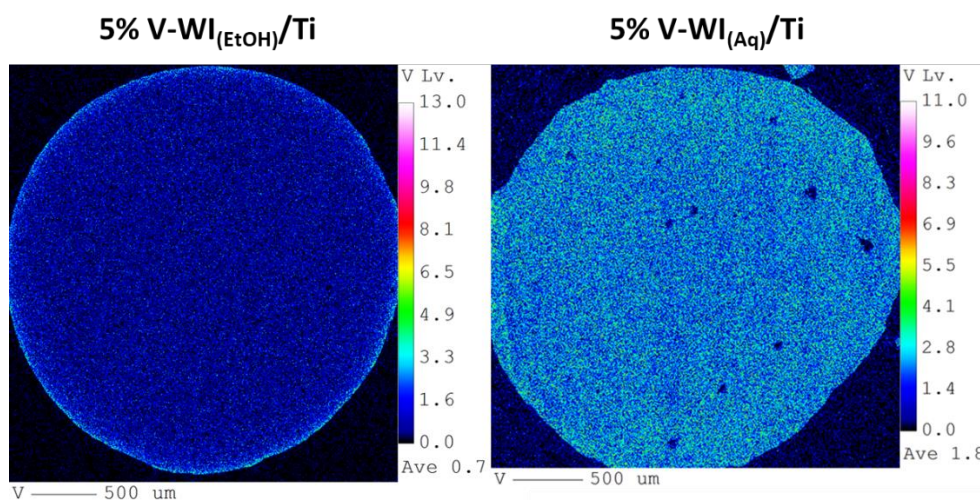


Figure 3-15 WDS scans of 5% V-WI_(EtOH)/Ti (left) and 5% V-WI_(Aq)/Ti (right)

In any case, it is clear that the 5% V-WI_(Aq)/Ti sample prepared using water as the solvent achieved a vanadium distribution that penetrated much further into the pellet than that obtained on the previously prepared samples, which only had the vanadium concentrated at the outer edge of the catalyst. UV/Vis testing was done along the outer edge of the catalyst and at points along the radius of the cross-section, to probe the existence of a vanadium gradient throughout the cross-section. The results of this analysis on the different areas of the pellet cross-section are presented in Figure 3-16. A clear gradient is observed throughout the pellet, with the bandgap energy value decreasing towards the pellet's center, evidencing more isolated vanadium domains; bandgap values suggesting

the presence of a two-dimensional monolayer at the outer edges of the pellet, while values corresponding to monomeric vanadium oxide domains observed at the center of the pellet.

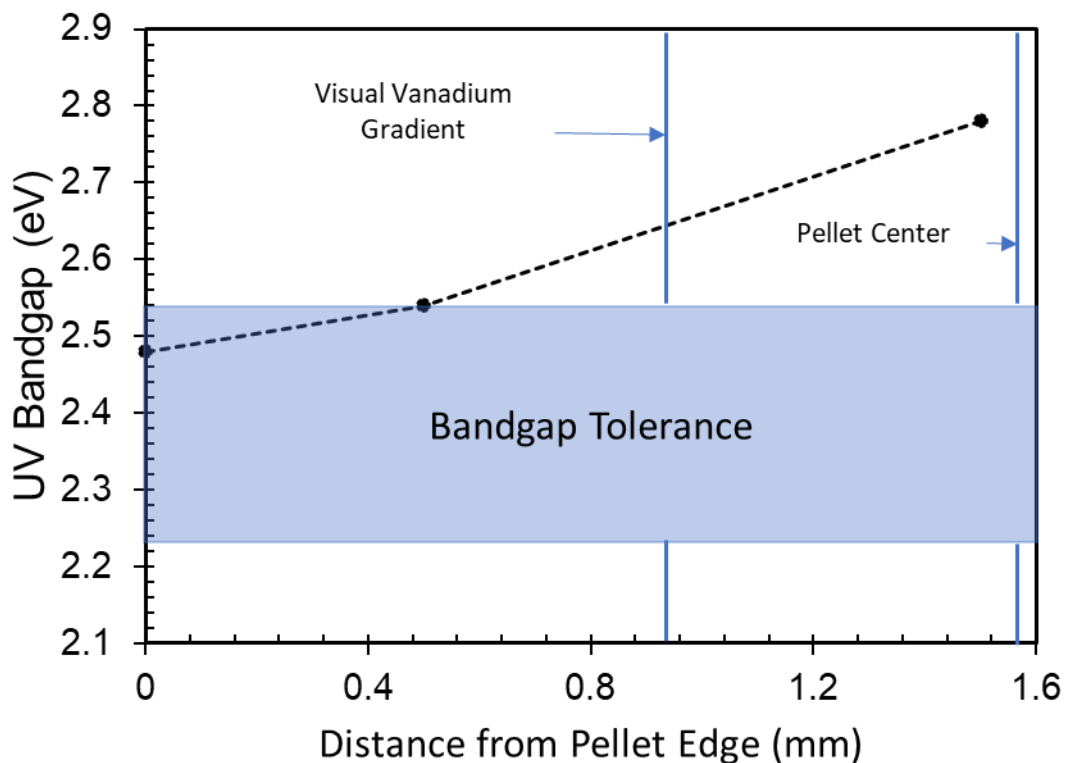


Figure 3-16 Bandgap Energy Gradient throughout the 5% V-WI_(Aq)/Ti Pellet

3.4.3 Catalytic Activity

The characterization results indicate that we were able to improve the vanadium distribution of a two-dimensional monolayer phase of vanadium oxide throughout a majority of the catalyst pellet. The 5% V-WI_(Aq)/Ti sample was evaluated to evaluate the impact of the catalyst pellet morphology would have on its catalytic activity. The results obtained are presented in Figure 3-17, showing steady-state conversions and selectivity as a function of temperature for two different space velocities.

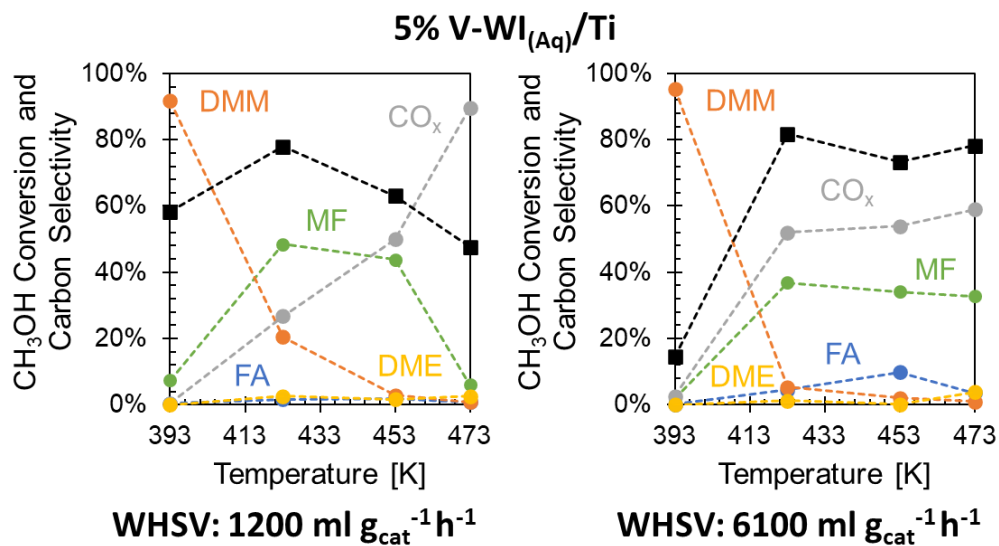


Figure 3-17 Catalyst Activity Data for the 5% V-WI_(Aq)/Ti Sample at Two Space Velocity Conditions. Black Square: Methanol Conversion, FA: Formaldehyde, MF: Methyl Formate. 2.44g of the 5% V-WI_(Aq)/Ti Whole Pellets assessed between 393K-473K, 20 kPa Methanol and 10 kPa Oxygen; balance Argon. 50SCCM/250SCCM

First, comparing the results with the 5% V-WI_(Aq)/Ti sample as opposed to those prepared using ethanolic oxalic acid solutions (Fig. 3-10), it is clear that increasing the depth of vanadium dispersion had a substantial positive effect on the catalytic activity and product selectivity. The 5% V-WI_(Aq)/Ti catalyst, evaluated at 1200 ml g_{cat}⁻¹h⁻¹, has an extremely high activity for methanol conversion and superior selectivity to DMM at 393K. The selectivity towards DMM was also near 100% for the 6100 ml g_{cat}⁻¹h⁻¹, high flowrate condition at 393K, albeit with a much lower conversion (60% at 1200 ml g_{cat}⁻¹h⁻¹ vs 15% at 6100 ml g_{cat}⁻¹h⁻¹). As the temperature increased, the amount of CO_x generated increased along with that of methyl formate for both conditions. However, at low space velocities methyl formate selectivity and overall conversion began to decrease with an increase of CO_x selectivity as a function of temperature. Meanwhile, at the high space velocity a plateau with temperature is observed in methanol conversion, methyl formate selectivity and CO_x selectivity from 423K onwards. It is important to mention that the high yields of CO_x at 423K and higher temperatures were not observed in the samples obtained using oxalic acid (Fig. 3-10).

Despite the increase in vanadium distribution to deeper regions within the pellet, selectivity towards methyl formate was still high past 393K at both space velocities. Similar levels of methyl formate production were also seen with the samples containing eggshell distributions, which we ascribed to vanadium-free TiO₂ sites catalyzing Tishchenko's formaldehyde conversion to methyl formate. As clearly observed (Figures 3-14 and 3-15) the 5% V-WI_(Aq)/Ti has a low amount of V-free TiO₂ sites, so the persistence of methyl formate in the product distribution is puzzling.

Selectivity towards formaldehyde was near zero, we could propose that that most of the formaldehyde is being over-oxidized to form CO_x as CO_x selectivity was significantly higher for the 5% V-WI_(Aq)/Ti sample. The large amount of CO_x observed in this case is uncharacteristic of this catalytic system, within the thermodynamic conditions used for the catalytic test and would occur either by overoxidation of formaldehyde or decomposition of methyl formate, both requiring significant higher temperatures than the ones used in our experiments (Deo and Wachs, 1994; Forzatti et al., 1997). Indeed taking into consideration that the catalyst surface morphology at the nanoscale is similar to the one observed in the 2% V-WI_(EtOH)/Ti catalyst, with the only difference being the distribution of this phase through the catalyst pellet; we can hypothesize that the high selectivity to CO_x is the result of localized hot spots inside the catalyst pellet generated during the exothermic partial oxidation of methanol to formaldehyde and/or DMM. These hot spots can be the site for the decomposition of methyl formate and/or the overoxidation of formaldehyde to CO_x.

To assess this hypothesis two calculations were used to determine the appearance of transport limitations in a catalytic system: the Weisz-Prater criterion and Prater number. These calculations were done in order to evaluate mass-transfer and heat-transfer limitations in the system. These equations are presented in Appendix B along with a detailed explanation of the derivation of their values and interpretation of results. For the 5% V-WI_(Aq)/Ti sample a Weisz-Prater Criterion value above 1 from 423-473K suggests the reaction rate is much quicker than the mass transfer of methanol to the active sites and as such the reaction resides in the diffusion-limited regime at these temperatures. This means that products are formed relatively quickly and with the deeper vanadium

penetration on the 5% V-WI_(Aq)/Ti sample these products interact with vanadium as they diffuse through the catalyst. Additionally, the calculated Prater number suggests a moderate to significant temperature gradient between the catalyst center and surface due to the exothermic nature of the methanol to carbon monoxide. This gradient is between 3-77K at 423K. To obtain a more specific value the exact thermal conductivity of the catalyst and porosity must be obtained experimentally. However, this range still illustrates that the system may contain substantial thermal gradients.

Both the Prater number and Weisz-Prater Criterion support the idea of the increased carbon monoxide production being attributed to formed products over-oxidizing from increased exposure to the active vanadium and an increasing temperature as the pellet center is reached. To confirm these numbers and hypothesis, experiments should be done in the kinetic regime to see how the conversion and product distributions are affected.

Verifying the impact which the transport limitations have on the catalytic activity on the large-scale can be done by mechanically crushing the pellets. Afterwards these smaller pellets are homogenized and tested on a differential microreactor. This action eliminated any diffusion limitations, evidenced by the Weisz-Prater Criterion being reduced to below 0.2. This value confirms the system is operating well within the kinetically controlled regime as such by reducing the size of the pellet, the mass and heat transfer restrictions are significantly minimized. If indeed heat transfer issues were responsible for the observed CO_x generation, the change in the reactor configuration would result in changes in selectivity once similar conversions had been achieved. The result of these experiments is presented below in Figure 3-18.

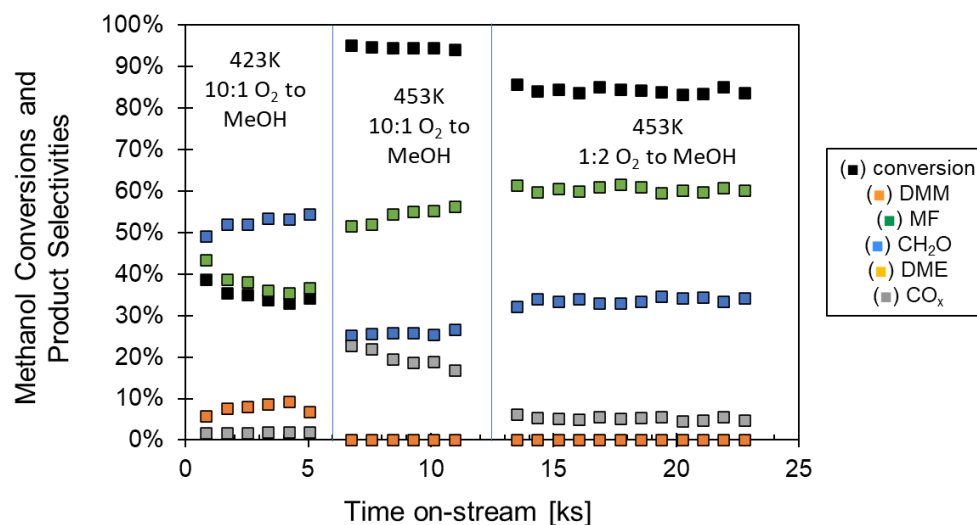


Figure 3-18 Effect of Crushing Pellet on Catalytic Activity. 100mg of the 5% V-WI_(Aq)/Ti crushed pellet (125-180 μm). 1 kPa Methanol with either 10 kPa or 0.5 kPa oxygen and balance Argon at 30,000 ml $\text{g}_{\text{cat}}^{-1}\text{h}^{-1}$

When examining the catalyst's activity of the sample once it is crushed and pressed into significantly smaller sized pellets (from 3180-10000 μm to 125-180 μm) it is quickly apparent that pellet size has greatly affected the product distribution of the catalyst, as evidenced by comparing the results for the 125-180 μm powder in Figure 3-18 with the results of the 1:2 for the 3180-10000 μm cylindrical pellets in Figure 3-17. At 423K methanol conversion is much lower on the small-scale albeit at a higher space velocity at about 35%. However, despite using a high oxygen to methanol ratio (10:1 for the case 125-180 μm powdered pellets vs 1:2 for the 3180-10000 μm cylindrical pellets) which would favor higher CO_x production, the CO_x selectivity was near 0% on the powdered pellets. At this condition formaldehyde was the primary product at about 55% selectivity while methyl formate had a selectivity at 35%. DMM finally had a selectivity near 10%. Comparing these results to the unaltered pellet, the formaldehyde selectivity increased significantly while the CO_x decreased significantly when the pellet was crushed.

Next the temperature for the powder pellets was increased to 453K, maintaining the 10:1 oxygen to methanol ratio, which is even more favourable to CO_x production. While CO_x increased to 20% selectivity, this was at a much higher conversion, nearing 100%. This

exceeded the conversion seen in the large-scale reactor at this temperature (63%, Fig 3-17) When considering the reduction of catalyst mass from the large-scale and small-scale (2.4g vs 0.1g) and reduction of total methanol pressure (20 kPa vs 1.0 kPa), the methanol rates per gram catalyst are comparable ($6.04 \text{ mol g}_{\text{cat}}^{-1}\text{h}^{-1}$ for the large-scale test vs. $8.25 \text{ mol g}_{\text{cat}}^{-1}\text{h}^{-1}$ on the small-scale) and, more importantly, the vanadia dispersion between both materials is exactly the same. As such, absent transport limitations, the product distributions should be similar between the integral and differential reactor experiments. Finally, the methanol to oxygen ratio was lowered to an equivalent ratio used for the large-scale DMM experiments depicted in Fig. 3-17 (1:2 oxygen to methanol, Fig 3-18) to directly compare the large-scale and small-scale conditions at 453K. Conversions obtained on the differential reactor at these oxygen rich conditions are slightly lower than those observed at a 1:2 oxygen to methanol ratio. Formaldehyde and methyl formate selectivity increased slightly, whereas selectivity to CO_x significantly decreased to 5% when the oxygen content in the stream decreased.

3.4.4 Discussion

Based on the characterization results, the distribution of the vanadium oxide phase throughout the pellet was severely improved through the removal of the oxalic acid from the vanadium precursor impregnating solution. Vanadium oxide achieved the required morphology for DMM production (two-dimensional monolayer) while penetrating deeper into the catalyst pellet. The effect of increasing the penetration depth of vanadium had significant effects on the catalytic activity. The 5% V-WI_(Aq)/Ti catalyst produced significantly more DMM at 393K than the ethanol impregnated samples (5% V-WI_(EtOH)/Ti and 2% V-WI_(EtOH)/Ti samples). The high yield obtained at this low temperature is atypical with literature reporting a lower DMM selectivity and conversion at similar space velocities (Kaichev et al., 2014). The increased productivity at low temperature could be due to the methanol having increased exposure to the active phase as it travels through the reactor. The drastic decrease in conversion seen when the space velocity is increased strengthens this hypothesis, as the lower residence time shortens the methanol's exposure to the active phase within the reactor and is therefore less likely to react.

Another aspect that was unique to the deeper vanadium penetration into the pellet, was that as temperature increased past 393K, significant over-oxidation occurred, i.e., increase in the CO/CO₂ yields. The yields were much higher than those obtained on the previous samples assessed which only generated minor CO_x production at 453-473K. In both the high and low space velocity conditions for the 5% V-WI_(Aq)/Ti sample, significant CO_x production was observed at and above 423K with a selectivity exceeding 50% as the temperature increased. For the low space velocity condition this increase in CO_x selectivity was accompanied by a decrease in methanol conversion for the 5% V-WI_(Aq)/Ti sample which was also observed for the 5% V-WI_(EtOH)/Ti sample. This decrease in methanol conversion can be attributed to the feed conditions used as the methanol to oxygen feed molar ratio was designed to be 2:1 methanol to oxygen (the stoichiometric amount for 100% formaldehyde selectivity). As the amount of oxygen is only available to convert methanol to formaldehyde, when over-oxidation to CO_x increases the oxygen becomes the limiting reagent as ½ mole extra of oxygen is consumed as the formaldehyde reacts to form carbon monoxide and 1 mole extra for carbon dioxide. As the CO_x selectivity increases the maximum conversion of methanol achieved should be lower due to an unavailability of oxygen in the feeding stream. It should be noted that at high space velocities the conversion did not decrease and plateaued with CO_x selectivity which goes against this hypothesis and results in oxygen conversions significantly over 100%. As such there may be other phenomena occurring at high space velocities.

When examining what is causing the unusual selectivity to CO_x when the catalyst pellets are used in the integral reactor while other vanadium/titanium powdered catalysts described in the literature exhibit very low CO_x production in the same temperature range (Deo and Wachs, 1994; Forzatti et al., 1997) the macro-distribution of the active catalyst phase in the pellets as well as the catalyst shape need to be examined. In industrial catalysis “hotspots” can be created within the catalyst pellet when there is high amount of heat generated inside the pellet from an exothermic reaction. The heat generated gets trapped inside the pellet due to inadequate thermal transport (Maymo and Smith, 1966). This amounts to a temperature gradient between the bulk fluid and the center of the catalyst where the center is much hotter than the bulk temperature. The oxidation and

acid reactions, that methanol needs to undergo to form DMM, are both exothermic leading to heat being generated. This behavior is similar to that reported on pellets used in the FORMOX © process, converting methanol to formaldehyde, which is also highly exothermic. As a first approach to rationalize the behaviour observed, the FORMOX © process can be examined to evaluate the formation of hot spots in the DMM process, as it too takes place in a fixed-bed reactor with catalysts containing a homogeneously distributed active-phase.

A recent study by Partopour and Dixon used CFD modelling of the FORMOX process reports that CO production is exclusive to the center of the catalyst as opposed to the outer edges, where a majority of formaldehyde production takes place (2020). This phenomenon occurs regardless of the shape of the catalyst, although those pellets with higher surface areas to volume ratios exposed to the bulk gas flow were able to limit the contact between the formed formaldehyde and the active phase (Rings, Trilobes) (Partopour and Dixon, 2020).

In our case, the catalyst samples prepared were obtained using cylindrical-shaped TiO₂ pellets. Cylinders in general have longer diffusion paths than other shapes due to a lower external surface area ($2L\pi r + \pi r^2$) to volume ($L\pi r^2$) ratio (assuming that the cylinder is void of pores) meaning less active-phase is exposed to the bulk flow of the gas which allows for longer contact time of the formed formaldehyde with the active-phase as it diffuses through the support. As the near homogenous distribution of 5% V-WI_(Aq)/Ti sample results in the creation of more VO_x/TiO₂ redox sites located closer to the geometrical center of the catalyst pellets, this could result on formaldehyde to further progress down the oxidation pathway, as it diffuses throughout the center the pellet, leading to higher temperatures generated as result of the exothermicity of the oxidation reactions. This in turn moves the thermodynamic window for the reaction to near complete methanol oxidation products. The increase in temperature also increases the reaction rates of oxidative dehydrogenation (ODH) of methanol ($4.1 \text{ mol (mol V)}^{-1}\text{h}^{-1}$ for 5% V-WI_(Aq)/Ti vs. $11.8 \text{ mol (mol V)}^{-1}\text{h}^{-1}$ for 5% V-WI_(EtOH)/Ti at 423K, low space velocity ($1000\text{-}1200 \text{ ml g}_{\text{cat}}^{-1}\text{h}^{-1}$)) thus increasing the rate of over-oxidation. Over-oxidation of formaldehyde was not observed in the 2% V-WI_(EtOH)/Ti and 5% V-

WI_(EtOH)/Ti samples as the vanadium did not penetrate past the surface of the pellet. The unavailability of redox centers past the outer layers of the cylindrical pellets could then explain why over-oxidation did not occur, with methyl formate being produced instead on the bare titania sites.

To further test this hypothesis and evaluate if the excess of CO_x production was indeed due to the creation of hotspots caused by the macroscopic distribution of the vanadia in the catalyst pellet and not a result of the domain size of the vanadium oxide clusters we first looked back at the UV/Vis results obtained for both samples. Examining the UV bandgap of the 5% V-WI_(Aq)/Ti pellet resulted in a monolayer dispersion with an outer edge bandgap of 2.48 eV. There was an observable vanadium gradient as evidenced in Figure 3-16 throughout this catalyst with the vanadium becoming more dispersed as the pellet was penetrated with about a third of the pellet within the optimum dispersion range. For the 5% V-WI_(EtOH)/Ti pellet and the 2% V-WI_(EtOH)/Ti pellet they too exhibited bandgaps with a monolayer dispersion (2.26 eV and 2.46 eV). The 2% V-WI_(EtOH)/Ti sample was much closer in dispersion to the 5% V-WI_(Aq)/Ti sample. The differing catalytic activities exhibited by these two samples illustrate how similar dispersions do not necessarily result in similar activity profiles when the catalysts have varying vanadium distributions (eggshell vs. homogenous), with the distribution playing a significant role.

The UV/results strongly suggest that the morphology of the vanadium clusters is similar, and hence should have the same intrinsic activity for partial oxidation of methanol in a kinetically controlled reaction regime. Thus, the explanation for the observed differences in selectivity need to be linked to transport limitations arising from the distribution of the active phase in the pellet, i.e., CO and CO₂ are generated in larger amounts when the vanadium sites reside deep inside the catalyst pellet. If this was not the case, running the process under the same conditions but mechanically altering the pellets in such a way that most of the vanadium centers are now not residing deep within the pellet (achieved by mechanically crushing the pellets) will result in the same product dispersion shown in Figure 33 at similar conversions. However, when Figures 3-17 and 3-18 are examined, the mechanically crushed pellets display a clearly different selectivity profile. While CO_x

was generated at excessive amounts on the cylindrical catalyst pellets at temperatures above 423K along the low and high ends of space velocities evaluated, when the pellet is crushed the selectivity towards CO_x significantly drops. Under similar conditions (2:1 methanol to O_2 ratio, 453K) the cylindrical pellets show a selectivity towards CO_x 5 times higher than that obtained over the mechanically crushed pellets. As a result, it can be concluded that the structure is causing the high amount of CO_x due to the formation of hot spots which is favouring formaldehyde oxidation as the formaldehyde diffuses through the catalyst.

During the catalytic testing of the crushed pellet little DMM production with significant selectivity to methyl formate and formaldehyde was observed in addition to the lower CO_x yields. This behaviour may be attributed to the fact that optimum conditions for DMM formation were not assessed with the space velocity at the small scale being $30000 \text{ ml g}_{\text{cat}}^{-1}\text{h}^{-1}$, and the optimum O_2 to methanol ratio only assessed at 453K, not at temperatures where DMM has shown to have high selectivity (393K or 423K). The increase in methyl formate may be due to exposure to titania from crushing the catalyst; however, further testing would be required to ensure it was undergoing the Tishchenko reaction on these sites and not another pathway.

While utilizing a different solvent effectively weakened the support-active phase interaction during impregnation resulting in a more distributed vanadium phase this caused new problems for selective DMM synthesis. Instead of an excess of methyl formate seen with previous eggshell distributed catalyst formulations, over-oxidation of formaldehyde was promoted leading to high yields of CO_x . Additionally, despite the higher vanadium distribution methyl formate was still prominent as not all titania sites were covered. As such methods to reduce the methyl formate are still needed in the catalytic formulation while avoiding over-oxidation.

3.5 Utilizing ALD to Address the Shortcomings of Previous Catalyst Iterations

3.5.1 Introduction

As described in Section 3.4, the distribution of the VO_x/TiO_2 centers on the catalyst pellets plays a critical role on the catalyst performance, that is not necessarily linked to the morphology or intrinsic redox activity of the vanadia catalytic centers. In addition to this consideration, as described in Chapter 2, the availability of vanadium-free titanium sites results in the formation of undesirable methyl formate, hence it is necessary to ensure a close interaction between both the vanadia and TiO_2 phases in order to optimize catalyst performance.

To address these issues, we moved away from using titanium as pellets, and instead selected a catalytically inert material: SiO_2 as the pellet substrate, our strategy assumes that the silica surface could be covered with a monolayer of TiO_2 which in turn would be fully coated with vanadia. This would ensure that all TiO_2 centers are covered by vanadia and thus catalytically unable to trigger the Tishchenko pathway leading to methyl formate production, while at the same time all vanadium would be interacting with TiO_2 thus ensuring an atomic efficient dispersion of the vanadia centers, all able to catalyze partial oxidation of formaldehyde and DMM formation. To achieve monolayer coating of TiO_2 we used atomic layer deposition (ALD) for the generation of the titania phase.

3.5.2 Depositing Titania onto SiO_2

We carry the deposition of TiO_2 following the procedure described in Section 3.1.2 to achieve a TiO_2 loading of 10 wt% in the SiO_2 pellet. To evaluate the presence of titania in the silica pellet, UV/Vis analysis and WDS mapping were conducted on the manufactured pellets. Pristine SiO_2 does not have a measurable band gap below 6.0 eV (Maj, 1988). The UV spectra measured at the outer edge of the $\text{TiO}_2/\text{SiO}_2$ pellet showed a bandgap of 3.2 eV, while the spectra measured at the center of the pellet resulted in a bandgap value of 3.4 eV. (Figure 3-19). The bandgap for pristine TiO_2 anatase sits at 3.2eV (Dette et al., 2014). The results obtained thus clearly indicate that a TiO_2 phase was deposited through the entirety of the pellet, the value of 3.2 eV measured at the outer

edges suggests that well-formed uniform titania domains have been created in this region of the pellet, while at the center the value of 3.4 eV suggest smaller sized titania domains.

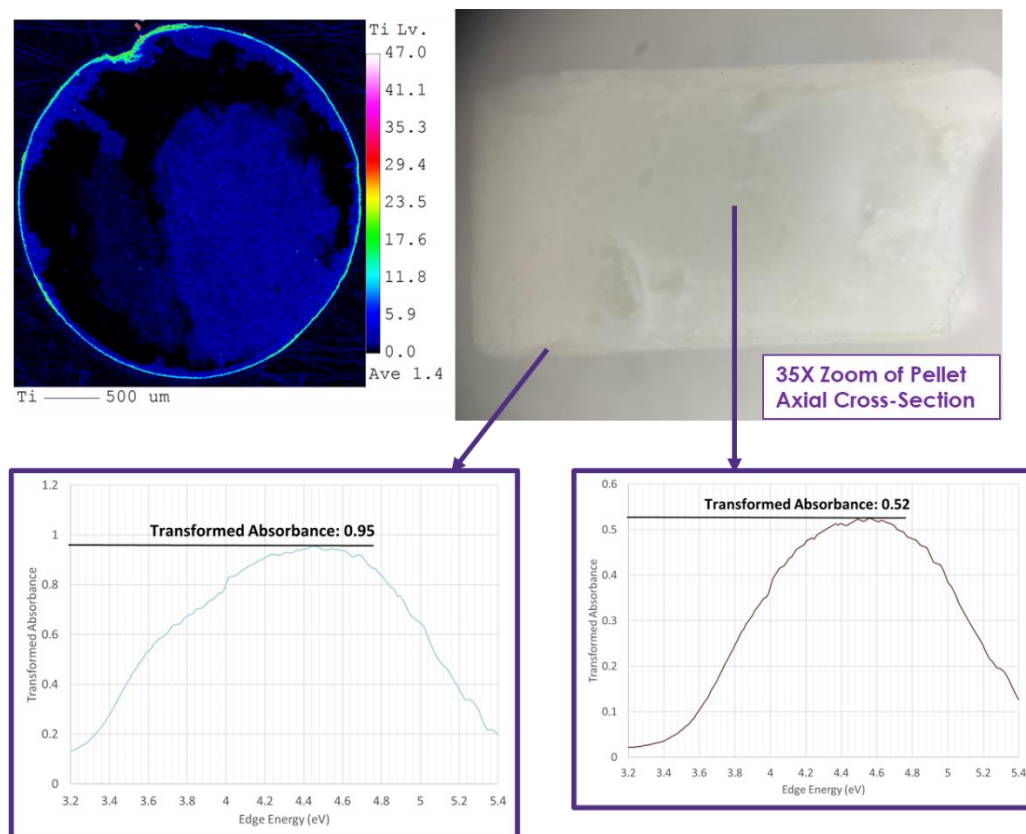


Figure 3-19 Titanium Distribution through Silica Pellet after ALD. Top Left WDS Scan showing Titanium throughout Cross-Section. Top Right and Bottom. Optical Picture Showing Cross-Section of Pellet with Transformed Absorbance Spectra at Different Cross-Section Areas

The results obtained from WDS mapping are also shown in Fig. 3-19. for the titanium distribution. It should be noted that the black colored areas within the pellet diameter on the map cannot be interpreted as regions where titania is not present. This is instead the result of sample charging that took place during analysis of the sample interfering with the WDS signal. This is also the case of the mapping of Si on these pellets, which show the “absence” of Si on the SiO₂ pellets due to charging of the sample shown below in

Figure 3-20. Examination of Figure 3-20 reveals that the titanium has penetrated all areas of the Silica pellet despite what the artefacts might suggest.

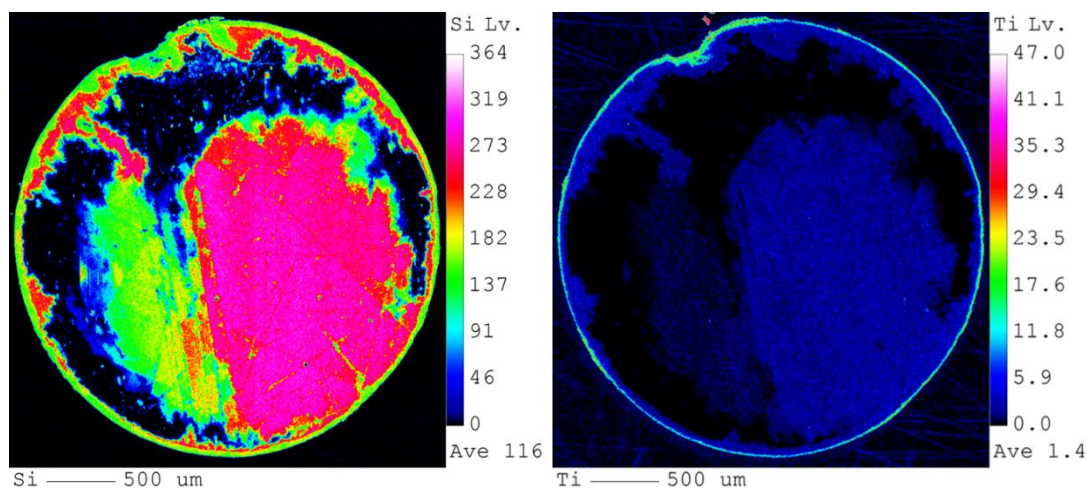


Figure 3-20 Comparison of Silicon (Left) and Titanium (Right) Distributions showing Signal Artefacts of a Pellet after ALD

Analysis of the cross-section UV/Vis and WDS maps shows that titanium penetrated the entirety of the catalyst, however the mapping results suggest a concentration gradient, with a larger titanium content in the outer layers of the catalyst pellet. This is also consistent with the difference in absolute absorbance values observed in the UV/Vis spectra, absorbance at the center of the pellet was lower than at the outer edge as seen in Figure 3-19. This suggests that the titanium concentration is lower towards the center of the pellet.

The results described above indicate that a titania phase had indeed been created in the SiO₂ pellets, but not with a uniform distribution or morphology, concentrations of TiO₂ are lower near the center of the pellet, and these titania domains are smaller in size with band gap energies values above those of TiO₂ anatase. It is well established that bandgap energies are associated with redox activity of metal oxides (Védrine, 2017), thus before proceeding with incorporating the vanadium oxide functionality we evaluated the catalytic activity of the TiO₂ coated silica pellets and compared it with that obtained over the bare TiO₂ pellet used to prepare the previous samples (Sections 3.2-3.4). The results of these experiments are presented in Table 3-4. The calculated oxidative

dehydrogenation (ODH) rates on the two samples are $0.07 \text{ mol (mol Ti)}^{-1}\text{h}^{-1}$ for Ti/Si and $0.01 \text{ mol (mol Ti)}^{-1}\text{h}^{-1}$ for the bare Ti pellet at 473K. While the conversions obtained looked similar, the amount of titanium present in the catalyst bed was much less for the Ti/Si pellets (130 mg) than for the pure TiO_2 pellets (3270 mg). Table 3-4 also shows the selectivity profiles observed at different temperatures. The Ti/Si sample forms almost exclusively DMM at 423K and 473K, while formaldehyde was exclusively produced on the Ti pellet. Very little methyl formate was seen on either pellet at this temperature range despite the excess of titanium Lewis sites on both samples. It did appear at low quantities on the Ti/Si pellet at 573K along with other acid products like DME at the expense of DMM selectivity all around 30-40%. The lack of methyl formate could be due to low conversions of methanol leading to lower concentrations of formaldehyde and thus the probability of two formaldehyde molecules interacting to undergo the Tishchenko reaction at a Lewis site decreased.

Table 3-4 Catalytic Activity for Vanadium Free Ti/Si Pellet and Ti Pellet in Large-Scale Reactor. MeOH: Methanol, FA: Formaldehyde, DME: Dimethyl Ether, MF: Methyl Formate, DMM: Dimethoxymethane. 1.38g (Ti/Si) and 3.27g (Ti) of whole pellets tested at 20 kPa methanol, 10 kPa oxygen, balance Argon (50 SCCM)

Sample	Temperature (K)	Space Velocity ($\text{ml g}_{\text{cat}}^{-1}\text{h}^{-1}$)	MeOH Conversion (%)	Selectivity			
				FA	DME	MF	DMM
Ti/Si Pellet	423K	2200	3%	0%	0%	5%	95%
Ti/Si Pellet	473K	2200	3%	1%	0%	6%	93%
Ti/Si Pellet	573K	2200	16%*	6%	37%	23%	31%
Ti Pellet	423K	900	1%	99%	0%	0%	1%
Ti Pellet	473K	900	1%	84%	0%	6%	10%

*Note at this condition a 3% selectivity to CO_x was observed as well

From the results on the large scale, it is clear that the ODH rate is much higher on the Ti/Si pellet than the bare Ti pellet. Additionally, the Ti/Si pellets almost exclusively formed acid pathway products as opposed to the bare Ti pellet which primarily produced formaldehyde at the same temperature range. As such we could propose that either the number of acid sites and/or the acid strength of the ALD manufactured Ti/Si pellet is much higher. For a better understanding of the reason for this increased acid strength, small-scale experiments on the Shimadzu GC were conducted with the Ti/Si as well as the bare Si pellets to determine the contributions of each phase on the catalytic activity. The results at 573K are presented below in Table 3-5. While the MeOH conversions are similar between the two samples, the bare silica produced exclusively acid products with an ODH rate of $0.001 \text{ mol g}_{\text{cat}}^{-1}\text{h}^{-1}$. In comparison, the Ti/Si sample still produced acid products but had a much higher ODH rate ($0.032 \text{ mol g}_{\text{cat}}^{-1}\text{h}^{-1}$)

Table 3-5 Catalytic Activity for Vanadium Free Ti/Si Pellet and Si Pellet on a Differential Reactor. MeOH: Methanol, FA: Formaldehyde, DME: Dimethyl Ether, MF: Methyl Formate, DMM: Dimethoxymethane. 60 mg (both Ti/Si and Si) and 3.27g (Ti) of crushed pellets (450-600 μm) tested at 5 kPa methanol, 2.5 kPa oxygen, balance Argon/Helium mixture. $13,000 \text{ ml g}_{\text{cat}}^{-1}\text{h}^{-1}$

Sample	MeOH Conversion (%)	Selectivity			
		FA	DME	MF	DMM
Si/Ti Crushed Pellet	8%	6%	64%	26%	4%
Bare Si Crushed Pellet	5%	0%	85%	0%	15%

From these results, it is clear that the ALD process modified the acid strength of the titania, by bonding it to the acidic SiO_2 . This strengthened the acid sites as opposed to the pure titania pellet leading to increased selectivity towards acid pathway products like DMM not seen on the pure titania pellet (Table 3-4). In addition, the catalytic activity was greatly increased on the titania monolayer with much higher redox activity (illustrated by the normalized rates) as opposed to the pure titanium dioxide pellet.

3.5.3 Wetness Impregnation of Vanadium onto Ti/Si

Vanadium oxide was loaded into the Ti/Si pellet utilizing an oxalic acid/ethanol solution maintaining a 5.0 wt% ratio between vanadium and titania. As such total vanadium loading on the pellet equated to 0.5 wt%. Characteristic analysis of this catalyst in the UV and WDS in Figure 3-21 showed the formation of a monomeric dispersion of vanadium along the outer layer of the catalyst (2.7 eV bandgap) with a titania pellet at the center (3.6 eV). This titania bandgap was shifted from the 3.2 eV value that is associated with anatase titanium, but this is consistent with the results from the bare Ti/Si pellet characterized in the previous section. WDS analysis of a similarly formulated but higher loaded (1.5 wt% vanadium) pellet cross-section showed the vanadium distribution was again limited to the outer edge of the catalyst in a sharp eggshell configuration. This is to be expected with the wetness impregnation in ethanol oxalic acid solution as seen in the 5% V-WI_{(EtOH)/Ti} and 2% V-WI_{(EtOH)/Ti} samples. Signal artefacts were observed in the WDS as illustrated in Figure 3-20 above.

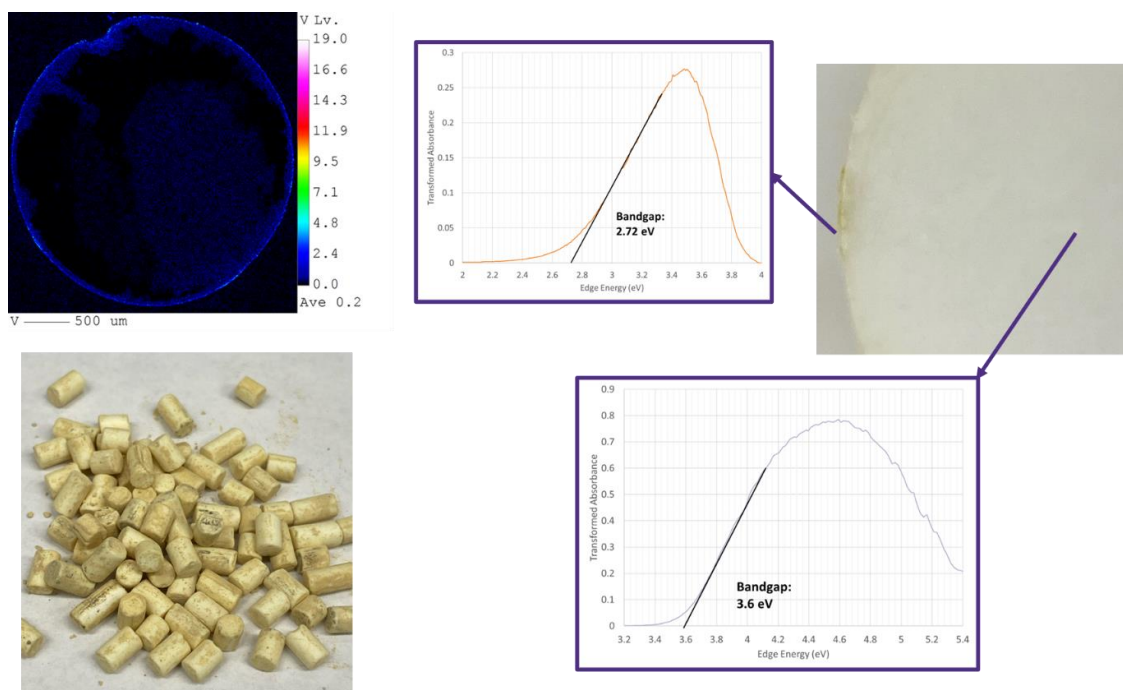


Figure 3-21 Vanadium Distribution for 0.5% V-WI_(EtOH)/Ti/Si Sample. Top Left: WDS scan showing Vanadium throughout cross-section (sample was similarly prepared but higher loaded than 0.5% vanadium to ensure a strong enough WDS signal). Bottom Left: Optical picture of whole pellets Right: Optical Picture Showing Cross-Section of Pellet with Transformed Absorbance Spectra with bandgaps at Different Cross-Section Areas

Overall characterization data for the distribution of both the titania and vanadia for the 0.5% V-WI_(EtOH)/Ti/Si pellets were consistent to the data obtained for both phases previously. The vanadium dispersion is in isolated monomeric form. The low loading of vanadium most likely contributed to this dispersion being obtained as the amount of vanadium on the 0.5% V-WI_(EtOH)/Ti/Si sample was 4 times lower than the next lower loaded sample (2% V-WI_(EtOH)/Ti) with similar initial pellet surface areas (bare titania vs bare silica). Reactivity data was obtained for this catalyst using the scale-up integral reactor and is shown in Figure 3-22, below.

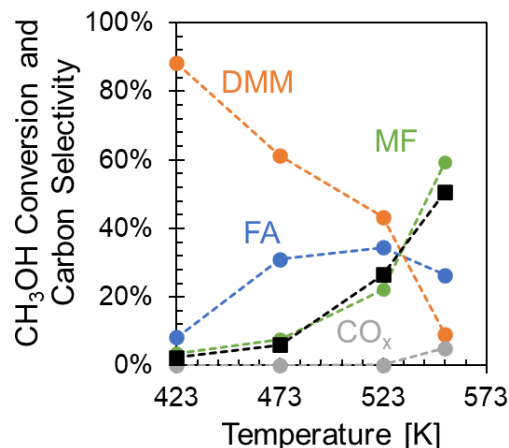


Figure 3-22 Catalyst Activity Data for the 0.5% V-WI_(EtOH)/Ti/Si Sample. Black Square: Methanol Conversion, FA: Formaldehyde, MF: Methyl Formate. 1.40 g of the 0.5% V-WI_(EtOH)/Ti/Si Whole Pellets evaluated between 423K-553K, 20 kPa Methanol and 10 kPa Oxygen; balance Argon. 2100 ml g_{cat}⁻¹h⁻¹

Compared to the samples prepared using wetness impregnation in ethanol and oxalic acid previously (Figure 33-10) obtained methanol conversion were much lower at 423 and 473K, but substantially higher than those obtained over the VO_x-free Ti/Si pellets, (Table 3-4). The conversion increased with temperature, achieving 51% at 553K. The conversion values obtained are consistent with the low vanadium loading in the catalyst and as such normalizing the total ODH rate per vanadium content for the sample results in a rate of 3.0 mol (mol V)⁻¹h⁻¹ at 423K, compared with the ODH rates calculated for the previous samples tested (4.1 mol (mol V)⁻¹h⁻¹ and 5.9 mol (mol V)⁻¹h⁻¹ ODH rate values, Section 3.2) show that the material has an adequate catalytic performance, with the vanadium used somewhat effectively.

The selectivity profile indicates that DMM production followed a similar drop with temperature as that seen in the previously tested catalysts (Figure 3-10); however, this decrease takes place only once a temperature of 353K is reached. Indeed, DMM was the dominant product even at 523K, while on the other catalysts evaluated, a DMM selectivity near zero is observed above 423K (Figure 3-10). At the same time, formaldehyde production on the 0.5% V-WI_(EtOH)/Ti/Si sample was very high achieving a maximum of 34% selectivity at 523K which is the highest value observed among the

catalyst we tested at this point. Methyl formate production was still observed on this sample. Although it is present at much lower quantities than previously seen at 423K and 473K, at higher temperatures (553K) it becomes the dominant product. CO_x was not produced in significant amounts until the final temperature condition (553K) was reached, but this amount was much smaller than that observed over other catalysts (Figure 3-10 and Figure 3-17) DME was not observed throughout the entire range of temperatures tested, this behaviour is similar to that observed over the 2% V-WI_(EtOH)/Ti pellet.

Ultimately, while this catalyst did not reach an adequate DMM yield due to the low conversions, the 0.5% V-WI_(EtOH)/Ti/Si pellets did achieve a much higher DMM: formaldehyde selectivity ratio (2:1 at 423K) than those obtained over the two previous catalytic formulations (8:1 ratio achieved on 2% V-WI_(EtOH)/Ti at 423K and 5000 ml gc⁻¹ h⁻¹). While this ratio obtained is optimal, the yields of these products are not high enough. As such although the 0.5% V-WI_(EtOH)/Ti/Si catalyst is an improvement over the previously tested two formulations, it is still not an adequate catalyst for producing a feedstock stream for long chain OME synthesis as methanol conversions need to be increased while maintaining the selectivity ratio seen at 423K.

3.5.4 Discussion

To rationalize the behavior observed for the 0.5% V-WI_(EtOH)/Ti/Si catalyst, we first must carry a morphology comparison between this formulation and the ones obtained over the TiO₂ pellets (Sections 3.2-3.4). As described above, the 0.5% V-WI_(EtOH)/Ti/Si sample had an egg-shell distribution of the vanadium oxide phase, with an extremely high nanoscale vanadium dispersion (segregated VO₄ monomers as per their edge energy value) indicating that in this formulation a vanadium monolayer was not achieved (Broomhead et al., 2022). As such the closest comparison to this formulation is the 2% V-WI_(EtOH)/Ti pellet catalysts prepared over a pure TiO₂ pellet which also exhibited a high dispersion of vanadia centers and eggshell distribution, but in a monolayer structure over the titanium surface. This difference in dispersion illustrates that the mass ratio of the vanadia to titania (1:20 for 0.5% V-WI_(EtOH)/Ti/Si, 1:50 for 2% V-WI_(EtOH)/Ti) is less important in regulating the nanoscale distribution of vanadia than the vanadium loading

per surface area of catalyst. This drastic increase in dispersion suggests that the ALD deposition of titania did not greatly affect the surface area of the silica pellet as both the titania and silica pellets had the same initial surface area. Hypothetically, if the vanadium had a similar or greater dispersion on the 0.5% V-WI_(EtOH)/Ti/Si despite 4 times lower the vanadium loading as compared to the 2% V-WI_(EtOH)/Ti sample this would evidence the surface area being smaller after titania deposition. There are currently conflicting reports in the literature on the effect of titania deposition to the surface area of silica, so this effect needs to be confirmed via BET analysis (Herrera et al., 2006; Quaranta et al., 1997).

When normalizing the ODH rate of methanol conversion for the 0.5% V-WI_(EtOH)/Ti/Si and the 2% V-WI_(EtOH)/Ti catalysts it is clear the vanadium is much more efficient at low temperatures at converting methanol to ODH products in the 2% V-WI_(EtOH)/Ti catalyst. This is consistent with reports in the literature indicating that isolated monomeric vanadia sites are less active than oligomeric structures for methanol ODH (Broomhead et al., 2022; Wachs 2013).

When comparing the product distribution, the behaviour between these two catalysts is also very different. At 423K the 2% V-WI_(EtOH)/Ti sample has high DMM selectivity followed by methyl formate as the primary by-product. The 0.5% V-WI_(EtOH)/Ti/Si sample has similar high selectivity to DMM, but formaldehyde is the primary-by-product. This contrasting behaviour is remarkable as both catalysts have distinct eggshell distributions meaning numerous TiO₂ Lewis sites are similarly exposed in both formulations (both have eggshell configurations for the vanadia phase). Methyl formate production is much higher for the 2% V-WI_(EtOH)/Ti sample. However, the amount of free titania with respect to vanadium oxide in both catalyst is similar with a molar Ti/V ratio of 21.6 mol Ti to 1 mol V for the 0.5% V-WI_(EtOH)/Ti/Si formulation (same as the 5% V-WI_(EtOH)/Ti sample) and 55.8 mol Ti to 1 mol V for the 2% V-WI_(EtOH)/Ti sample. While the 2% V-WI_(EtOH)/Ti catalyst has a higher Ti/V ratio, the 0.5% V-WI_(EtOH)/Ti/Si formulation has much less methyl formate production compared to the 5% V-WI_(EtOH)/Ti sample as well, which has the same Ti/V ratios for both catalysts.

Thus, the observed lower selectivity toward methyl formate observed on the 0.5% V-WI_(EtOH)/Ti/Si sample cannot be rationalized in terms of the amount of exposed titanium on the catalyst surface but could suggest that anchoring the titania to the silica pellet alters the strength and/or number of Lewis sites present on the titania structure, decreasing its ability to catalyze the Tishchenko reaction. A decrease on the number of Lewis acid sites is a plausible explanation if one takes into consideration the characterization results: the larger domains of titanium oxide (band gap energy values similar to those of crystalline anatase) are present in the outer layers of the silica pellets, while the inner core is formed by smaller titanium domains. The presence of Lewis centers on metal oxides is directly correlated with the domain size of these structures since Lewis sites are coordinatively unsaturated cations; a result of oxygen vacancies (defects) on crystals (Busca, 1998). Larger metal oxide domains thus host a larger number of these defects (Yun and Herrera, 2017). Thus, the outer layers of the TiO₂/SiO₂ pellets would have a similar density of Lewis acids sites as those on the pristine TiO₂ pellets, while the inner core has a lower number of these acid sites. Upon vanadia incorporation, an eggshell distribution is achieved (Figure 3-21), and thus the titanium phase rich of Lewis acid centers at the outer edge (Figure 3-19) gets covered by vanadia, leaving only isolated titania Lewis sites on the pellet inner core, at a much lower density than on pristine TiO₂.

Moreover, the effect of a low density of Lewis sites on the formation of methyl formate gets exacerbated as its production is dependent upon the concentration of formaldehyde in the system. Given that the vanadium monomers present on the 0.5% V-WI_(EtOH)/Ti/Si formulation are inactive towards formaldehyde production (Broomhead et al., 2022), the net result is a significantly lower selectivity towards methyl formate production since the process is dependent not only of the availability of Lewis acid sites but also the presence of formaldehyde, which is observed only at low concentrations at 423K and 473K.

However, when conversions increase for the 0.5% V-WI_(EtOH)/Ti/Si at higher temperatures (523K and 553K), the methyl formate production increases but “unreacted” formaldehyde is observed at high concentrations. The increased formaldehyde selectivity at these conditions could either be a result of a decrease in availability of Lewis acid sites

able to catalyze the Tishchenko formaldehyde to methyl formate conversion resulting from the interaction between the titania and silica altering TiO_2 Lewis centers, or the availability of other reaction pathways for methyl formate production taking predominance under the high temperature conditions. Liu and Iglesia reported that high methyl formate selectivity observed on supported ruthenium oxide catalysts was due to the dehydrogenation of an hemiformal and not via the Tishchenko reaction (2005), this pathway might be available to formaldehyde in our system at higher temperatures. Further analyses are required to elucidate the key mechanism taking place under these conditions.

3.5.5 ALD Impregnation of Vanadium onto $\text{TiO}_2/\text{SiO}_2$

At this point all samples prepared which were able to achieve high ODH conversions of methanol also produced a high amount of methyl formate. Using the knowledge gained at this point, we modified our catalyst synthesis protocol. As discussed in the previous section, the deposition of vanadia onto the ALD Ti/Si pellet, using wetness impregnation resulted in an eggshell morphology for the vanadia phase. Thus, we now set to incorporate the vanadium oxide phase in the ALD-prepared Ti/Si pellets, using ALD. This strategy, once again, attempts to blanket all the titania sites present on the pellet and form a vanadia monolayer on top of the TiO_2 monolayer present on the SiO_2 pellet. By utilizing a 1:1 molar ratio of vanadium to titania the titanium dioxide could be entirely covered and theoretically enfold all Lewis acid centers present in TiO_2 , eliminating the amount of methyl formate being produced. Two weight loadings were prepared and evaluated, the 1:1 molar ratio of vanadium to titanium which equated to 11 wt% loading of vanadium, and a slightly lower 8 wt% vanadium content.

3.5.5.1 Characterization of Vanadium-ALD Pellets

To evaluate the vanadium phase distribution throughout the catalyst WDS mapping was conducted, the results are shown in Figure 3-23. The WDS maps show that for both loadings the dispersion is near homogenous throughout the pellet. There exists some gradient towards the outer edge of the pellet with higher concentrations of vanadia observed towards the external surface. This is more apparent with the 11% V-ALD/Ti/Si

sample. To determine the extent of the gradient for the vanadium dispersion, UV data was taken at the outer edge and center of the pellets. This relevant UV data is presented in Table 3-6.

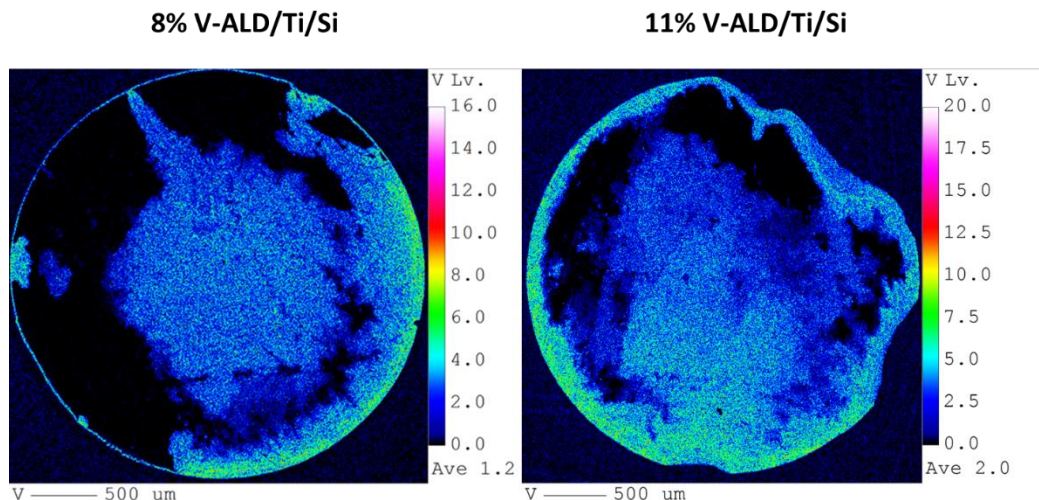


Figure 3-23 Vanadium WDS Scans of 8% V-ALD/Ti/Si (left) and 11% V-ALD/Ti/Si (right)

Table 3-6 UV Bandgap at Different Sections of V-ALD/Ti/Si Pellets

Vanadium Loading (wt%)	UV Bandgap (Outer)	UV Bandgap (Inner)
11	2.12 eV	2.34 eV
8	2.17/2.32 eV*	2.42 eV

**Note the 8 wt% VO_x/TiO₂/SiO₂ samples did not have a homogenous colour to the outer shell of the pellets with one side appearing distinctly browner than the other, which appeared yellow, as such UV was taken for both colours (Left value Brown Section; Right Value Yellow Section)*

The UV bandgap values show once again there is a vanadium gradient throughout the catalyst pellet cross-section. Vanadium is more concentrated and more crystalline towards the outer edge of the catalyst with both samples having bandgaps associated with crystalline vanadium along their outer edge. The dispersion was less concentrated and more dispersed towards the center with both samples achieving a monolayer distribution. The varying bandgap along the outer edge of 8% V-ALD/Ti/Si sample suggest that

vanadium may also be migrating throughout the synthesis process and as such becomes more concentrated in certain sections of the catalyst, although this was not evident in the WDS mapping (the 8% V-ALD/Ti/Si sample had more extensive interference due to sample charge making this difficult to differentiate). While the outer edge of the samples' bandgap is below the threshold required for adequate DMM formation the center is well-dispersed and makes up a much higher volume of active sites as evidenced by the WDS maps. As such catalytic testing should reveal a high propensity to DMM and formaldehyde production as vanadium has completely been spread throughout the pellet minimizing bare titania sites.

3.5.5.2 Reactivity Testing and the Consequences of Distribution and Dispersion on Catalytic Activity

The results of the catalytic testing on these two samples (8% V-ALD/Ti/Si and 11% V-ALD/Ti/Si), carried at two different WHSV are shown in Figure 3-24.

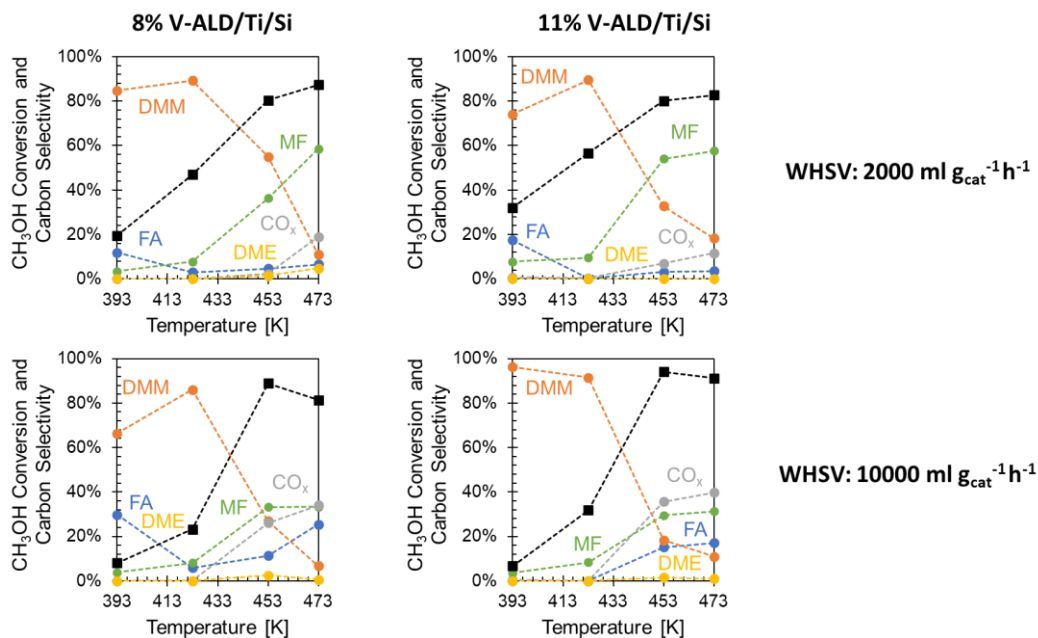


Figure 3-24 Catalytic Activity for V-ALD/Ti/Si Catalysts at Two Space Velocity Conditions. Black Square: Methanol Conversion, FA: Formaldehyde, MF: Methyl Formate. 1.47g of the 8% V-ALD/Ti/Si and 1.74g of the 11% V-ALD/Ti/Si whole pellets assessed between 393K-473K, 20 kPa methanol and 10 kPa oxygen; balance argon. 50SCCM (2000 ml g_{cat}⁻¹h⁻¹ for 8% V-ALD/Ti/Si and 1700 ml g_{cat}⁻¹h⁻¹ for 11% V-ALD/Ti/Si) and 250SCCM (10200 ml g_{cat}⁻¹h⁻¹ for 8% V-ALD/Ti/Si and 8600 ml g_{cat}⁻¹h⁻¹ for 11% V-ALD/Ti/Si) were tested

Both the 1:1 molar vanadium to titanium sample (11% V-ALD/Ti/Si) and the 8% V-ALD/Ti/Si sample are able to reach substantial methanol conversions despite the fact that they were tested at nearly double the space velocities used for the V/Ti samples prepared using TiO₂ pellets. For the 8% V-ALD/Ti/Si catalyst at the low space velocity conditions conversions increased with temperature from 20% at 393K to 87% at 473K. DMM selectivity was also high, reaching a maximum at 89% at 423K before decreasing with temperature, a trend also seen on the previously tested catalytic formulations (Figures 3-17, 3-18, and 3-22). Formaldehyde was present at low concentrations with a maximum selectivity of 12% at 393K before decreasing to 3% once the temperatures reached 423K, at higher temperatures formaldehyde selectivity values recovered to just 7%. Compared to the previously tested catalytic formulations, selectivity to methyl formate was lower;

however, despite the low amount of exposed titania it was still observed at 453 and 473K. DME and CO_x were not detected below 473K.

At the high space velocity regime, conversions obtained were low, until temperatures above 453K were reached, where conversions attained values above 80%. The DMM selectivity reached a maximum of 86% at 423K before decreasing significantly with temperature. Formaldehyde initially formed in high quantities (30% selectivity at 393K) following a similar trend as that observed at low space velocity conditions, decreasing with temperature before increasing back to 25% at 473K. At this high space velocity methyl formate selectivity was lower plateauing at 33% at 453K. DME was not observed in significant amounts. CO_x had a significantly higher selectivity, compared to that observed at the lower space velocity, detected at 453K and achieving a maximum of 33% at 473K.

The behaviour observed at higher temperatures and high space velocity for the 8% V-ALD/Ti/Si catalyst, specifically the higher CO_x selectivity, compared to the case of the catalyst assessed at low space velocity, is atypical. It is expected that increasing space velocity decreases the residence time and thus the interaction of the catalyst with the formed formaldehyde, minimizing the amount of formaldehyde that continues down the oxidation pathway. The CO_x selectivity being higher with an increased space velocity could be caused by hot spot formation due to higher amounts of methanol reacting at this condition and thus higher quantity of energy being released per gram of catalyst, leading to more distinct non-uniform temperature profiles.

When examining the higher loaded 1:1 molar vanadium to titanium catalyst formulation (11% V-ALD/Ti/Si) at low space velocities, the sample exhibits better conversions at lower temperatures (393K and 423K) than the 8% V-ALD/Ti/Si formulation (32 and 57% vs 20 and 47%, respectively). Compared to the 8% V-ALD/Ti/Si sample the trends in product selectivity remained relatively unchanged, likely due to similar vanadium distributions and dispersions on these two catalyst pellets. DMM achieved a maximum yield at 423K (2.3 mol_{DMM} g_{cat}⁻¹h⁻¹ molar rate production). Methyl formate production reached a similar maximum to the lower loaded 8 wt% sample but this maximum was

achieved at lower temperatures (453K) before plateauing on the 11% V-ALD/Ti/Si. As such the drop-off for DMM selectivity was steeper between 423K and 453K for the 11% V-ALD/Ti/Si vs the 8% V-ALD/Ti/Si. CO_x selectivity was substantially lower for the higher loaded 11 wt% catalyst. These changes, albeit small, might be caused by the differences in vanadium dispersion as they all are ODH products and therefore linked to the redox ability of the catalysts.

Finally, when the 11% V-ALD/Ti/Si sample was assessed at the high space velocity conditions, the obtained trends had some differences to those observed on the 8 wt% V-ALD/Ti/Si catalyst evaluated under the same conditions. The two key differences were the 11% V-ALD/Ti/Si catalyst had zero selectivity to formaldehyde production at 393K, and a near 100% DMM selectivity achieved at this temperature. Additionally, the amount of CO_x generated was higher, reaching a 40% selectivity at 393K. The conversion at these temperatures were also higher than the one obtained on the 8% V-ALD/Ti/Si catalyst with >90% of methanol converted.

This is in opposition to previous results where 80% was the maximum attainable conversion due to over-oxidation limiting conversion, because of the lack of oxygen in the feedstock stream. Over the 5% V-WI_(EtOH)/Ti sample, methanol conversions decreased below 80% once CO_x became a dominant product; however, this is not observed for the 11 wt% and 8wt% V-ALD/Ti/Si samples at high flowrates (also not seen on the 5% V-WI_(Aq)/Ti sample). As such, over-achieving oxygen efficiency in the catalyst at these conditions should be further explored and might suggest other pathways are available or the generation of oxidation products such as direct dehydrogenation of methanol to formaldehyde given in Equation 2-8 in Section 2.3.

The results obtained indicate that methyl formate is still being produced at high temperatures (453K- 473K). One of our key objectives when incorporating vanadia through ALD was to ensure that the titania Lewis sites were covered and unavailable for catalysis of the Tishchenko pathway. In Section 3.4 we also observed the formation of methyl formate under conditions that would have suppressed its formation, and we speculated that perhaps methyl formate was being formed through a different kinetic

pathway. To probe this hypothesis, we conducted an additional set of experiments using formaldehyde instead of methanol in the reaction feed over the 11% V-ALD/Ti/Si catalyst. If the Tishchenko route is available for formaldehyde over available Lewis acid centers, the production of methyl formate will substantially increase with formaldehyde present in the reaction stream. The results of these experiments are shown on Figure 3-25, in the form of product formation rates along with the reactor feed composition.

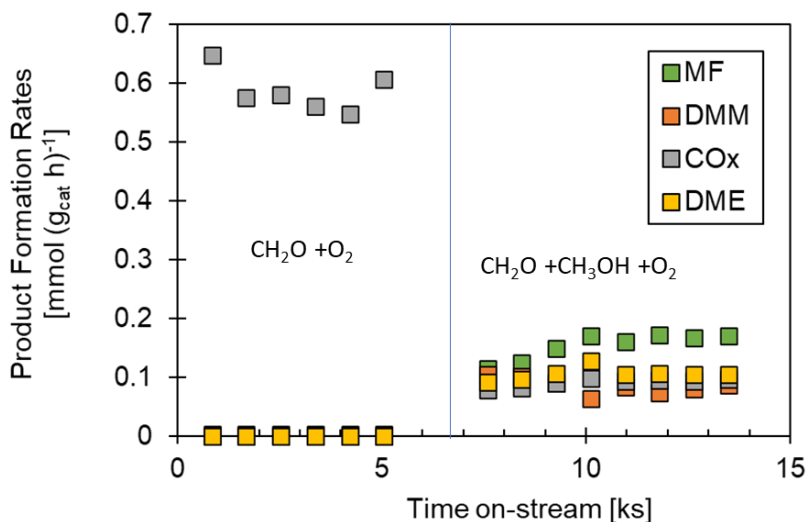


Figure 3-25: Rates of Formation for Different Products in a Pure Formaldehyde and Formaldehyde/Methanol Feed. MF: Methyl Formate, DMM: Dimethoxymethane, CO_x: CO/CO₂, DME: Dimethyl Ether. 110mg of the 11% V-ALD/Ti/Si crushed pellet (125-180 μm). 1 kPa Formaldehyde, 10 kPa oxygen, with the addition of 1 kPa Methanol after 5000 seconds, and balance Argon on stream at 27300 ml g_{cat}⁻¹h⁻¹

When formaldehyde and O₂ are the only components fed to the reactor (no methanol) the only products formed were those of formaldehyde combustion: CO/CO₂ (CO_x). Methyl formate was not observed indicating that the Tishchenko reaction pathway has been suppressed. After two hours 1 kPa of methanol was added to the feed mixture. Once methanol was present in the feed stream; DME, DMM and methyl formate were observed. DME is formed through the dehydration of methanol. DMM is produced when formaldehyde and methanol form hemiformals (in both the gas and liquid phase) that can acetalize (see Section 2.4.1). The presence of methyl formate occurring only when

methanol is a component of the reactor feed indicates that methanol must be present for methyl formate to form, indicating that production is taking place either through the acetalization of a formate complex or the oxidation of a formed hemiformal complex (Sun et al., 2019). A key observation is that the CO_x production also drops substantially with the introduction of the methanol, this is strong indication that the complete combustion pathway for formaldehyde is suppressed in the presence of methanol, perhaps through the creation of a formate esterification route given below in Equations 3-3 and 3-4.



In fact, there are three viable alternative pathways for the methyl formate to form. It could still undergo the Tishchenko reaction but using reduced Vanadium +4 sites acting as Lewis acid centers instead of exposed TiO_2 sites (Broomhead et al., 2022). Though we did not observe methyl formate in the absence of methanol, methyl formate could be formed over the 11% V-ALD/Ti/Si catalyst under conditions where oxygen limits the conversion, potentially not allowing all active vanadium sites to re-oxidize (i.e., not closing the Mars-van Krevelen cycle), creating these reduced V^{+4} species. The other two pathways for methyl formate production were presented in Section 2.3, these being either hemiformal oxidation or formate acetalization. Liu and Iglesia reported that hemiformal dehydrogenation over formate acetalization was the preferred pathway for methyl formate production in ruthenium-based catalysts (2005). From the results of Figure 41, CO_x production was reduced sixfold with the introduction of methanol to a formaldehyde/oxygen stream. This would suggest at the tested conditions (453K) formaldehyde has the ability to oxidize to formic acid which decomposes to CO. As such, it is possible that the significant decrease in CO_x is, at least partly, caused by this formic acid forming a formate complex which subsequently acetalizes. While DMM was also produced once methanol was introduced and captures some of the formaldehyde molecules that would pursue other pathways such as CO_x generation, the mass balance indicates that DMM was not produced in sufficient quantities to account for the strong

suppression of the CO_x rate production. In the end, to confidently elucidate which pathway is dominant to produce methyl formate over sites different than those TiO_2 Lewis acid centers, further testing is required.

In any case, it is clear that the Tishchenko pathway has been suppressed in the 11% V-ALD/Ti/Si catalyst. The measured rate of methyl formate production in the presence of formaldehyde and oxygen and absence of methanol shown in Figure xxx can be correlated back to the amount of exposed titania Lewis sites in the catalyst. Broomhead et al. reported a linear relationship between methyl formate formation rates, in the presence of formaldehyde and oxygen only, and exposed titania sites (i.e., not covered by vanadium) measured at 423K on powdered TiO_2 supported catalysts prepared using different vanadium loadings (2022). The relationship is shown below in Figure 3-26, together with the rate for methyl formate formation obtained under similar conditions in the 11% V-ALD/Ti/Si catalyst pellet formulation. While our experiments the experiment done in Figure 42 was carried at a slightly higher temperature (453K vs 423K) the data is comparable. All previous catalyst samples assessed on this work have shown increased methyl formate production at 453K vs 423K. Additionally, 453K achieves high rates of formaldehyde dimerization via the Tishchenko reaction from literature albeit on a different catalytic system (Ai, 1984). As such the results obtained and those from Broomhead et al. are comparable. The methyl formate production rate being near zero in the 11% V-ALD/Ti/Si catalyst formulation thus suggests that this catalyst possess near zero exposed TiO_2 sites, in other words, for the perspective of the gas phase, the surface of the catalyst topologically resembles that of bulk vanadium oxide, though with a titanium layer under it: ALD deposition of vanadia was successful in covering the titanium sites and eliminating the acid Lewis centers on the catalyst, while maintaining the high catalytic activity of the VO_x/TiO_2 system.

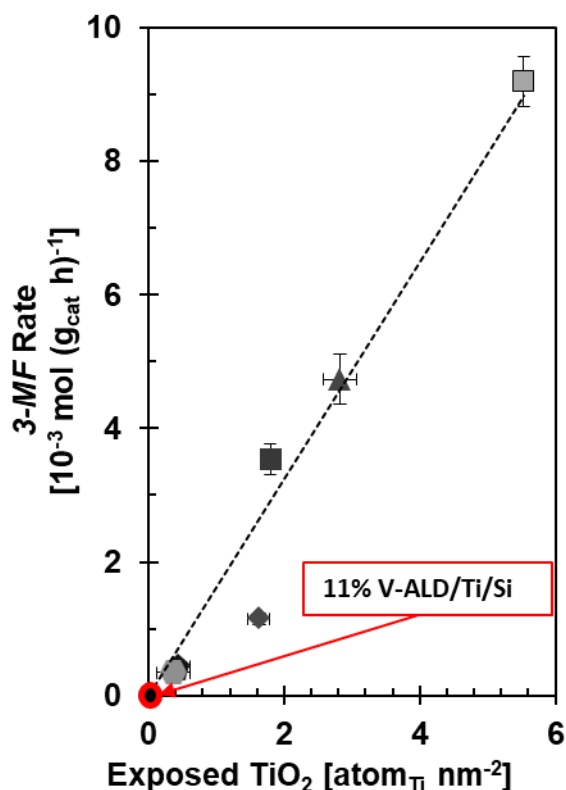


Figure 3-26 Relationship between Methyl Formate Rate and Exposed Titania adapted from Broomhead et al., 2022. 11% V-ALD/Ti/Si marked in red overlapping the symbol for crystalline V₂O₅. From highest to lowest TiO₂, 1% V/Ti, 2% V/Ti, 3% V/Ti, 5%, V/Ti (overlapped), 10% V/Ti (overlapped), all powder samples. Powdered Samples were tested by Broomhead et al. using 100 mg of sample in 1 kPa of formaldehyde, balance helium at 423K with space velocities between 14000-5000 ml g_{cat}⁻¹h⁻¹

3.5.5.3 Summary

We have achieved the required vanadium dispersion and distribution that we hypothesized would provide an appropriate product stream (Formaldehyde + DMM) and could be used for the production of long-chain OMEs, without the need of additional co-feed. A homogenous distribution of the vanadium oxide phase was attained on the catalysts obtained using ALD sequential deposition of TiO₂ and VO_x on SiO₂ pellets at vanadium loadings of 8 and 11% while simultaneously ensuring a degree of nanoscale dispersion consistent of that of a vanadium monolayer throughout the catalyst. The lower

loaded 8% V-ALD/Ti/Si catalyst had a proclivity towards higher production of redox products than the slightly more agglomerated 11% V-ALD/Ti/Si sample, as evidenced by their normalized ODH rates ($2.6 \text{ mmol}_{\text{DMM}} (\text{mol V})^{-1}\text{h}^{-1}$ vs $3.6 \text{ mmol}_{\text{DMM}} (\text{mol V})^{-1}\text{h}^{-1}$ at $423\text{K } 2000 \text{ ml g}_{\text{cat}}^{-1}\text{h}^{-1}$). This explains the significant increase towards formaldehyde production seen at high space velocities for the 8% V-ALD/Ti/Si sample as well as the higher CO_x selectivity at lower space velocities. The 8% V-ALD/Ti/Si sample had UV signals consistent with a more dispersed vanadium dispersion throughout the pellet which is tied with a better redox ability (Wachs, 2013; Broomhead et al., 2022).

The homogenous distribution of vanadium at the macroscale that was achieved for both the 8% V-ALD/Ti/Si and 11% V-ALD/Ti/Si catalysts also played a significant role in product selectivity. By giving methanol increased exposure to the active phase, the methanol conversions obtained over both catalysts were among the highest reported. This, despite the actual vanadium content in the reactor bed being relatively low, clearly indicating that a high level of vanadium atomic efficiency has been achieved on these materials: *all vanadium present in the pellets is likely involved in the catalytic process.* This was evidenced by the high DMM yield achieved by the 11% V-ALD/Ti/Si sample at $423\text{K } 2000 \text{ ml g}_{\text{cat}}^{-1}\text{h}^{-1}$. Moreover, despite the complete penetration of the active-phase through the pellet, and the formation of a well dispersed monolayer of vanadium oxide through the pellet, over-oxidation resulting from the presence of hotspots did not occur at the level observed in the 5% V-WI_(Aq)/Ti samples. CO_x production in fact was lower than that observed over the eggshell distributed catalysts (5% V-WI_(EtOH)/Ti). This would suggest that that by utilizing ALD to create a TiO_2 monolayer anchored over SiO_2 , the Si-O-Ti moieties created affected the redox potential of the V-O-Ti bonds, perhaps making them less active for formaldehyde oxidation. Further analysis must be done to probe this hypothesis and understand why this is occurring.

Chapter 4

4 Conclusions and Recommendations

4.1 Conclusions and Summary

The substitution and potential replacement of traditional diesel fuel with oxy methyl ethers (OMEs) obtained from renewable sources is a highly promising strategy in the path to decarbonization of the fuel and transportation industry. A key pathway to accomplishing the industrial manufacture of OMEs is a first stage process which converts methanol to dimethoxymethane (DMM) and formaldehyde directly in a single reactor unit. To achieve this objective a catalyst with the right redox and acid strength is required to accomplish both the methanol partial oxidation and the subsequent acetalization step of the resulting formaldehyde. Although several catalysts have been studied extensively for this process, and a clear understanding of the mechanism and reaction kinetics has emerged, very little emphasis has been put on the steps required to use the mechanistic knowledge gained at the molecular scale to create a catalyst viable for industrial production of DMM. To bridge this gap, chemical kinetics must be incorporated into a framework that includes materials manufacturing, as well as mass and heat transfer.

This thesis set to establish a link between the studies done on the bench-scale of the laboratory for the V/Ti system for DMM production and translate the knowledge of the molecular catalyst requirements to a macro-scale catalytic system. This was done by altering the distribution of the pellet while maintaining the molecular dispersion of vanadia selective to DMM formation. The molecular knowledge provided us with the requirements of a highly active vanadium monolayer that we tried to replicate on the large-scale pellets. Our synthesis efforts and subsequent characterization and catalytic test results led to the following key conclusions:

- In the catalyst pellets, the creation of egg-shell distribution results in a significant amount of methyl formate production, attributed to the presence of a large amount of active Lewis centers on TiO_2 that are not covered by the vanadia phase.

- Changing the solvent formulation used for the impregnation of the vanadia phase in the pellets (oxalic acid ethanol solution vs. water) allows for a control on the distribution of the vanadia phase through the TiO₂ pellet.
- Eggshell formulations where the vanadia phase has achieved a deep degree of penetration (nearing homogenous distribution) throughout the pellet results in a decrease of methyl formate production, however the presence of hot spots under reaction conditions is apparent, these hot spots trigger the formation of combustion products during DMM synthesis.
- Atomic layer deposition protocols for catalyst pellet preparation result on homogeneous distribution of the catalytic phase; moreover, by successfully covering all the titania Lewis sites using a 1:1 vanadium to titanium ratio formaldehyde could not undergo the Tishchenko reaction. However, methyl formate formation still occurred through different reaction pathways.

4.2 Direction for Future Work

Our work successfully accomplished the initial goal of this thesis: eliminating the Tishchenko reaction by tailoring the active-phase distribution. The strategy used, however, opened new pathways for the production of undesired methyl formate. As such, alternative process variables should be examined to boost formaldehyde production that not only involve distributing the vanadium deeper into the pellet. By altering the oxygen to methanol feed ratio in areas that produced high amounts of DMM, formaldehyde production may improve as was observed at the small-scale. Alternatively, poisoning of the titania sites exposed in eggshell dispersion catalysts may work to increase formaldehyde yields. Our results also seem to suggest that the Lewis sites are altered by distributing a titania monolayer over a silica pellet, making these titania sites less likely to form methyl formate; however more testing needs to be carried out to test this hypothesis and to better understand the effect the Ti-O-Si moiety has on the system at large. Finally, the suggestion that oxygen was over-converted, which we witnessed in several samples, indicating the potential of decomposition occurring to the reactants and products should be further investigated.

Overall, while we were not able to optimum 1:1 formaldehyde to DMM ratio that was sought, we did provide extensive evidence on how the effect of vanadium distribution throughout a 3D surface impacted the reactive system. Additional work is required now focused on the molecular interaction between less known species (Ti-O-Si) as well as the possibility of oxygen deficient zones operating under different kinetic regimes to increase formaldehyde yields in a DMM catalyst for an industrial process.

References

- Afandizadeh, S., & Foumeny, E. A. (2001). Design of packed bed reactors: Guides to catalyst shape, size, and loading selection. *Applied Thermal Engineering*, *21*(6), 669–682. [https://doi.org/10.1016/S1359-4311\(00\)00072-7](https://doi.org/10.1016/S1359-4311(00)00072-7)
- Ai, M. (1984). Dimerization of formaldehyde to methyl formate on SnO₂-W₂O₃ catalysts. *Applied Catalysis*, *9*(3), 371–377. [https://doi.org/10.1016/0166-9834\(84\)80008-1](https://doi.org/10.1016/0166-9834(84)80008-1)
- Akiya, N., & Savage, P. E. (1998). Role of water in formic acid decomposition. *AIChE Journal*, *44*(2), 405–415. <https://doi.org/10.1002/aic.690440217>
- Andersson, A., Holmberg, J., & Häggblad, R. (2016). Process Improvements in Methanol Oxidation to Formaldehyde: Application and Catalyst Development. *Topics in Catalysis*, *59*(17), 1589–1599. <https://doi.org/10.1007/s11244-016-0680-1>
- Armor, J. N. (2011). A history of industrial catalysis. *Catalysis Today*, *163*(1), 3–9. <https://doi.org/10.1016/j.cattod.2009.11.019>
- Bagheri, S., Muhd Julkapli, N., & Bee Abd Hamid, S. (2014). Titanium Dioxide as a Catalyst Support in Heterogeneous Catalysis. *The Scientific World Journal*, *2014*, 727496. <https://doi.org/10.1155/2014/727496>
- Bahmanpour, A. M., Hoadley, A., & Tanksale, A. (2014). Critical review and exergy analysis of formaldehyde production processes. *Reviews in Chemical Engineering*, *30*(6), 583–604. <https://doi.org/10.1515/revce-2014-0022>
- Baltes, C., Vukojević, S., & Schüth, F. (2008). Correlations between synthesis, precursor, and catalyst structure and activity of a large set of CuO/ZnO/Al₂O₃ catalysts for methanol synthesis. *Journal of Catalysis*, *258*(2), 334–344. <https://doi.org/10.1016/j.jcat.2008.07.004>
- Bañares, M. A., Alemany, L. J., Jiménez, M. C., Larrubia, M. A., Delgado, F., Granados, M. L., Martínez-Arias, A., Blasco, J. M., & Fierro, J. L. G. (1996). The Role of Vanadium Oxide on the Titania Transformation under Thermal Treatments and Surface Vanadium States. *Journal of Solid State Chemistry*, *124*(1), 69–76. <https://doi.org/10.1006/jssc.1996.0209>
- Baranowski, C. J., Bahmanpour, A. M., & Kröcher, O. (2017). Catalytic synthesis of polyoxymethylene dimethyl ethers (OME): A review. *Applied Catalysis B: Environmental*, *217*, 407–420. <https://doi.org/10.1016/j.apcatb.2017.06.007>
- Bergwerff, J. A., Lysova, A. A., Espinosa-Alonso, L., Koptug, I. V., & Weckhuysen, B. M. (2008). Monitoring Transport Phenomena of Paramagnetic Metal-Ion Complexes Inside Catalyst Bodies with Magnetic Resonance Imaging. *Chemistry – A European Journal*, *14*(8), 2363–2374. <https://doi.org/10.1002/chem.200700990>
- Bernholc, J., Horsley, J. A., Murrell, L. L., Sherman, L. G., & Soled, S. (1987). Brønsted acid sites in transition metal oxide catalysts: Modeling of structure, acid strengths, and support effects. *The Journal of Physical Chemistry*, *91*(6), 1526–1530. <https://doi.org/10.1021/j100290a047>

- Bitter, J. H., van der Lee, M. K., Slotboom, A. G. T., van Dillen, A. J., & de Jong, K. P. (2003). Synthesis of Highly Loaded Highly Dispersed Nickel on Carbon Nanofibers by Homogeneous Deposition–Precipitation. *Catalysis Letters*, 89(1), 139–142. <https://doi.org/10.1023/A:1024744131630>
- Blaszkowski, S. R., & van Santen, R. A. (1996). The Mechanism of Dimethyl Ether Formation from Methanol Catalyzed by Zeolitic Protons. *Journal of the American Chemical Society*, 118(21), 5152–5153. <https://doi.org/10.1021/ja954323k>
- Breitkreuz, C. F., Hevert, N., Schmitz, N., Burger, J., & Hasse, H. (2022). Synthesis of Methyl and Poly(oxymethylene) Dimethyl Ethers from Dimethyl Ether and Trioxane. *Industrial & Engineering Chemistry Research*, 61(23), 7810–7822. <https://doi.org/10.1021/acs.iecr.2c00790>
- Broomhead, W. T., Tian, W., Herrera, J. E., & Chin, Y.-H. C. (2022). Kinetic Coupling of Redox and Acid Chemistry in Methanol Partial Oxidation on Vanadium Oxide Catalysts. *ACS Catalysis*, 12(19), 11801–11820. <https://doi.org/10.1021/acscatal.2c01852>
- Bruyère, V. I. E., Rodenas, L. A. G., Morando, P. J., & Blesa, M. A. (2001). Reduction of vanadium(V) by oxalic acid in aqueous acid solutions. *Journal of the Chemical Society, Dalton Transactions*, 24, 3593–3597. <https://doi.org/10.1039/B103320B>
- Burattin, P., Che, M., & Louis, C. (1998). Molecular Approach to the Mechanism of Deposition–Precipitation of the Ni(II) Phase on Silica. *The Journal of Physical Chemistry B*, 102(15), 2722–2732. <https://doi.org/10.1021/jp980018k>
- Burger, J., Siegert, M., Ströfer, E., & Hasse, H. (2010). Poly(oxymethylene) dimethyl ethers as components of tailored diesel fuel: Properties, synthesis and purification concepts. *Fuel*, 89(11), 3315–3319. <https://doi.org/10.1016/j.fuel.2010.05.014>
- Busca, G. (1998). Spectroscopic characterization of the acid properties of metal oxide catalysts. *Catalysis Today*, 41(1), 191–206. [https://doi.org/10.1016/S0920-5861\(98\)00049-2](https://doi.org/10.1016/S0920-5861(98)00049-2)
- Cabaleiro, D., Nimo, J., Pastoriza-Gallego, M. J., Piñeiro, M. M., Legido, J. L., & Lugo, L. (2015). Thermal conductivity of dry anatase and rutile nano-powders and ethylene and propylene glycol-based TiO₂ nanofluids. *The Journal of Chemical Thermodynamics*, 83, 67–76. <https://doi.org/10.1016/j.jct.2014.12.001>
- Capel-Sanchez, M. C., Blanco-Brieva, G., Campos-Martin, J. M., de Frutos, M. P., Wen, W., Rodriguez, J. A., & Fierro, J. L. G. (2009). Grafting Strategy to Develop Single Site Titanium on an Amorphous Silica Surface. *Langmuir*, 25(12), 7148–7155. <https://doi.org/10.1021/la900578u>
- Carpenter, P. K. (1997). Peak Overlaps in EDX/WDX of Titanium and Vanadium. *Microscopy Today*, 5(5), 20–20. <https://doi.org/10.1017/S1551929500061629>
- Choi, N. H., Kwon, S., & Kim, H. (2013). Analysis of the Oxidation of the V(II) by Dissolved Oxygen Using UV-Visible Spectrophotometry in a Vanadium Redox Flow Battery. *Journal of The Electrochemical Society*, 160(6), A973. <https://doi.org/10.1149/2.145306jes>

- Demirbas, A. (2007). Progress and recent trends in biofuels. *Progress in Energy and Combustion Science*, 33(1), 1–18. <https://doi.org/10.1016/j.pecs.2006.06.001>
- Deo, G., & Wachs, I. E. (1994). Reactivity of Supported Vanadium Oxide Catalysts: The Partial Oxidation of Methanol. *Journal of Catalysis*, 146(2), 323–334. <https://doi.org/10.1006/jcat.1994.1071>
- Dette, C., Pérez-Osorio, M. A., Kley, C. S., Punke, P., Patrick, C. E., Jacobson, P., Giustino, F., Jung, S. J., & Kern, K. (2014). TiO₂ Anatase with a Bandgap in the Visible Region. *Nano Letters*, 14(11), 6533–6538. <https://doi.org/10.1021/nl503131s>
- Doornkamp, C., & Ponec, V. (2000). The universal character of the Mars and Van Krevelen mechanism. *Journal of Molecular Catalysis A: Chemical*, 162(1), 19–32. [https://doi.org/10.1016/S1381-1169\(00\)00319-8](https://doi.org/10.1016/S1381-1169(00)00319-8)
- Fogler, H. S. (2006). *Elements of Chemical Reaction Engineering* (4th ed.). Pearson Education.
- Forzatti, P., Tronconi, E., Elmi, A. S., & Busca, G. (1997). Methanol oxidation over vanadia-based catalysts. *Applied Catalysis A: General*, 157(1), 387–408. [https://doi.org/10.1016/S0926-860X\(97\)00026-4](https://doi.org/10.1016/S0926-860X(97)00026-4)
- Gao, X., & Wachs, I. E. (2000). Investigation of Surface Structures of Supported Vanadium Oxide Catalysts by UV–vis–NIR Diffuse Reflectance Spectroscopy. *The Journal of Physical Chemistry B*, 104(6), 1261–1268. <https://doi.org/10.1021/jp992867t>
- Gornay, J., Sécordel, X., Tesquet, G., Ménorval, B. de, Cristol, S., Fongarland, P., Capron, M., Duhamel, L., Payen, E., Dubois, J.-L., & Dumeignil, F. (2010). Direct conversion of methanol into 1,1-dimethoxymethane: Remarkably high productivity over an FeMo catalyst placed under unusual conditions. *Green Chemistry*, 12(10), 1722–1725. <https://doi.org/10.1039/C0GC00194E>
- Gothe, M. L., Silva, K. L. C., Figueredo, A. L., Fiorio, J. L., Rozendo, J., Manduca, B., Simizu, V., Freire, R. S., Garcia, M. A. S., & Vidinha, P. (2021). Rhenium – A Tuneable Player in Tailored Hydrogenation Catalysis. *European Journal of Inorganic Chemistry*, 2021(39), 4043–4065. <https://doi.org/10.1002/ejic.202100459>
- Grael, O., Puigmartí-Luis, J., & Muñoz-Rojas, D. (2021). Liquid atomic layer deposition as emergent technology for the fabrication of thin films. *Dalton Transactions*, 50(19), 6373–6381. <https://doi.org/10.1039/D1DT00232E>
- Guerrero-Pérez, M. O. (2017). Supported, bulk and bulk-supported vanadium oxide catalysts: A short review with an historical perspective. *Catalysis Today*, 285, 226–233. <https://doi.org/10.1016/j.cattod.2017.01.037>
- Harriott, P. (1975). Thermal conductivity of catalyst pellets and other porous particles: Part I: Review of models and published results. *The Chemical Engineering Journal*, 10(1), 65–71. [https://doi.org/10.1016/0300-9467\(75\)88018-X](https://doi.org/10.1016/0300-9467(75)88018-X)

- Herrera, J. E., Kwak, J. H., Hu, J., Wang, Y., & Peden, C. H. (2005, November 4). *Novel Wox Catalysts Grafted on Mesoporous Silica by Atomic Layer Deposition: Role of Tungstates Morphology in Methanol Dehydration*. American Institute of Chemical Engineers Annual Meeting, AIChE Annual Meeting. <https://www.aiche.org/conferences/aiche-annual-meeting/2005/proceeding/paper/601f-novel-wox-catalysts-grafted-on-mesoporous-silica-atomic-layer-deposition-role-tungstates-0>
- Herrera, J. E., Kwak, J. H., Hu, J. Z., Wang, Y., & Peden, C. H. F. (2006). Synthesis of nanodispersed oxides of vanadium, titanium, molybdenum, and tungsten on mesoporous silica using atomic layer deposition. *Topics in Catalysis*, 39(3), 245–255. <https://doi.org/10.1007/s11244-006-0063-0>
- Hill, C. G., & Wilson, J. H. (1991). Raman spectroscopy of iron molybdate catalyst systems: Part II. Preparation of supported catalysts. *Journal of Molecular Catalysis*, 67(1), 57–77. [https://doi.org/10.1016/0304-5102\(91\)85034-Y](https://doi.org/10.1016/0304-5102(91)85034-Y)
- Hlavacek, Vladimir. (1970). Aspects in Design of Packed Catalytic Reactors. *Industrial & Engineering Chemistry*, 62(7), 8–26. <https://doi.org/10.1021/ie50727a004>
- Holder, C. F., & Schaak, R. E. (2019). Tutorial on Powder X-ray Diffraction for Characterizing Nanoscale Materials. *ACS Nano*, 13(7), 7359–7365. <https://doi.org/10.1021/acsnano.9b05157>
- Hu, J. Z., Kwak, J. H., Herrera, J. E., Wang, Y., & Peden, C. H. F. (2005). Line narrowing in ^1H MAS spectrum of mesoporous silica by removing adsorbed H_2O using N_2 . *Solid State Nuclear Magnetic Resonance*, 27(3), 200–205. <https://doi.org/10.1016/j.ssnmr.2004.11.004>
- Hu, L., Qi, W., & Li, Y. (2017). Coating strategies for atomic layer deposition. *Nanotechnology Reviews*, 6(6), 527–547. <https://doi.org/10.1515/ntrev-2017-0149>
- International Energy Agency. (2022). *World Energy Outlook 2022*.
- Jin, X., Sun, W., Chen, C., Wei, T., Cheng, Y., Li, P., & Li, Q. (2014). Efficiency enhancement via tailoring energy level alignment induced by vanadium ion doping in organic/inorganic hybrid solar cells. *RSC Advances*, 4(86), 46008–46015. <https://doi.org/10.1039/C4RA08671F>
- Kaichev, V. V., Popova, G. Ya., Chesalov, Yu. A., Saraev, A. A., Zemlyanov, D. Y., Beloshapkin, S. A., Knop-Gericke, A., Schlögl, R., Andrushkevich, T. V., & Bukhtiyarov, V. I. (2014). Selective oxidation of methanol to form dimethoxymethane and methyl formate over a monolayer $\text{V}_2\text{O}_5/\text{TiO}_2$ catalyst. *Journal of Catalysis*, 311, 59–70. <https://doi.org/10.1016/j.jcat.2013.10.026>
- Klokic, S., Hochegger, M., Schober, S., & Mittelbach, M. (2020). Investigations on an efficient and environmentally benign poly(oxymethylene) dimethyl ether (OME3-5) fuel synthesis. *Renewable Energy*, 147, 2151–2159. <https://doi.org/10.1016/j.renene.2019.10.004>
- Kolah, A. K., Mahajani, S. M., & Sharma, M. M. (1996). Acetalization of Formaldehyde with Methanol in Batch and Continuous Reactive Distillation Columns. *Industrial*

& *Engineering Chemistry Research*, 35(10), 3707–3720.
<https://doi.org/10.1021/ie950563x>

- Langenberg, S., Carstens, T., Hupperich, D., Schweighofer, S., & Schurath, U. (2020). Technical note: Determination of binary gas-phase diffusion coefficients of unstable and adsorbing atmospheric trace gases at low temperature – arrested flow and twin tube method. *Atmospheric Chemistry and Physics*, 20(6), 3669–3682. <https://doi.org/10.5194/acp-20-3669-2020>
- Lautenschütz, L., Oestreich, D., Haltenort, P., Arnold, U., Dinjus, E., & Sauer, J. (2017). Efficient synthesis of oxymethylene dimethyl ethers (OME) from dimethoxymethane and trioxane over zeolites. *Fuel Processing Technology*, 165, 27–33. <https://doi.org/10.1016/j.fuproc.2017.05.005>
- Lee, J. E., Ok, Y. S., Tsang, D. C. W., Song, J., Jung, S.-C., & Park, Y.-K. (2020). Recent advances in volatile organic compounds abatement by catalysis and catalytic hybrid processes: A critical review. *Science of The Total Environment*, 719, 137405. <https://doi.org/10.1016/j.scitotenv.2020.137405>
- Lekhal, A., Glasser, B. J., & Khinast, J. G. (2001). Impact of drying on the catalyst profile in supported impregnation catalysts. *Chemical Engineering Science*, 56(15), 4473–4487. [https://doi.org/10.1016/S0009-2509\(01\)00120-8](https://doi.org/10.1016/S0009-2509(01)00120-8)
- Li, G., Hu, L., & Hill, J. M. (2006). Comparison of reducibility and stability of alumina-supported Ni catalysts prepared by impregnation and co-precipitation. *Applied Catalysis A: General*, 301(1), 16–24. <https://doi.org/10.1016/j.apcata.2005.11.013>
- Li, M., Long, Y., Deng, Z., Zhang, H., Yang, X., & Wang, G. (2015). Ruthenium trichloride as a new catalyst for selective production of dimethoxymethane from liquid methanol with molecular oxygen as sole oxidant. *Catalysis Communications*, 68, 46–48. <https://doi.org/10.1016/j.catcom.2015.04.031>
- Liu, H., & Iglesia, E. (2003). Selective One-Step Synthesis of Dimethoxymethane via Methanol or Dimethyl Ether Oxidation on $H_{3+n}V_nMo_{12-n}PO_4$ Keggin Structures. *The Journal of Physical Chemistry B*, 107(39), 10840–10847. <https://doi.org/10.1021/jp0301554>
- Liu, H., & Iglesia, E. (2005). Selective Oxidation of Methanol and Ethanol on Supported Ruthenium Oxide Clusters at Low Temperatures. *The Journal of Physical Chemistry B*, 109(6), 2155–2163. <https://doi.org/10.1021/jp0401980>
- Machiels, C. J., & Sleight, A. W. (1982). Kinetic isotope effect in the selective oxidation of methanol to formaldehyde over some molybdate catalysts. *Journal of Catalysis*, 76(1), 238–239. [https://doi.org/10.1016/0021-9517\(82\)90254-8](https://doi.org/10.1016/0021-9517(82)90254-8)
- Maj, S. (1988). Energy gap and density in SiO₂ polymorphs. *Physics and Chemistry of Minerals*, 15(3), 271–273. <https://doi.org/10.1007/BF00307516>
- Maricq, M. M., Chase, R. E., Podsiadlik, D. H., Siegl, W. O., & Kaiser, E. W. (1998). The Effect of Dimethoxy Methane Additive on Diesel Vehicle Particulate Emissions. *SAE Transactions*, 107, 1504–1511.

- Masamoto, J., Ohtake, J., & Kawamura, M. (1994). *Process for producing formaldehyde and derivatives thereof* (European Union Patent No. EP0327343B1). <https://patents.google.com/patent/EP0327343B1/en?q=0327343>
- Maymo, J. A., & Smith, J. M. (1966). Catalytic oxidation of hydrogen—Intrapellet heat and mass transfer. *AIChE Journal*, *12*(5), 845–854. <https://doi.org/10.1002/aic.690120505>
- Mengason, M., & Ritchie, N. (2017). Overcoming Peak Overlaps in Titanium- and Vanadium-Bearing Materials with Multiple Linear Least Squares Fitting. *Microscopy and Microanalysis*, *23*(3), 491–500. <https://doi.org/10.1017/S1431927617000265>
- Mettan, X., Jaćimović, J., Barišić, O. S., Pisoni, A., Batistić, I., Horváth, E., Brown, S., Rossi, L., Szirmai, P., Farkas, B., Berger, H., & Forró, L. (2019). Tailoring thermal conduction in anatase TiO₂. *Communications Physics*, *2*(1), Article 1. <https://doi.org/10.1038/s42005-019-0224-7>
- Millar, G. J., & Collins, M. (2017). Industrial Production of Formaldehyde Using Polycrystalline Silver Catalyst. *Industrial & Engineering Chemistry Research*, *56*(33), 9247–9265. <https://doi.org/10.1021/acs.iecr.7b02388>
- Munnik, P., de Jongh, P. E., & de Jong, K. P. (2015). Recent Developments in the Synthesis of Supported Catalysts. *Chemical Reviews*, *115*(14), 6687–6718. <https://doi.org/10.1021/cr500486u>
- Neimark, A. V., Kheifets, L. I., & Fenelonov, V. B. (1981). Theory of preparation of supported catalysts. *Industrial & Engineering Chemistry Product Research and Development*, *20*(3), 439–450. <https://doi.org/10.1021/i300003a006>
- Nobbs, J. H. (1985). Kubelka—Munk Theory and the Prediction of Reflectance. *Review of Progress in Coloration and Related Topics*, *15*(1), 66–75. <https://doi.org/10.1111/j.1478-4408.1985.tb03737.x>
- Omari, A., Heuser, B., Pischinger, S., & Rüdinger, C. (2019). Potential of long-chain oxymethylene ether and oxymethylene ether-diesel blends for ultra-low emission engines. *Applied Energy*, *239*, 1242–1249. <https://doi.org/10.1016/j.apenergy.2019.02.035>
- O'Neill, B. J., Jackson, D. H. K., Lee, J., Canlas, C., Stair, P. C., Marshall, C. L., Elam, J. W., Kuech, T. F., Dumesic, J. A., & Huber, G. W. (2015). Catalyst Design with Atomic Layer Deposition. *ACS Catalysis*, *5*(3), 1804–1825. <https://doi.org/10.1021/cs501862h>
- Partopour, B., & Dixon, A. G. (2020). Effect of particle shape on methanol partial oxidation in a fixed bed using CFD reactor modeling. *AIChE Journal*, *66*(5), e16904. <https://doi.org/10.1002/aic.16904>
- Pavid, K. (2019, June 6). *We need more scarce metals and elements reach the UK's greenhouse gas goals*. Natural History Museum. <https://www.nhm.ac.uk/discover/news/2019/june/we-need-more-metals-and-elements-reach-uks-greenhouse-goals.html>

- Peláez, R., Marín, P., & Ordóñez, S. (2021). Effect of formaldehyde precursor and water inhibition in dimethoxymethane synthesis from methanol over acidic ion exchange resins: Mechanism and kinetics. *Biofuels, Bioproducts and Biorefining*, 15(6), 1696–1708. <https://doi.org/10.1002/bbb.2266>
- Pudge, G. J. F., Hutchings, G. J., Kondrat, S. A., Morrison, K., Perkins, E. F., Rushby, A. V., & Bartley, J. K. (2022). Iron molybdate catalysts synthesised via dicarboxylate decomposition for the partial oxidation of methanol to formaldehyde. *Catalysis Science & Technology*, 12(14), 4552–4560. <https://doi.org/10.1039/D2CY00699E>
- Quaranta, N. E., Soria, J., Corberán, V. C., & Fierro, J. L. G. (1997). Selective Oxidation of Ethanol to Acetaldehyde on V₂O₅/TiO₂/SiO₂ Catalysts. *Journal of Catalysis*, 171(1), 1–13. <https://doi.org/10.1006/jcat.1997.1760>
- Radko, M., Kowalczyk, A., Bidzińska, E., Witkowski, S., Górecka, S., Wierzbicki, D., Pamin, K., & Chmielarz, L. (2018). Titanium dioxide doped with vanadium as effective catalyst for selective oxidation of diphenyl sulfide to diphenyl sulfonate. *Journal of Thermal Analysis and Calorimetry*, 132(3), 1471–1480. <https://doi.org/10.1007/s10973-018-7119-9>
- Rhodes, C. J. (2016). The 2015 Paris Climate Change Conference: Cop21. *Science Progress*, 99(1), 97–104. <https://doi.org/10.3184/003685016X14528569315192>
- Rodriguez, A. F., & Herrera, J. E. (2023). Hacia el desarrollo de alternativas sostenibles al combustible diésel: Síntesis de 1,1-dimetoximetano (OME1) a través de catálisis bifuncional. *Revista de Química*, 37(1), 13–21. <https://doi.org/10.18800/quimica.202301.002>
- Russo, V., Mastroianni, L., Tesser, R., Salmi, T., & Di Serio, M. (2020). Intraparticle Modeling of Non-Uniform Active Phase Distribution Catalyst. *ChemEngineering*, 4(2), Article 2. <https://doi.org/10.3390/chemengineering4020024>
- Satoh, S., & Tanigawa, Y. (2002). *Process for producing methylal* (United States Patent No. US6379507B1). <https://patents.google.com/patent/US6379507B1/en?q=U.S.+Patent+6379507>
- Satsuma, A., Takenaka, S., Tanaka, T., Nojima, S., Kera, Y., & Miyata, H. (2002). Studies on the preparation of supported metal oxide catalysts using JRC-reference catalysts: II. Vanadia–titania catalyst: effect of starting solution and phase of titania. *Applied Catalysis A: General*, 232(1), 93–106. [https://doi.org/10.1016/S0926-860X\(02\)00089-3](https://doi.org/10.1016/S0926-860X(02)00089-3)
- Schmitz, N., Burger, J., Ströfer, E., & Hasse, H. (2016). From methanol to the oxygenated diesel fuel poly(oxymethylene) dimethyl ether: An assessment of the production costs. *Fuel*, 185, 67–72. <https://doi.org/10.1016/j.fuel.2016.07.085>
- Schmitz, N., Homberg, F., Berje, J., Burger, J., & Hasse, H. (2015). Chemical Equilibrium of the Synthesis of Poly(oxymethylene) Dimethyl Ethers from Formaldehyde and Methanol in Aqueous Solutions. *Industrial & Engineering Chemistry Research*, 54(25), 6409–6417. <https://doi.org/10.1021/acs.iecr.5b01148>

- Schwarz, J. A., Contescu, C., & Contescu, A. (1995). Methods for Preparation of Catalytic Materials. *Chemical Reviews*, 95(3), 477–510. <https://doi.org/10.1021/cr00035a002>
- Shafeeq, K. M., Athira, V. P., Kishor, C. H. R., & Aneesh, P. M. (2020). Structural and optical properties of V₂O₅ nanostructures grown by thermal decomposition technique. *Applied Physics A*, 126(8), 586. <https://doi.org/10.1007/s00339-020-03770-5>
- Soares, A. P. V., Portela, M. F., & Kiennemann, A. (2005). Methanol Selective Oxidation to Formaldehyde over Iron-Molybdate Catalysts. *Catalysis Reviews*, 47(1), 125–174. <https://doi.org/10.1081/CR-200049088>
- Sorenson, S. C., Glensvig, M., & Abata, D. L. (1998). Dimethyl Ether in Diesel Fuel Injection Systems. *SAE Transactions*, 107, 438–449.
- Sun, J., Li, H., Song, H., Wu, Q., Zhao, Y., & Jiao, Q. (2015). Synthesis of methylal from methanol and formaldehyde catalyzed by Brønsted acid ionic liquids with different alkyl groups. *RSC Advances*, 5(106), 87200–87205. <https://doi.org/10.1039/C5RA18598J>
- Sun, R., Delidovich, I., & Palkovits, R. (2019). Dimethoxymethane as a Cleaner Synthetic Fuel: Synthetic Methods, Catalysts, and Reaction Mechanism. *ACS Catalysis*, 9(2), 1298–1318. <https://doi.org/10.1021/acscatal.8b04441>
- Tatibouët, J. M. (1997). Methanol oxidation as a catalytic surface probe. *Applied Catalysis A: General*, 148(2), 213–252. [https://doi.org/10.1016/S0926-860X\(96\)00236-0](https://doi.org/10.1016/S0926-860X(96)00236-0)
- Thavornprasert, K., Capron, M., Jalowiecki-Duhamel, L., & Dumeignil, F. (2016). One-pot 1,1-dimethoxymethane synthesis from methanol: A promising pathway over bifunctional catalysts. *Catalysis Science & Technology*, 6(4), 958–970. <https://doi.org/10.1039/C5CY01858G>
- Thavornprasert, K., Capron, M., Jalowiecki-Duhamel, L., Gardoll, O., Trentesaux, M., Mamede, A.-S., Fang, G., Faye, J., Touati, N., Vezin, H., Dubois, J.-L., Couturier, J.-L., & Dumeignil, F. (2014). Highly productive iron molybdate mixed oxides and their relevant catalytic properties for direct synthesis of 1,1-dimethoxymethane from methanol. *Applied Catalysis B: Environmental*, 145, 126–135. <https://doi.org/10.1016/j.apcatb.2013.01.043>
- Thrane, J., Mentzel, U. V., Thorhauge, M., Høj, M., & Jensen, A. D. (2021). A Review and Experimental Revisit of Alternative Catalysts for Selective Oxidation of Methanol to Formaldehyde. *Catalysts*, 11(11), Article 11. <https://doi.org/10.3390/catal11111329>
- Tracey, A. S., Gresser, M. J., & Parkinson, K. M. (1987). Vanadium(V) oxyanions. Interactions of vanadate with oxalate, lactate and glycerate. *Inorganic Chemistry*, 26(5), 629–638. <https://doi.org/10.1021/ic00252a002>
- Védrine, J. C. (2017). Heterogeneous Catalysis on Metal Oxides. *Catalysts*, 7(11), Article 11. <https://doi.org/10.3390/catal7110341>

- Venezia, B., Cao, E., Matam, S. K., Waldron, C., Cibin, G., Gibson, E. K., Golunski, S., Wells, P. P., Silverwood, I., Catlow, C. R. A., Sankar, G., & Gavriilidis, A. (2020). Silicon microfabricated reactor for *operando* XAS/DRIFTS studies of heterogeneous catalytic reactions. *Catalysis Science & Technology*, *10*(23), 7842–7856. <https://doi.org/10.1039/D0CY01608J>
- Vertin, K. D., Ohi, J. M., Naegeli, D. W., Childress, K. H., Hagen, G. P., McCarthy, C. I., Cheng, A. S., & Dibble, R. W. (1999). *Methylal and Methylal-Diesel Blended Fuels for Use in Compression-Ignition Engines* (SAE Technical Paper No. 1999-01-1508). SAE International. <https://doi.org/10.4271/1999-01-1508>
- Wachs, I. E. (2013). Catalysis science of supported vanadium oxide catalysts. *Dalton Transactions*, *42*(33), 11762–11769. <https://doi.org/10.1039/C3DT50692D>
- Wachs, I. E., & Weckhuysen, B. M. (1997). Structure and reactivity of surface vanadium oxide species on oxide supports. *Applied Catalysis A: General*, *157*(1), 67–90. [https://doi.org/10.1016/S0926-860X\(97\)00021-5](https://doi.org/10.1016/S0926-860X(97)00021-5)
- Wang, F., Zhu, G., Li, Z., Zhao, F., Xia, C., & Chen, J. (2015). Mechanistic study for the formation of polyoxymethylene dimethyl ethers promoted by sulfonic acid-functionalized ionic liquids. *Journal of Molecular Catalysis A: Chemical*, *408*, 228–236. <https://doi.org/10.1016/j.molcata.2015.07.028>
- Weaver, F. L., Hough, A. R., Highman, B., & Fairhall, L. T. (1951). The Toxicity of Methylal. *British Journal of Industrial Medicine*, *8*(4), 279–283.
- Wu, J., Zhu, H., Wu, Z., Qin, Z., Yan, L., Du, B., Fan, W., & Wang, J. (2015). High Si/Al ratio HZSM-5 zeolite: An efficient catalyst for the synthesis of polyoxymethylene dimethyl ethers from dimethoxymethane and trioxymethylene. *Green Chemistry*, *17*(4), 2353–2357. <https://doi.org/10.1039/C4GC02510E>
- Yu, H., Zeng, K., Fu, X., Zhang, Y., Peng, F., Wang, H., & Yang, J. (2008). RuO₂·xH₂O Supported on Carbon Nanotubes as a Highly Active Catalyst for Methanol Oxidation. *The Journal of Physical Chemistry C*, *112*(31), 11875–11880. <https://doi.org/10.1021/jp804003g>
- Yuan, M., Dong, M., Tian, Z., Che, Y., Tian, Y., Qiao, Y., Zhang, J., & Li, D. (2022). Reaction mechanisms and catalysis in the one-step synthesis of methylal via methanol oxidation. *Journal of the Energy Institute*, *103*, 47–53. <https://doi.org/10.1016/j.joei.2022.05.006>
- Yuan, Y., Liu, H., Imoto, H., Shido, T., & Iwasawa, Y. (2000). Performance and Characterization of a New Crystalline SbRe₂O₆ Catalyst for Selective Oxidation of Methanol to Methylal. *Journal of Catalysis*, *195*(1), 51–61. <https://doi.org/10.1006/jcat.2000.2990>
- Yuan, Y., Shido, T., & Iwasawa, Y. (2000). The new catalytic property of supported rhenium oxides for selective oxidation of methanol to methylal. *Chemical Communications*, *0*(15), 1421–1422. <https://doi.org/10.1039/B003870I>
- Yun, D. (2016). Mechanism of ethanol partial oxidation over titania supported vanadia catalysts: Geometric and electronic structure consequences on reaction kinetics. *Electronic Thesis and Dissertation Repository*. <https://ir.lib.uwo.ca/etd/4082>

- Yun, D., & Herrera, J. E. (2017). A novel methodology for in situ redox active site titration of TiO₂-supported vanadia during ethanol partial oxidation catalysis. *Journal of Catalysis*, 350, 72–85. <https://doi.org/10.1016/j.jcat.2017.04.001>
- Yun, D., Wang, Y., & Herrera, J. E. (2018). Ethanol Partial Oxidation over VO_x/TiO₂ Catalysts: The Role of Titania Surface Oxygen on Vanadia Reoxidation in the Mars–van Krevelen Mechanism. *ACS Catalysis*, 8(5), 4681–4693. <https://doi.org/10.1021/acscatal.7b03327>
- Zabilska, A., Clark, A. H., Moskowitz, B. M., Wachs, I. E., Kakiuchi, Y., Copéret, C., Nachttegaal, M., Kröcher, O., & Safonova, O. V. (2022). Redox Dynamics of Active VO_x Sites Promoted by TiO_x during Oxidative Dehydrogenation of Ethanol Detected by Operando Quick XAS. *JACS Au*, 2(3), 762–776. <https://doi.org/10.1021/jacsau.2c00027>
- Zandbergen, M. W., Beale, A. M., & Weckhuysen, ir. B. M. (2012). On the Microdistributions of Cr-Ion Complexes within mm-Sized γ -Al₂O₃ Catalyst Bodies upon Impregnation as Studied by UV/Vis and Raman Microspectroscopy. *ChemCatChem*, 4(2), 217–227. <https://doi.org/10.1002/cctc.201100333>
- Zhang, J., Fang, D., & Liu, D. (2014). Evaluation of Zr–Alumina in Production of Polyoxymethylene Dimethyl Ethers from Methanol and Formaldehyde: Performance Tests and Kinetic Investigations. *Industrial & Engineering Chemistry Research*, 53(35), 13589–13597. <https://doi.org/10.1021/ie501231a>
- Zhang, L. (2018). *CHAPTER 1 Introduction to Formaldehyde*. 1–19. <https://doi.org/10.1039/9781788010269-00001>
- Zhang, Q., Wang, W., Zhang, Z., Han, Y., & Tan, Y. (2016). Low-Temperature Oxidation of Dimethyl Ether to Polyoxymethylene Dimethyl Ethers over CNT-Supported Rhenium Catalyst. *Catalysts*, 6(3), Article 3. <https://doi.org/10.3390/catal6030043>
- Zhang, Y. (2020). Preparation of heterogeneous catalysts based on CWAO technology. *Journal of Physics: Conference Series*, 1549(3), 032052. <https://doi.org/10.1088/1742-6596/1549/3/032052>
- Zheng, Y., Tang, Q., Wang, T., Liao, Y., & Wang, J. (2013). Synthesis of a Green Fuel Additive Over Cation Resins. *Chemical Engineering & Technology*, 36(11), 1951–1956. <https://doi.org/10.1002/ceat.201300360>
- Zheng, Y., Tang, Q., Wang, T., & Wang, J. (2015). Kinetics of synthesis of polyoxymethylene dimethyl ethers from paraformaldehyde and dimethoxymethane catalyzed by ion-exchange resin. *Chemical Engineering Science*, 134, 758–766. <https://doi.org/10.1016/j.ces.2015.05.067>

Appendices

Appendix A: Large-Scale Catalytic Testing Experimental Setup

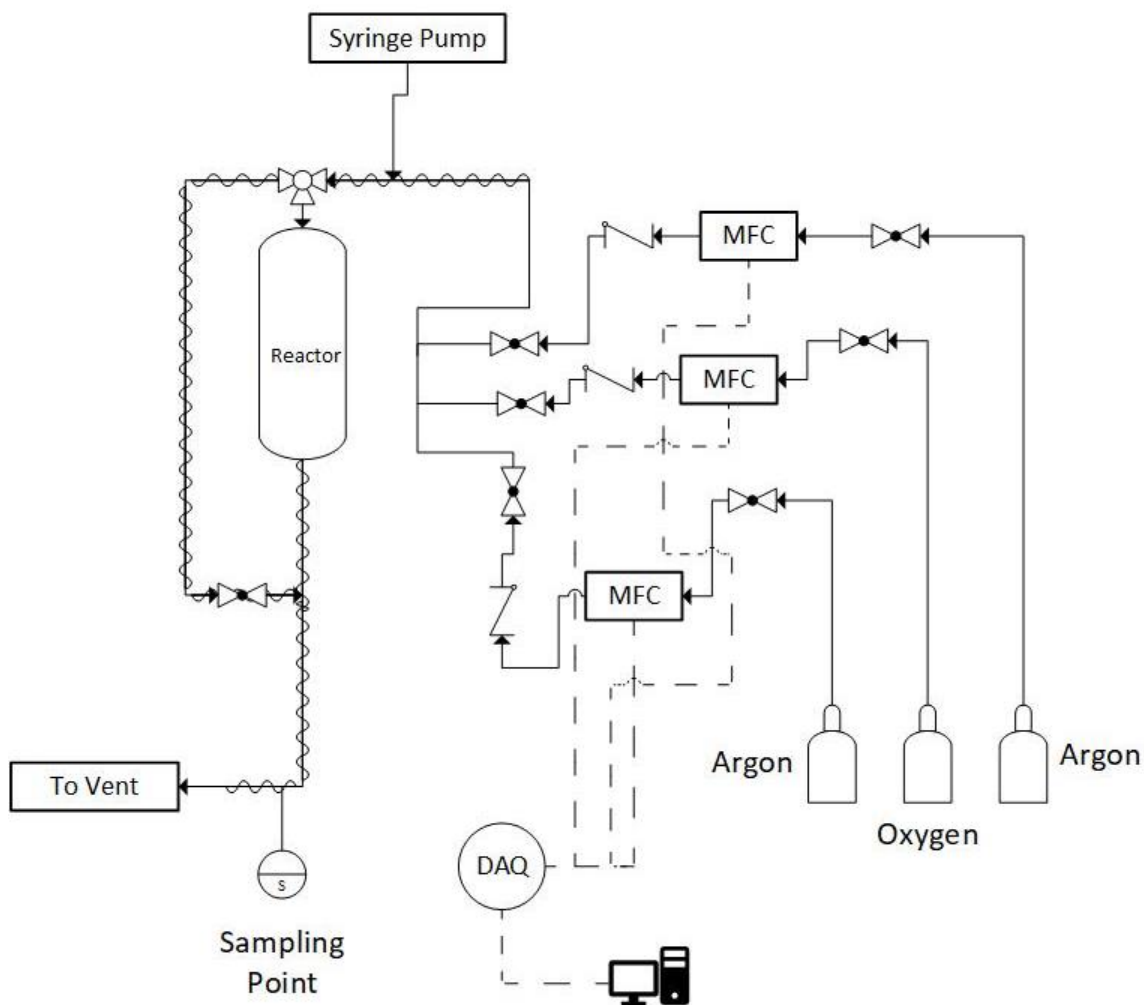


Figure A-1 P&ID Diagram of Large-Scale Experimental System. MFC: Mass-Flow Controller; DAQ: Data Acquisition Terminal

Appendix B: Determining Mass and Heat Transfer Limitations using Calculations

The Weisz-Prater criterion can determine if a reaction is operating in the kinetic limited or mass-transfer limited regime (Fogler, 2006). The calculation to determine this criterion

is given below in Equation A-1 showing that the criterion is a ratio between the observed kinetic rate and effective diffusivity.

$$C_{WP} = \frac{-r'_{ODH(Obs)}\rho_c R_{pellet}^2}{D_{TA}^e C_{MEOH,S}} \quad (A - 1)$$

When the observed rate is very high, and the diffusivity is low, this number is very large, and the system is in the mass-transport limited regime. Alternatively, if these conditions are reversed the reaction is kinetic limited as the diffusivity is much faster than the observed rate. Alternatively this can be communicated as a Weisz-Prate criterion greater than 1 results in the reaction being relegated by the mass transfer of the molecule through the pellet and a criterion below 1 results in the reaction kinetics relegating the system. As this equation is valid only for 1st order reactions the oxidative dehydrogenation of methanol to formaldehyde was used for the normalized rate term (Venezia et al., 2020). The effective transitional diffusivity was calculated using the Knudsen diffusion and the molecular diffusivity of methanol into argon obtained using the Fuller, Schettler, and Giddings correlation which provides an adequate estimation for the conditions of the experimental system (Langenburg, 2020). Porosity and Tortuosity were estimated to be 0.7 and 3 respectively (Fogler, 2006). The density of the catalyst pellet was estimated using the pure titanium pellet. Finally, concentration of methanol at the surface of the pellet was assumed to be the same as that in the bulk of the system. With these approximations the Weisz-Prater criterion for the 5% V-WI_(Aq)/Ti sample can be calculated at the given temperatures given below in Figure A-2.

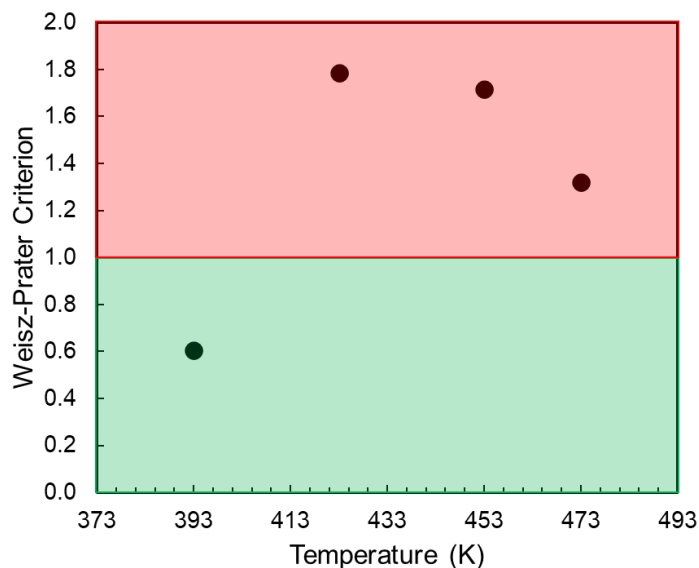


Figure A-2 Weisz-Prater Criterion for 5% V-WI(Aq)/Ti Sample at 50 SCCM. Note the green region is the kinetically controlled regime while red represents the mass-transport controlled regime

Similarly for heat transfer the Prater number can be used to determine the presence of a temperature gradient throughout the pellet, which can be due to poor thermal conductivity or excessive heat generated. It is given below in Equation A-2.

$$\beta = \frac{T_{MAX} - T_s}{T_s} = \frac{-\Delta H_{RX} D_{TA}^e C_{MEOH,S}}{k_t T_s} \quad (A - 2)$$

A larger Prater number represents a greater gradient in temperature from the surface of the catalyst towards the center and can be described as a ratio of the heat generated as the product travels towards the center of the catalyst compared to the ability for the catalyst to dissipate this energy. For this equation the enthalpy of reaction for methanol to carbon monoxide was used as this was the dominant reaction at higher temperatures. The thermal conductivity was estimated using the known thermal conductivity for bulk anatase TiO₂ (7.4 W m⁻¹K⁻¹) (Cabaleiro et al., 2015). With this value correlations from Harriott can be used for a similar porous system to obtain a value of (0.18 W m⁻¹K⁻¹). While this value obtains a low temperature gradient of 7K at 423K, other researchers have obtained thermal conductivities for titanium dioxide ranging from 0.423 and 0.016 W m⁻¹K⁻¹

demonstrating the variability of this property and thus the Prater number on physical construction of the titania (Cabaleiro et al., 2015; Mettan et al., 2019). While these values represent a temperature gradient of 3K and 77K at 423K respectively, the true value is somewhere between these numbers.

Ultimately the Prater number is highly dependent on the thermal conductivity of the pellet which itself is highly dependent on the structure of the pellet and its porosity (Harriott, 1975). To obtain a more accurate Prater number and thus a more accurate representation of the temperature gradient, the exact porosity and thermal conductivity must be obtained experimentally. However, the assumptions above can be used as a good starting point illustrating that the system may be highly sensitive to heat fluctuations throughout the pellet.

Curriculum Vitae

Name: Sebastian Cook
Post-secondary Education and Degrees: University of Western Ontario
London, Ontario, Canada
2016-2021 B.E.Sc.

Honours and Awards: Province of Ontario Graduate Scholarship
2021-2022
Dr. Argyrios Margaritis Memorial Scholarship
2021

Related Work Experience Teaching Assistant
The University of Western Ontario
2021-2023